Investigating the Antagonization of dIgA-pIgR Mucosal Immune Pathways by the SARS-CoV-2 Accessory Protein ORF8

Frederique Laprise

Division of Microbiology and Immunology, Faculty of Science

McGill University, Montreal

April 2024

A thesis submitted to McGill University in partial fulfillment of the requirements of the degree of Master of Science

TABLE OF CONTENTS

LIST OF ABBREVIATIONS

ACE2: angiotensin converting enzyme 2

ADCC: antibody-dependent cellular cytotoxicity

ALI: air-liquid interface

AM: alveolar macrophages

APC: antigen-presenting cell

ARDS: acute respiratory distress syndrome

ASC: antibody secreting cell

ATF6: activating transcription factor 6

ATL3: GTPase 3 (ATL3)

BLI: bio-layer interferometry

BRM: tissue-resident memory B cell

cGAS: cyclic GMP-AMP synthase

CM: convoluted membrane

COPD: chronic obstructive pulmonary disease

CoV: coronavirus

CTL: cytotoxic t lymphocyte

CTPS1: CTP synthase 1

D: domain

dIgA: dimeric IgA

DMT1: divalent metal transporter 1

DMV: double-membrane vesicle

E: envelope

ER: endoplasmic reticulum

ERGIC: endoplasmic reticulum-Golgi intermediate compartment

FP: fusion peptide

FPN1: ferroportin 1

HBEC: human bronchial epithelial cell

HCoV: human coronavirus

IBD: inflammatory bowel syndrome

IBV: avian infection bronchitis virus

IFITM: interferon induced transmembrane protein

IFN: interferon

Ig: immunoglobulin

IL: interleukin

ILC: innate lymphoid cells

IRE1a: inositol-requiring transmembrane kinase endoribonuclease-1a

ISG: interferon stimulated genes

JC: joining chain

Kb: kilobase

LCC: liquid covered culture

M: membrane

MCP-1: monocyte chemoattractant protein 1

MDCK: Madin-Darby canine kidney

MERS: middle eastern respiratory syndrome

MHC-I: major histocompatibility complex I

N: nucleocapsid

nAb: neutralizing antibody

NF-κB: nuclear factor kappa-light-chain-enhancer of activated B cells

NLR: nod-like receptor

NSP: non-structural protein

OAS3: 2', 5'-oligodenylate synthetase

ORF: open reading frame

PERK: protein kinase R-like endoplasmic reticulum kinase

PGE2: prostaglandin 2

pIgA: pIgR-IgA

pIgR: polymeric Ig receptor

PRR: pattern-recognition receptor

RBC: red blood cell

RBD: receptor-binding domain

RdRp: RNA-dependent RNA-polymerase

RETREG1: reticulophagy regulator 1

RLR: RIG-I-like receptor

RO: replication organelle

rpIgR: recombinant pIgR

rTFR1: recombinant TFR1

S: spike

SARS: severe acute respiratory syndrome

SC: secretory component

sgRNA: sub-genomic RNA

sIg: secretory immunoglobulin

sIgA: secretory immunoglobulin A

SIgAD: selective IgA deficiency

ss: single strand

STAT: signal transducer and activator of transcription

STING: stimulator of interferon genes

TEER: trans-epithelial electrical resistance

TFR: transferrin receptor

TGF-β: transforming growth factor-β

TLR: toll-like receptor

TMPRSS2: transmembrane protease serine 2

T_{RM}: tissue-resident memory T cell

TRS: transcription regulatory sequence

UPR: unfolded protein response

VOC: variant of concern

VOI: variant of interest

ZIP: zinc transporter

ABSTRACT

1. English

Despite the deployment of safe and effective vaccines, SARS-CoV-2 transmission continues to pose a threat to global health and remains closely monitored due to its high mutation rate. Current intramuscular vaccines alleviate COVID-19 severity but are limited in their capacity to prevent breakthrough SARS-CoV-2 infections due to inadequate mucosal immunity stimulation, which has prompted the active pursuit of mucosal vaccines. Consequently, it is essential to understand SARS-CoV-2 antagonization mechanisms, particularly involving the mucosal immune system, which are not well understood. Recent findings have highlighted a marked reduction in the expression of crucial immune receptors in COVID-19 patients, including the polymeric Ig receptor (pIgR); however, the underlying viral mechanisms are unknown. This key mucosal immunity receptor maintains homeostasis by facilitating transcytosis and secretion of dimeric IgA (dIgA) across epithelial cells into the lung mucosa to neutralize infectious pathogens. Recently, I discovered that SARS-CoV-2 accessory protein Open Reading Frame 8 (ORF8) antagonization of pIgR expression is accompanied by modulation in cellular localization of both ORF8 and pIgR. These findings have led to the hypothesis that SARS-CoV-2 ORF8 intercepts and exploits the dIgA-pIgR mucosal immune pathway to promote SARS-CoV-2 infection of lung epithelial cells. This project aimed to elucidate the molecular mechanisms of ORF8-mediated pIgR downregulation by investigating the interaction between both proteins via co-immunoprecipitation and mutagenesis. We discovered that ORF8-mediated downregulation of pIgR was highly dependent on its binding affinity with pIgR, a feature which appeared to rely on ORF8 capacity to dimerize. We further demonstrated that both dIgA and soluble ORF8 bind domain 1 of pIgR independently of one another. Furthermore, we sought to determine the effect of ORF8 from

SARS-CoV-2 and its variants in the antagonization of dIgA transport by pIgR. Within cells, we observed that ORF8 antagonized dIgA binding to pIgR, while soluble ORF8 alternatively appeared to highjack the pIgR-dIgA complex for internalization. Overall, these findings provide new insights into our understanding of SARS-CoV-2 mucosal immune evasion and inform pandemic preparedness.

2. French

Malgré le déploiement de vaccins efficaces, la transmission du SRAS-CoV-2 continue de représenter une menace pour la santé mondiale et reste étroitement surveillée en raison de son taux de mutation élevé. Les vaccins intramusculaires actuels atténuent la gravité de la COVID-19, mais leur capacité à prévenir les infections par le SRAS-CoV-2 est limitée en raison d'une stimulation inadéquate de l'immunité des muqueuses, ce qui a suscité la recherche active de vaccins pour les muqueuses. Par conséquent, il est essentiel de comprendre les mécanismes d'antagonisation du SRAS-CoV-2, en particulier ceux qui impliquent le système immunitaire des muqueuses, qui ne sont pas bien compris. Des découvertes récentes ont mis en évidence une réduction marquée de l'expression de récepteurs immunitaires cruciaux chez les patients atteints de COVID-19, notamment le récepteur d'Ig polymérique (pIgR), mais les mécanismes sous-jacents sont inconnus. Ce récepteur essentiel de l'immunité des muqueuses maintient l'homéostasie en facilitant la transcytose et la sécrétion d'IgA dimérique (dIgA) à travers les cellules épithéliales dans la muqueuse pulmonaire pour neutraliser les agents pathogènes infectieux. J'ai récemment découvert que l'antagonisation de l'expression du pIgR par la protéine accessoire SARS-CoV-2 Open Reading Frame 8 (ORF8) s'accompagne d'une modulation de la localisation cellulaire de l'ORF8 et du pIgR. Ces résultats ont conduit à l'hypothèse que SARS-CoV-2 ORF8 intercepte et exploite la voie immunitaire muqueuse dIgA-pIgR pour promouvoir l'infection des cellules épithéliales

pulmonaires par SARS-CoV-2. Ce projet vise à élucider les mécanismes moléculaires de la régulation négative du pIgR par l'ORF8 en étudiant l'interaction entre les deux protéines par mutagenèse. Nous avons découvert que la régulation négative de pIgR par ORF8 dépendait fortement de son affinité de liaison avec pIgR, une caractéristique qui semble dépendre de la capacité d'ORF8 à se dimériser. Nous avons également démontré que dIgA et l'ORF8 soluble se lient au domaine 1 de pIgR indépendamment l'un de l'autre. En outre, nous avons cherché à déterminer l'effet d'ORF8 du SARS-CoV-2 et de ses variants dans l'antagonisation du transport de dIgA par pIgR. Dans les cellules, nous avons observé que ORF8 était capable d'antagoniser la liaison de dIgA à pIgR, tandis que l'ORF8 soluble semblait alternativement d’exploiter le complexe pIgR-dIgA pour son internalisation. Dans l'ensemble, nous pensons que cette étude fera progresser nos connaissances sur l'évasion immunitaire des muqueuses par le SARS-CoV-2 et contribuera à la préparation aux pandémies futurs.

ACKNOWLEDGMENT

My experience through graduate school has been extremely enriching and gratifying. I first joined Dr. Chen Liang's lab to research the impact of SARS-CoV-2 on mucosal immunity for my honours research project during my bachelor's in microbiology and immunology. Dr. Liang's support and dedication to research fuelled my passion for virology and inspired my choice to pursue academic research.

I am extremely grateful to Dr. Liang for giving me the opportunity to purse my master's degree in his lab. His guidance and mentorship have allowed me to grow as a scientist and acquire both academic and professional skills which I will carry into my future endeavours. Our weekly individual and group meetings have nurtured my communication, critical thinking, and scientific inquiry skills. I am further thankful to Dr. Liang for giving me the opportunity to participate in international conferences, which taught me the importance of collaboration and communication within the scientific community. Furthermore, Dr. Liang gave me the rewarding opportunity to be a teaching assistant for *MIMM466: Viral Pathogenesis*, an undergraduate course which he coordinates.

Throughout my stay in the lab, I was fortunate to work amongst a team of bright, motivated, and incredible scientists. I would like to express my deepest appreciation to Ariana Arduini, Dr. Zhen Wang, and Qinghua Pan for taking the time to train me when I first joined the lab, as well as always being available to answer my questions without hesitation. These women have demonstrated a deep compassion and dedication to their work and have inspired the researcher I am today. I would also like to express my gratitude to current and past lab members of the Dr. Liang lab for their constant support, perseverance, and in contributing to positive and enjoyable

work environment. Finally, I would like to thank CIHR and FRQS for providing grants during my master's and CIHR to provide the funds for this project.

Lastly, I would like to thank my supervisory committee members Dr. Andrew Mouland and Dr. Irah King for their constructive feedback, guidance, and advice. I would like to thank all Dr. Liang members for their constant support, particularly Cesar Collazos, Qinghua Pan, Ariana Arduini, Harshita Katiyar, Yishi Lin, Megan Solomon, Myles McLean, Dr. Zhen Wang, and Jacqueline Sung.

PREFACE

The candidate has adhered to thesis requirements in accordance with the McGill University Graduate Program Studies guidelines. The Candidate has chosen to organize her thesis in the traditional format which consists of the following: comprehensive literature review, project rationale, hypothesis, and aims, followed by materials and methods, results, discussion, summary, and conclusion, and ending with a formatted bibliography and appendix.

CONTRIBUTION OF AUTHORS

Dr. Liang conceived the project and collaborated with the candidate to design the experiments and the protocols. The candidate performed the experiments, data collection, analysis, preparation of the figures, and writing of the manuscript with feedback and input from Dr. Liang. Ariana Arduini performed mutagenesis to clone the ORF8 mutants. Qinghua Pan performed experiments using primary human bronchial epithelial cells.

CHAPTER 1: INTRODUCTION TO SARS-CORONAVIRUSES AND MUCOSAL IMMUNITY

The emergence of SARS-CoV-2 in 2019 led to a global emergency which resulted in over 7 million deaths. However, the pandemic further shed light on SARS-Coronavirus biology and the importance of studying viral zoonotic transmission, evolution, and immune escape mechanisms in contribution to therapeutic development and pandemic preparedness. To this end, we have discovered the accessory protein ORF8 of SARS-CoV-2 as a pivotal antagonist of IgA-mediated mucosal immunity. In this introduction, we will discuss the emergence and adaptation of SARS-Coronaviruses, antiviral mucosal immunity, and the role of SARS-COV-2 ORF8 in immunomodulation.

1. Human SARS-Coronaviruses

1.1. Emergence of human Coronaviruses

Coronaviruses (CoVs) are enveloped positive single-stranded (ss) RNA viruses of the *Coronaviridae* family, which are classified into four genera: *Alpha-, Beta-, Gamma-,* and *Delta-coronavirus*[1]. Notably, their genomes are among the largest known viral RNAs, spanning approximately 30 kilobases (Kb)[2]. Within Open Reading Frame (ORF) 1a and ORF1b, CoVs encode 16 non-structural proteins (NSPs), while it encodes four structural proteins including Spike glycoprotein (S), Envelope (E), Membrane (M), and Nucleocapsid (N) outside of ORF1a/b[3]. However, the number of accessory proteins varies across different CoVs[3].

The ancestor amongst the four CoV genera dates back 300 million years, consistent with the divergence of mammals and birds[3–5]. This emphasizes the co-evolutionary relationship between CoVs and their hosts, such that Gamma- and Delta-coronaviruses have been demonstrated to primarily infect avians, while Alpha- and Beta-coronaviruses rather target mammals, including

humans[1,6]. The first pathogenic CoV, avian infectious bronchitis virus (IBV), was discovered in 1931 amongst diseased baby chicks[7]. However, it was not until 1966 that the first human CoV (HCoV), HCoV-229E, was identified[8,9]. The following year, HCoV-OC43 was discovered from organ culture of clinical samples, raising the awareness of the potential animal-to-human transmission and the role of coronaviruses in human health[10]. To date, five more HCoVs have been identified, notably severe acute respiratory syndrome (SARS)-CoV in 2002, HCoV-NL63 and HCoV-HKU1 in 2004, Middle East respiratory syndrome (MERS)-CoV in 2012, and SARS-CoV-2 in 2020[11–15]. Of these, HCoV-229E, HCoV-OC43, HCoV-NL63, and HCoV-HKU1 are endemic and associated with mild cold-like symptoms, while SARS-CoV, MERS-CoV, and SARS-CoV-2 are pandemic coronaviruses associated with high pathogenicity and severe respiratory diseases[9]. Understanding the evolutionary dynamics which led to the emergence of these HCoVs highlights key pathways of zoonotic transmission and host interactions, which we will discuss in further detail.

CoVs are distinguished by their large genomic diversity, in part due to the rapid adaptations of these viruses to different hosts. Most HCoVs have ancestral links to either bat CoVs (HCoV-NL63, HCoV-229E, SARS-CoV, and SARS-CoV-2) or murine CoVs (HCoV-OC43, and HCoV-HKU1) [1,16–22]. However, direct transmission of CoV from bats or rodents to humans has yet to be observed[1,16–22]. In fact, HCoVs rather emerge through various intermediate hosts ranging from wild to domesticated mammals, which contribute towards eventual viral spillover and adaptation to humans[1,9]. Interspecies spillover imposes stringent selection conditions for the virus to adapt its interactions with the hosts through acquisition of mutations via the low fidelity and error-prone RNA-dependent RNA-polymerase (RdRp)[23–25]. This sporadic selective pressure across the whole genome of all HCoVs, with emphasis on Spike glycoprotein, has been demonstrated to be highest

within intermediate hosts, followed by humans, while bats present little to no selection as the natural reservoir[26]. These findings support the hypothesis that CoVs in bats may not be optimally adapted for emergence in humans[27,28]. This entails that ecological, epidemiological, and compatibility bottleneck events in bats are insufficient for successful CoV spillover to humans, hence requiring adaptation in an intermediate host which has increased contact and shares key physiological traits with humans[27]. These selection events have contributed towards the genomic diversity and pathogenicity of HCoVs.

1.2. Emergence and epidemiology of pathogenic human SARS-Coronaviruses

In the past two decades, three main epidemic and pandemic HCoVs have emerged, SARS-CoV in 2002, MERS-CoV in 2012, and SARS-CoV-2 in 2019[29]. During the Coronavirus Disease 2019 (COVID-19) pandemic, a lot of parallels were drawn to the SARS-CoV pandemic due to structural and epidemiological similarities between these two viruses which share 79% nucleotide similarity[30,31]. Genomes of SARS-CoV and SARS-CoV-2 span around 29.7-29.8 kb, encoding 4 structural proteins (S, M, E, N), and 16 NSPs (NSP1-16) (Fig. 1A-B) [32]. Main differences reside in their accessory proteins, SARS-CoV encodes 8 accessory proteins (ORF3a, 3b, 6, 7a, 8a, 8b, and 9b), while SARS-CoV-2 encodes 9 accessory proteins (ORF3a, 3b, 6, 7a, 7b, 8, 9b, 9c, and 10) (Fig. 1A-B) [32].

1.2.1. SARS-CoV emergence

SARS-CoV emerged in Guangdong Province, China, in 2002 [33]. The initial outbreak was linked to workers in the live animal markets in Shenzhen municipality, with high seroprevalence of anti-SARS-CoV IgG titres in traders of live animals[33,34]. SARS-CoV was subsequently isolated from Himalayan palm civets, racoon dogs, and Chinese ferret-badgers[35]. Molecular analyses linked SARS-CoV to CoVs found in palm civets through shared homology of signature variation

residues (SNVs) between the Spike glycoprotein (S) of SARS-CoV and SARS-CoV-like animal CoVs[36]. However, the lack of widespread infection amongst both wild and farmed palm civets suggests its role as an amplifying host rather than a reservoir[35,37]. Surveillance of wildlife coronaviruses identified the horseshoe bat as the natural reservoir of SARS-like CoVs (SL-CoVs) which shared over 92% sequence identity to SARS-CoV isolated from humans and palm civets, with the most variable regions in S and ORF10[21,38].

1.2.2. SARS-CoV epidemiology and immunobiology

Over the course of 2 years, SARS-CoV resulted in 8096 cases globally, with a mortality rate of 10% (744 deaths)[29]. Clinical presentations were marked by persistent fever in 99-100% of patients, accompanied with non-productive cough, myalgia, and chills/rigor in up to 75% of patients[39]. Neutralizing antibodies have been shown to block viral entry, while T cell responses play an important protective role during SARS-CoV infection[40,41]. Clearance of SARS-CoV infection has been associated with robust and long-lasting cytotoxic T lymphocyte (CTL) responses, whilst antibody responses do not seem to be maintained post infection[42,43]. On the other hand, lymphopenia marked by a strong downregulation of $CD4^+$ T cells has been shown to correlate with severe disease, acute respiratory distress syndrome (ARDS), and lung damage[44,45]. However, the contribution of pro-inflammatory (IFN-γ, interleukin (IL)-6, IL-8, and monocyte chemoattractant protein 1 (MCP-1)) versus immunosuppressive (transforming growth factor-β (TGF-β) and prostaglandin 2 (PGE2)) cytokines towards ARDS in SARS-CoV remains poorly understood, with contradicting data supporting that both pro-inflammatory and immunosuppressive environments can lead to lung damage and severe disease pathology[46–49]. In mice, severe disease is rather the cause of inefficient immune activation due to the stimulation of inhibitory alveolar macrophages by SARS-CoV, which results in deficient T cell responses[50].

Unlike SARS-CoV-2, asymptomatic infection with SARS-CoV was rare, allowing aggressive quarantine measures coupled with the development of efficient surveillance strategies and rigorous contact tracing to effectively control and halt the spread of SARS-CoV in 2004, without the development of antivirals or vaccines[51]. Due to a rapid halt of the SARS-CoV epidemic, viral mechanisms underlying severe disease pathogenesis and immune evasion have been vastly understudied.

1.2.2. SARS-CoV-2 emergence

The Coronavirus Disease 2019 (COVID-19) pandemic, caused by SARS-CoV-2, has claimed over 7.03 million lives since its emergence from Wuhan, China, in 2019[52,53]. After its emergence, SARS-CoV-2 was rapidly linked to the horseshoe bat-CoV RATG13 as its most likely predecessor, sharing around 96% nucleotide identity[30,54]. This supported that bats were the likely reservoir for SARS-CoV-2 and while the intermediate host has yet to be confirmed, the most probable hypothesis is pangolins due to the high phylogenetic similarity between pangolin CoV-2020 and SARS-CoV-2[55,56]. The capacity of pangolin-CoV S to bind human angiotensin converting enzyme 2 (ACE2) receptor together with its high structural similarity to RATG13 S have further reinforced pangolins as potential intermediate hosts[57,58]. In contrast, other groups have put forward the possibility of ferrets, minks, raccoon dogs, and white tailed deer having the capacity to act as amplifying hosts due to their susceptibility to SARS-CoV-2 infection and, in some cases, their capacity to transmit the virus back to humans[59]. However, lack of a scientific consensus towards SARS-CoV-2 intermediate host merits caution.

1.2.3. SARS-CoV-2 epidemiology and immunobiology

Due to its high transmissibility, pathogenicity and mutational rate, SARS-CoV-2 continues to have a global impact since the frequent emergence of variants of concern (VOCs) and

variants of interest (VOIs) challenges the efficiency of COVID-19 vaccines[60,61]. The clinical manifestation of the disease is broad, and depends on factors such as age, sex, and overall health condition[52,62,63]. Younger patients tend to develop milder symptoms such as fever, fatigue, and dry cough, while older, immunocompromised patients who suffer from comorbidities are at a higher risk of developing more severe forms of the disease including hypoxemia, hypoxia, pneumonia, septic shock and multiple organ dysfunction or failure [52,62,63]. The wide spectrum of symptoms has been shown to be attributed to differences in the proficiency of host immune responses. In fact, studies have shown that asymptomatic patients tend to mount adequate virus-specific regulatory T cell responses, while symptomatic patients tend to have limited regulatory T cells responses[64]. Additionally, hypoxemia severity is closely correlated with lower levels of immune cells, suggesting that SARS-CoV-2 favours a cellular state of immune depletion[63,65,66]. Altogether, these studies suggest that the antagonization of the host immune system by SARS-CoV-2 is critical for viral pathogenesis, yet the specific mechanisms behind these interactions remain to be further investigated.

Despite the wide spectrum of COVID-19 disease severity, nearly all patients with severe COVID-19 present similar clinical profiles of ARDS and lung damage[67]. In COVID-19 patients, ARDS is characterized by the cytokine storm which is associated with increased inflammatory markers such as IL-1β, IL-6, IL-7, and IL-10[67,68]. The continued expression of these cytokines and other inflammatory mediators allow the persistence of both local and systemic hyperinflammation[67,68]. This response is thought to originate in part from SARS-CoV-2 cytopathic properties which promote an increased secretion of IL-1β from the pyroptosis of infected cells, a key event for the initiation and maintenance of the cytokine storm[67,68]. Additionally, the systemic immunopathology of COVID-19 involves an impaired natural killer cell response, lymphopenia,

and lymphocyte dysfunction which contribute to disease severity by increasing susceptibility of co-infections, ARDS respiratory failure, and multiple organ failure from excessive tissue damage[67,69]. Further understanding SARS-CoV-2 biology and viral mechanisms of immune evasion will deepen our understanding of SARS-CoV-2 pathogenicity, as well as inform both therapeutic development and future pandemic preparedness.

2. SARS-CoV-2 Biology

2.2. SARS-CoV-2 Life Cycle

SARS-CoV-2 life cycle starts with the engagement of the S glycoprotein with its receptor, ACE2, expressed ubiquitously across respiratory, gastrointestinal, urogenital, liver, and vascular epitheliums[70–72]. Prior to cellular entry, Spike is cleaved at the S1/S2 polybasic cleavage site by furin in infected cells during viral replication[73]. Consequently, the S glycoprotein comprises two non-covalently linked subunits, S1 which contains the receptor-binding domain (RBD) to mediate receptor binding and S2 which contains the fusion peptide (FP) to mediate viral and cellular membrane fusion[70,74]. Binding of S1 RBD to ACE2 allows the tethering of SARS-CoV-2 virions to the surface of lung epithelial cells[70]. Two major viral entry mechanisms have been defined for SARS-COV-2, the first via membrane fusion at the surface of cells which express the transmembrane protease serine 2 (TMPRSS2), the second by endocytosis for cells who do not (Fig. 1C)[75]. Membrane fusion is mediated by cleavage of S2 into S2' by TMPRSS2 at the cell surface[73]. This allows the exposure of the FP which initiates the formation of the fusion pore through which the viral genome enters into the host cell cytoplasm[73,76]. In contrast, in the absence of cell-surface TMPRSS2, binding of S glycoprotein to ACE2 triggers clathrin-mediated endocytosis of the virion[77]. Within late endosomes or lysosomes, cathepsin L cleaves at the S2' site, exposing the FP for membrane fusion and subsequent cellular entry of the viral genome[78,79].

After entry, the positive sense viral RNA is translated to produce polyprotein (pp) 1a and through a programmed ribosomal frameshift, further produce pp1ab [70,80]. These two viral polyproteins are processed by two viral proteases, NSP3 (papain-like protease; PL^{pro}) and NSP5 (main protease, M^{pro}) to release mature NSP1 to NSP16[70,80–82]. Specifically, NSP3 catalyzes the cleavage and release of NSP1-4, while NSP5 catalyzes the cleavage and release of NSP5-16[70].

Of the NSPs, NSP1 has been shown to act as a potent antagonist of host mRNA translation through its capacity to bind host 40S ribosome and mediate cleavage of host mRNA[82–84]. NSP4 has been shown to remodel ER membranes, acting in concert with NSP3 and NSP6 to form SARS-CoV-2 replication organelles (ROs), named double-membrane vesicles (DMVs)[85–87]. These ROs are crucial to viral replication which begins with the synthesis of full-length negative-sense SARS-CoV-2 RNA (Fig. 1C)[82].

SARS-CoV-2 RNA replication and transcription are carried out by the synchronous activities of NSP7 to NSP16. NSP7, NSP8 and NSP12 form SARS-CoV-2 RNA-dependent RNA polymerase holoenzyme in the RTC, with NSP12 acing as the RdRp to replicate the full-length viral RNA and NSP7/8 acting as co-factors[82,88]. Nascent viral RNA produced by the RdRp is proofread by NSP14 with its 3'-5' exonuclease activity [70,82,89]. Furthermore, NSP14 and NSP16 catalyze viral RNA capping, with NSP14 carrying the N7-MTase activity and NSP16 functioning as a methyltransferase. These functions of NSP14 and NSP16 are stimulated by NSP10[82,90]. NSP13 is an RNA helicase, it promotes viral RNA synthesis by unwinding RNA secondary structures, while NSP9 contributes to viral RNA replication by binding to single-stranded RNA [82].

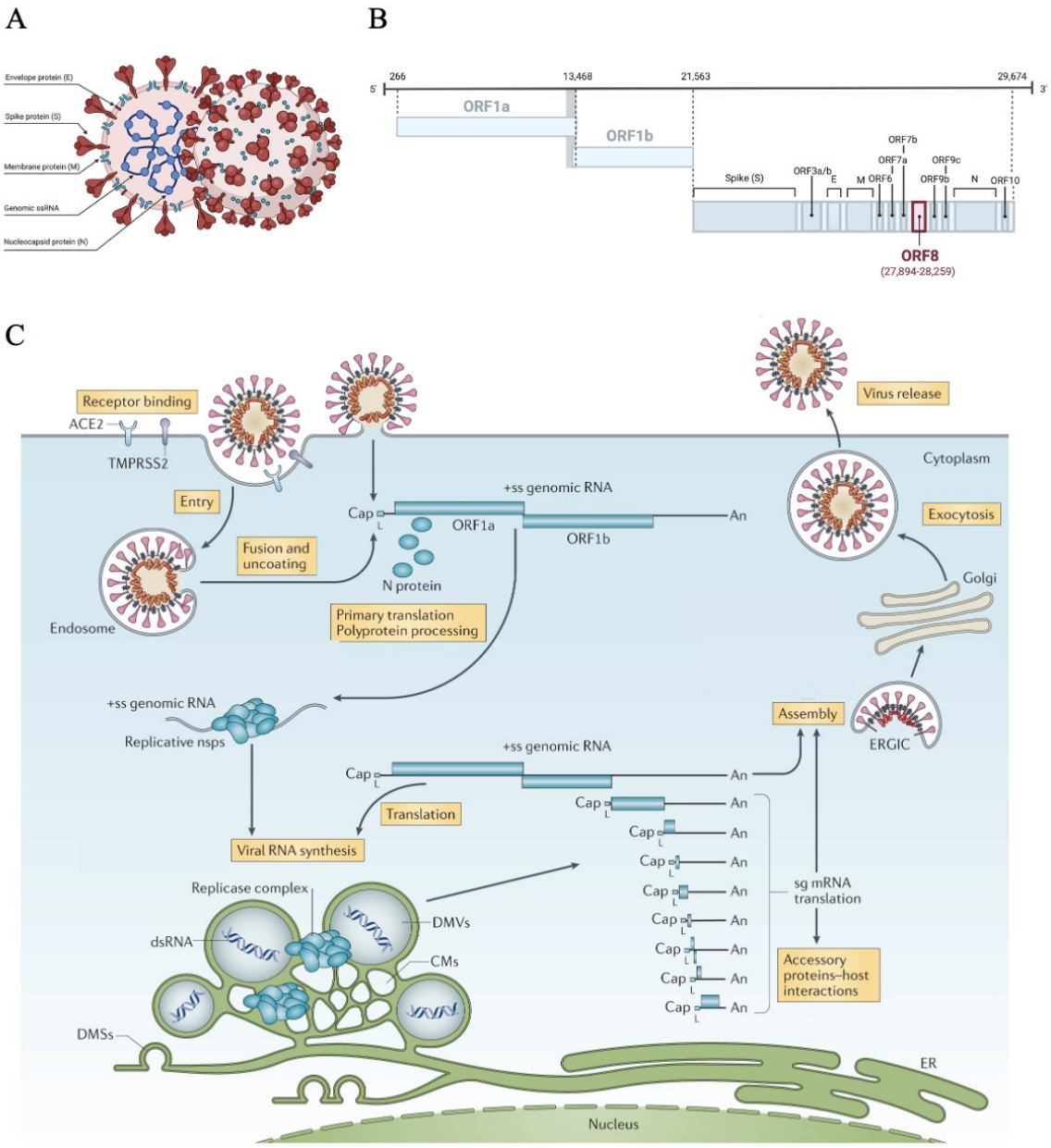

Figure 1. SARS-CoV-2 structure, genome, and life cycle. (**A**) Schematic of SARS-CoV-2 structural proteins which make up the virion. (**B**) SARS-CoV-2 genome structure with emphasis on ORF8 accessory protein. (**C**) SARS-CoV-2 life cycle is initiated by the entry of the virus either dependently or independently of TMPRSS2. Release of the viral genome will lead to replication as well as discontinuous transcription, allowing the production of NSP, structural, and ORF proteins. The virus particle will assemble at the ERGIC, after which it will exit the cell via the lysosomal pathway. Schematics adapted from (**A**) *Pizzato M, et al (2023)*[56], (**B**) *Arduini A, Laprise F, & Liang C (2023)*[124], and (**C**) *V'kovski P, et al (2021)*[70].

Finally, NSP15 is an endoribonuclease which cleaves 5'-polyuridines in viral negative-strand RNA, thus preventing activation of MDA5-mediated antiviral responses[82,91].

In addition to the synthesis of full-length viral genomic RNA, SARS-CoV-2 needs to transcribe subgenomic RNA (sgRNA) to express its structural and accessory proteins that are encoded in the 3' region of viral RNA (Fig. 1C). This is achieved by the function of transcription regulatory sequences (TRS) that are located immediately upstream of the coding sequences of structural and accessory proteins, which coordinate discontinuous transcription[70]. Since sgRNAs are monocistronic, only the ORF at the 5' end are translated[70]. Structural and accessory proteins (ORF3a, ORF3b, ORF6, ORF7a, ORF7b, ORF8, ORF9, ORF10, ORF14) are found near the 3' end of the genome and are all products of discontinuous transcription (Fig. 1B-C)[70,80]. SARS-CoV-2 accessory proteins have been characterized for their crucial roles in mediating immune evasion. ORF3a, ORF6, and ORF7a/b antagonize phosphorylation and nuclear translocation of signal transducer and activator of transcription 1 and 2 (STAT1/2) to antagonize expression of interferon stimulated genes (ISGs), while ORF3b, ORF6, and ORF8 inhibit nuclear translocation of IRF3 to prevent the expression of interferons, altogether functioning as potent IFN antagonists [92–99]. Similarly, ORF9b and ORF10 have been shown to antagonize type I IFN through both indirect and direct interactions with MAVS[92,100,101]. Finally, ORF9c interacts with the nuclear factor kappa-light-chain-enhancer of activated B cells (NF-κB), however its effect on antiviral responses have yet to be determined[102].

SARS-CoV-2 particles are formed by S, E, M and N proteins (Fig. 1A, C). After synthesis in DMVs, viral genomic RNA exits the ROs, condenses with cytosolic N and undergoes phase separation while S, E, and M are synthesized at the endoplasmic reticulum (ER)[103–105]. Although the detailed virion assembly and release mechanisms have yet to be fully elucidated, current data

support the model that viral structural proteins S, E and M travel to the ER-Golgi Intermediate Compartment (ERGIC), where M protein oligomerizes and recruits S, E and N/viral RNA to form virus particles [80,103,106–108]. After assembly, SARS-CoV-2 particles egress via the lysosomal secretory pathway, rather than employ the host conventional secretory pathway via the trans-Golgi network[109]. SARS-CoV-2 ORF3a protein has been shown to facilitate this mechanism by mediating deacidification of lysosomes and regulation of autophagy[110]. Extensive research is underway to better understand the role of viral proteins and their contribution in viral replication and these findings are expected to contribute towards therapeutic development and pandemic preparedness.

2.3. Immune responses to SARS-CoV-2

The first line of defence against SARS-CoV-2 involves the recognition of viral components by cell-surface pattern recognition receptors (PRR)[111]. E protein is sensed by Toll-like receptor 2 (TLR2), while S glycoprotein is primarily recognized by TLR4 and to a lesser extent by TLR1 and TLR6[111–113]. This triggers the activation of MyD88- and TRIF-dependent pro-inflammatory signalling pathways [111–113]. Within infected cells, viral RNA is sensed by RIG-I/MDA-5, which triggers the production of type I and III IFN, and subsequently stimulates the synthesis of ISGs[111,114]. These antiviral effector proteins work collectively to impede SARS-CoV-2 entry (such as IFITM and Ly6E) and replication (such as IFIT1, IFIT3, IFIT5)[111,115,116]. SARS-CoV-2 has been found to incite the formation of NLRP3 inflammasomes *in vitro*, likely contributing to the pro-inflammatory response in COVID-19[111,117]. Furthermore, mitochondrial damage by SARS-CoV-2 infection results in the activation of the cyclic GMP-AMP synthase (cGAS)-stimulator of interferon genes (STING) signalling pathway, further contributing to the type I IFN response against SARS-CoV-2[111,118]. However, stimulation of innate immunity by SARS-CoV-2 has

contributed to the unchecked activation of pro-inflammatory cytokines and cytokine storm observed in severe COVID-19 cases, as previously described[111].

Adaptive immunity is mounted after innate immune responses, and plays an equal and important role in controlling SARS-CoV-2 infection and COVID-19 progression [119]. Adaptive immunity begins by presentation of viral antigens by antigen-presenting cells (APCs) to T cells and B cells in lymph nodes, which leads to the activation of naïve T and B lymphocyte and their migration to the pulmonary space [119]. A potent T cell response together with neutralizing antibodies (nAb) production by B cells can clear SARS-CoV-2 infection [119]. However, patients with severe COVID-19 disease suffer from a dysfunctional T cell response and a lack in Treg cells, allowing a harmful inflammatory environment to persist[119,120]. Due to CD4+ T cell dysregulation, excessive antibody responses are observed in severe disease, which is characterized with high levels of serum IgG and IgA[119]. An unrestrained type I IFN response, excessive antibody responses, together with the lack of Treg cells, promote unchecked inflammation and progression towards the cytokine storm and ARDS[119,121]. To overcome host immune defences, SARS-CoV-2 uses its proteins to counteract pivotal immune mechanisms of both innate and adaptive immunity to promote immune evasion and viral replication.

2.4. SARS-CoV-2 immune evasion

During viral infection, innate immune responses act as first line defences to protect the host[122]. This typically includes the recruitment of antiviral effector proteins and the induction of type I IFN and type III IFN antiviral responses in consequence to cellular detection of viral proteins and viral nucleic acids[122,123]. To successfully infect the host and spread, SARS-CoV-2 has adapted to use many of its proteins to target host antiviral pathways [122]. As described above, these strategies include the antagonization of viral RNA sensing, blockade of IFN signalling, shutoff of host

translation, and obstruction of nuclear import and export[122]. Among these viral antagonization mechanisms, my interest lies within ORF8, notably due to its capacity of secretion and dimerization, which suggests potentially novel viral mechanisms of systemic immunomodulation unique to SARS-CoV-2[124]. I will therefore focus on reviewing the structure, evolutionary landscape, and reported functions of SARS-CoV-2 ORF8, as well as highlight the current knowledge gaps regarding the role of ORF8 in viral pathogenicity.

2.4.1. Accessory protein ORF8 structure and evolution

SARS-CoV-2 ORF8 is a small secreted accessory protein. It has been of notable interest due to its large interactome network and its capacity to modulate host cellular pathways to promote immune evasion and viral replication[102,124]. Positioned amongst one of the most hypervariable regions of SARS-CoV-2-like and SARS-CoV-like genomes, following the spike protein, it serves as a strong recombination hotspot[125–127]. Despite its expression in other *Sarbecoviruses*, it only shares 55.4% nucleotide similarity with full-length SARS-CoV ORF8 and 93% nucleotide similarity with bat-CoV RATG13 ORF8, the closest relative of SARS-CoV-2[128]. SARS-CoV-2 ORF8 is structurally distinct from SARS-CoV ORF8 as it forms a dimer which is held via three intramolecular disulfide bonds (C25-C90, C37-C102, C61-C83) within the monomeric subunits, and an intermolecular disulfide bond (C20-C20), four salt bridges (D199-R115, R115-E92), and hydrogen bonds (F120-K53, K53-S24, Q18-L22, R52-I121) between the monomeric subunits[124,129–133]. Furthermore, ORF8 contains an Ig-like domain within its β-sandwich, which is thought to mediate SARS-CoV-2 ORF8 immune mimicry and evasion of host immune pathways[126,129].

Being one of the most hypervariable proteins of *Sarbecoviruses*, it is no surprise that SARS-CoV-2 ORF8 has evolved throughout the course of the pandemic in parallel with the

emergence of VOCs and VOIs[124]. One of the earliest amino acid changes within *ORF8* was the L84S, which is expected to hinder dimer interactions and Ig-like domain binding[124,126,127,129,134,135]. In addition, the S24L and V62L ORF8 mutants have become common amongst emerging viral variants, while the C20 dimerization and N78 glycosylation sites have remained conserved across VOCs and VOIs[124,126,136–138]. In SARS-CoV-2 pathogenic VOCs, such as Delta (B.1.617) and Alpha (B.1.1.7), ORF8 mutations (deletion of D199-F120 and Q27stop, respectively) have been associated with a decrease in ORF8's function through loss in dimer stability or expression[133,139,140]. Interestingly, loss of function mutations in ORF8 have emerged alongside S glycoprotein mutations which increase viral infectivity, suggesting a potential compensation of pathogenicity and transmissibility for SARS-CoV-2 to persist[124,139,141,142]. However, recent findings suggest that a complete loss of ORF8 impedes ancestral and variant SARS-CoV-2 transmission, supporting the crucial role of this accessory protein for successful SARS-CoV-2 infection and transmission[143].

2.4.2. Contribution of ORF8 in SARS-CoV-2 immune evasion

Over the past three years, the role of ORF8 in host immune evasion and mimicry has been studied by several groups. Importantly, ORF8 has been detected in the plasma of COVID-19 patients, and its levels correlate with disease severity[144,145]. Further supporting a role of ORF8 in SARS-CoV-2 pathogenicity, a 382-nucleotide deletion in ORF8 emerged in a small cohort in Singapore which exhibited milder COVID-19 disease symptoms and progression[146,147]. A comparable deleterious mutation in ORF8 was observed in a lymphoma patient, indicating the possibility of a loss in selective pressure on SARS-CoV-2 pathogenic genes under immunosuppression [124,139,148]. These findings mirror the split of *ORF8* gene and its eventual loss during the SARS-CoV outbreak in 2003 [124,136,149]. The functions of SARS-CoV ORF8 and its split

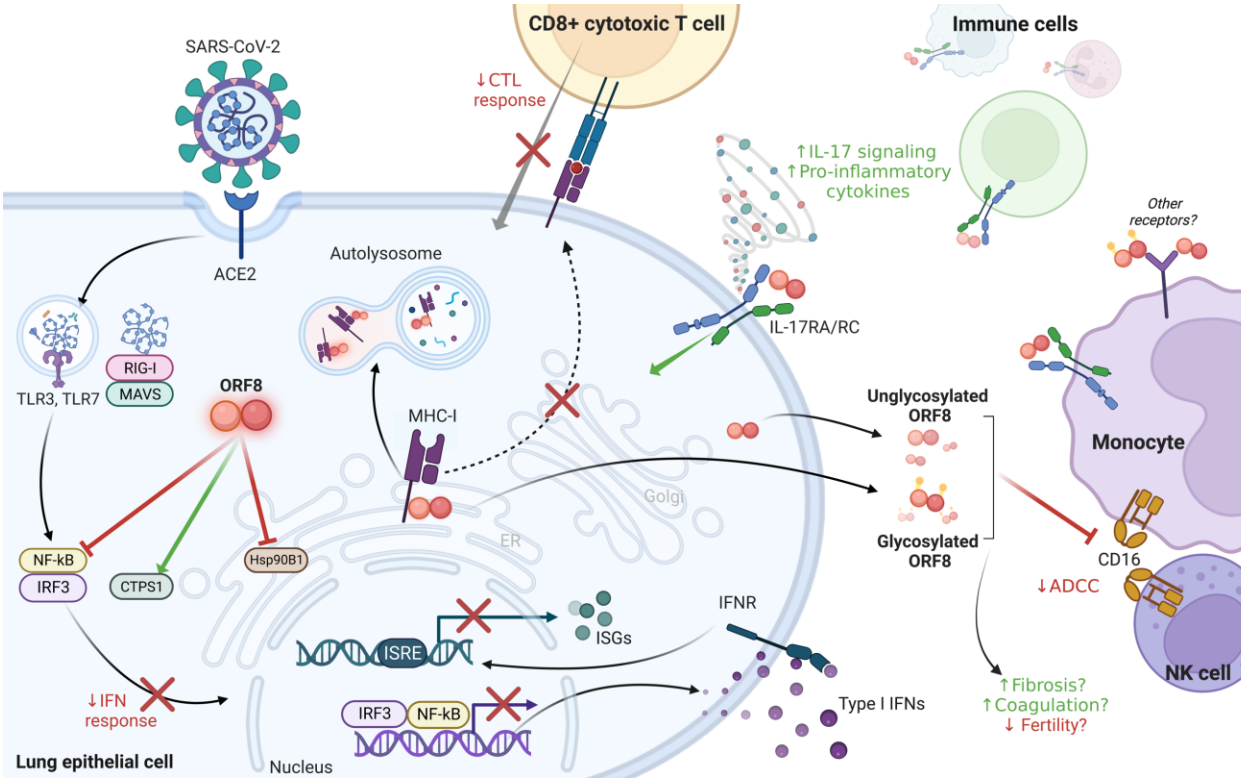

Figure 2. Immunomodulation of host cellular and systemic immunity by SARS-CoV-2 ORF8. Within cells, SARS-CoV-2 ORF8 antagonizes IFN responses via antagonization of NF-κB activation. Furthermore, it promotes the lysosomal degradation of MHC-I which leads to a deficient CTL response. As a soluble protein. ORF8 acts as an IL-17 mimic by binding IL-17RA and promoting pro-inflammatory cytokine signalling. Finally, ORF8 interacts with CD16 at the surface of monocytes and NK cells, suppressing ADCC. Figure adapted from *Arduini A, Laprise F, & Liang C* (2023)[124].

products ORF8a and ORF8b have yet to be fully understood. Nonetheless, the rapid dominance of this SARS-CoV mutant indicates a possible trade-off between host adaptability and viral pathogenicity[35,124,149,150]. Taken together, the changes of ORF8 during both the SARS-CoV epidemic and SARS-CoV-2 pandemic support an important role of ORF8 in viral immune evasion and pathogenicity.

SARS-CoV-2 ORF8 functions can be categorized into two main areas: contributing to viral replication and promoting immune evasion[124]. Regarding viral replication, ORF8 has been shown

to help remodel the ER and facilitate the formation of convoluted membranes (CM) and DMVs, through activation of adaptive unfolded protein response (UPR) sensors including inositol-requiring transmembrane kinase endoribonuclease-1a (IRE1a), protein kinase R-like endoplasmic reticulum kinase (PERK), and activating transcription factor 6 (ATF6)), inhibition of ER-phagy receptors atlasin GTPase 3 (ATL3) and reticulophagy regulator 1 (RETREG1), and sequestration of ER chaperones BiP and calnexin[151–153]. In addition, monomeric SARS-CoV-2 ORF8 contains the histone H3 regulatory site 'ARKS' sequence, and has been linked with the downregulation of histone acyltransferase KAT2A transcription, leading to modulations in histone post-translational modifications and chromatin compaction, in favour of SARS-CoV-2 replication[124,154,155]. However, this latter finding was recently challenged by other groups due to the lack of reproducibility of the data as well as ORF8 residence in the ER lumen [151,156,157]. Finally, ORF8 was reported to antagonize the packaging of S glycoprotein into progeny virions, resulting in decreased cell-surface S glycoprotein expression, thus reducing antibody-mediated detection of SARS-CoV-2 infected cells[141,142].

In addition to its role in SARS-CoV-2 replication, it is recognized that the primary function of ORF8 is to modulate and evade host immunity (Fig. 2)[124]. The known mechanisms include antagonization of IFN and CTL response, as well as its function as a virokine (Fig. 2)[124]. ORF8 appears to antagonize type I IFN response by a few different ways which are cell-type dependent. In cervical cancer cell line HeLa and kidney epithelial cell line HEK293T, ORF8 represses mRNA expression of IFN-β and NF-κB (Fig. 2)[99,158]. Furthermore, its capacity to bind and activate CTP synthase 1 (CTPS1) has been linked with antagonization of nuclear translocation of IRF3, hence inhibiting RIG-I/MDA-5-MAVS signalling (Fig. 2)[99,124,159,160]. In lung cell line A549, ORF8 counters IFN-γ response via the formation of intracellular aggregates, thus suppressing expression

of antiviral effectors such as IFN-induced transmembrane 1 (IFTIM1) and 2', 5'-oligodenylate synthetase (OAS3)[124,161]. ORF8 has also been reported by several groups to downregulate the expression of major histocompatibility complex I (MHC-I), thus antagonizing the CTL response which plays a major role in clearing infected cells (Fig. 2)[124]. MHC-I downregulation was first observed in nasopharyngeal swabs of SARS-CoV-2 patients, and it was later confirmed in SARS-CoV-2 infected cells that ORF8 targets MHC-I to lysosomes for degradation[124,162,163]. In contrast, some groups did not detect direct interaction between ORF8 and MHC-I, but have noticed that ORF8, together with ORF6, antagonizes MHC-I induction by targeting effectors of the downstream signalling pathway[124,163]. Although a clear consensus on the mechanism behind MHC-I antagonization by ORF8 has yet to be reached, these findings do support the function of ORF8 in evading CTL-mediated killing of SARS-CoV-2-infected cells (Fig. 2)[124,162].

In its secreted form, ORF8 can act systemically as an IL-17A mimic and by binding to Fc receptors (Fig. 2)[124]. ORF8 has been reported to activate pro-inflammatory signalling by binding to the IL-17A receptor (IL-17R) in murine models, peripheral blood monocytes (PBMCs) and monocytic cell lines THP1 and U937 (Fig. 2)[145,164–167]. Furthermore, this function may be specific to un-glycosylated ORF8, supporting possible pathways of unconventional secretion[166]. Additionally, ORF8 has been shown to interact with CD16a on monocytes and natural killer (NK) cells, decreasing both its cell-surface expression as well at its capacity to mediate antibody-dependent cellular cytotoxicity (ADCC) in assays using convalescent and vaccinated COVID-19 serum samples (Fig. 2)[124,168]. Altogether, these findings support both soluble and intracellular ORF8 as critical modulators of host immunity, in favour of virus replication and immune escape. In addition, the capacity of ORF8 to interact with IL-17R, MHC-I, and CD16a suggests its possible interaction with the broad host Ig domain superfamily, which remains to be further investigated[124].

3. Lung Mucosal Immunity

3.1. Mucosal immune landscape

The mucosa of our respiratory tract is constantly exposed to various chemicals and potential pathogens from inhaled air[169]. Hence, maintaining immune homeostasis in the airways is crucial in preventing respiratory diseases. As such, our body has evolved complex mechanisms ranging from innate to adaptive immune pathways to sense and neutralize infectious particles[169]. During infection, airway epithelial cells act as the first line of defence through their capacity to sense incoming pathogens via a variety of PRRs, including TLRs, RIG-I-like receptors (RLR), and Nod-like receptors (NLR)[65,169,170]. Activation of these receptors leads to induction of type I, type II, or type III IFN responses and are linked with pro-inflammatory cytokine secretion[169].

Tissue-resident immune cells have been shown to play a crucial role in bridging innate and adaptive immunity. First, dendritic cells monitor the alveolar space for invading pathogens, rapidly initiating pro-inflammatory and adaptive immune responses[171]. Circulating neutrophils can be recruited to the lungs upon either infection or sterile inflammation, where they undergo functional changes into an "activated" phenotype[169,172]. This allows the neutrophils to mediate core-inflammatory signalling pathways in the lungs by modulating their cell-surface receptors and metabolic functions to perform robust pathogen killing via granule exocytosis and apoptosis induction[169,173,174]. Another critical subset of lung-resident immune cells are alveolar macrophages (AM). Being largely present in the alveolar space, their main function is to phagocytose pathogens and promote antigen-presentation[169]. Furthermore, their interaction with regulatory T cells and alveolar epithelial cells allows for infection-dependent immunomodulation of both pro- and anti-inflammatory signalling [169,175,176]. Additionally, innate lymphoid cells (ILCs) have been shown to

be involved in inflammatory antimicrobial responses at mucosal barriers due to their capacity to release cytokines in response to direct activation by infected cells[169,177].

In recent years, there has been growing evidence for the existence of both tissue-resident memory B (BRMs) and T (T_{RM}) cells in the lungs[178,179]. Although BRMs are antigen-experienced, they are not pathogen-specific. This entails that they are recruited to tissues following a primary infection but they can respond to a broad range of microbes including *S. pneumococcus* and influenza, where they can be rapidly relocated in response to a secondary infection[179–181]. Although the exact location of BRMs is still debated, they have been found to rapidly differentiate into antibody-secreting cells (ASCs) in response to pathogens, highlighting their critical contribution to antibody-mediated adaptive mucosal immunity[179,182]. In addition to BRMs, T_{RM} cells migrate to and persist in mucosal barriers, such as the lungs, after infection and can become activated following a subsequent challenge at the site of infection[178]. Although the specific mechanism of T_{RM} cells remains under investigation, they have been shown to contribute in shaping the protective immune response against various pathogens, including a wide range of viruses[183].

An important function of the mucosal adaptive immune response is to produce antibodies which contribute to the primary defence against pathogens[184]. The secretory immunoglobulins (sIgs) population is mostly consisted of dimeric immunoglobulin A (dIgA) and pentameric immunoglobulin M (pIgM)[184]. In response to infection, IgM is the first antibody produced, then production of IgA allows for a specific and early neutralizing response during infection[185,186]. As a product of Ig class switching, IgA has two subtypes. IgA1 makes up the majority of the IgA pool on mucosal surfaces whereas IgA2 is found in the colon[187]. While plasma B cells produces monomeric IgA which goes into blood circulation, subepithelial BMRs produce IgA as a dimer (dIgA) consisting of two monomeric IgAs linked with a joining chain (JC)[188]. The following

sections provide a detailed account of the secreted (dimeric) IgA (sIgA), including its role in mucosal immunity and its mechanism of secretion across mucosal epithelia.

3.2. IgA-mediated mucosal immunity and the polymeric Ig receptor (pIgR)

sIgA is the dominant antibody class in mucosal secretions, thus it plays a pivotal role in maintaining immune homeostasis at mucosal surfaces[189,190]. In the lungs, the main functions of sIgAs are to capture and clear pathogens via coating, cross-linking, agglutination, and to promote mucociliary transport of airway secretions[191,192]. Of interest, the structure of sIgA is distinct from dIgA[192]. To be secreted, dIgA must be transported from the lung subepithelial space to the mucosal lumen. This process, termed transcytosis, is mediated by the polymeric Ig receptor (pIgR) located at the basolateral surface of epithelial cells[193].

Human pIgR is a type I transmembrane protein which contains six extracellular domains, a transmembrane domain, and an intracellular domain[193]. The extracellular domain contains five Ig-like domains in tandem which mediate binding with dIgA and pIgM, while the sixth domain contains a proteolytic cleavage site that, upon cleavage by proteases, allows the release of sIgA after transcytosis[193,194]. When un-ligated, the ectodomain of pIgR, known as the secretory component (SC), adopts a closed conformation with primary interactions between domain (D) 1 and D5, D1 and D4, and finally D1 and D2[192,195]. In its closed conformation, D1-D4-D5 forms a large interface with their respective complementarity determining regions (CDRs) facing outwards, suggesting that JC binding initially occurs with D1 and D5[192,195]. This initial interaction promotes a conformational change within pIgR, separating D1 and D5 to allow D1 CDR1 to mediate the main interaction between SC and the JC of dIgA, while D3-D4-D5 become extended, leaving D4-D5 to have a minor interaction with both the Fc and JC of dIgA[192,195].

Following binding of dIgA to pIgR, the pIgR-IgA (pIgA) complex gets internalized via clathrin-mediated endocytosis at the basolateral pole, then the complex traffics via the conventional endosomal pathway[193,196]. Once arriving at the apical pole of epithelial cells, D6 undergoes endo-proteolytic cleavage, allowing the release and diffusion of dIgA bound to SC of pIgR (sIgA) into the mucosal lumen[193]. In addition, constitutive transcytosis of un-ligated pIgR allows the release of SC into the mucosa. SC participates in immune exclusion by preventing access of pathogens to the epithelium in unison with sIgA[193,197–199]. In cells, pIgR is upregulated by host cytokines such as IL-1, IL-17, IFN-γ, TNF-α as a result of activation of NF-κB and IRF1 by microbial products[193,200]. Owing to its crucial role in mucosal immunity, dysregulation of IgA transcytosis and pIgR expression has been implicated in various pulmonary diseases.

3.3. IgA and pIgR in diseases

Early studies investigating pIgR-knockout mice demonstrated that the disruption of IgA transcytosis and secretion led to higher serum IgA levels and subsequent gut microbiota changes which promoted inflammatory bowel disease (IBD), consistent with clinical data[193,201,202]. Similarly, the knockout of pIgR from mice hepatocytes has been shown to aggravate autoimmune hepatitis due to mucosal barrier dysfunctions caused by a decrease in sIgA[203]. In contrast, pIgR levels are clinically associated with cardio-renal syndrome, such that an increase in pIgR correlates with kidney disease and an increase in urinary sIgA and SC[194,204].

In the lungs, a variety of pulmonary diseases have been linked with altered levels of sIgA and changes in pIgR expression. One such example is chronic obstructive pulmonary disease (COPD), a degenerative lung disease where disease severity correlates with deficiencies in sIgA, resulting in dysfunctional local immune response[205–207]. COPD is characterized by excessive pulmonary inflammation which decreases the expression of pIgR in bronchial epithelial cells due

to increased epithelial TGF-β expression[207–209]. It has been reported that pIgR is similarly downregulated by IL-4 and IL-13 in asthma, leading to an impaired sIgA response[210]. Furthermore, asthma is increasingly prevalent in patients suffering from selective IgA deficiency (SIgAD), an immunodeficiency disease characterized by low to undetectable IgA levels, further emphasizing the role of sIgA in preventing inflammatory pulmonary diseases[207,211,212]. In the past few years, the role of sIgA in pulmonary diseases has gained more attention due to its link with SARS-CoV-2 and COVID-19 disease severity[207].

3.4. IgA-mediated mucosal immunity during SARS-CoV-2 infection

The systemic antibody response to SARS-CoV-2 has been extensively investigated, notably to assess vaccine efficacy and understand COVID-19 progression. In patients infected with SARS-CoV-2, potent neutralizing antibody (nAb) responses against N and S glycoprotein are observed in serum IgA, IgM, and IgG [213]. Although total serum nAb responses can be maintained up to 6-8 months-post infection, systemic neutralizing IgA has been shown to be rapidly lost as early as 2 months post-infection [214,215]. Similarly, intramuscular vaccination has been successful in generating potent serum neutralizing IgG responses[216]. Serum and secretory IgA responses are elicited by vaccination of pre-immunized patients, but these are not maintained and do not respond to subsequent immunization with boosters[216,217]. This may be of concern because sIgA is known to play a pivotal role in controlling early infection as it dominates the early nAb response[218]. Furthermore, low serum nAb responses in mild COVID-19 patients are inversely correlated with sIgA, where low serum nAb titres and high neutralizing sIgA titres in mucosal secretions correlate with positive disease prognosis[216,219]. This suggests that transient nAb presence in serum observed in mild to moderate COVID-19 disease may be linked to an increased nAb secretion in the mucosa of the respiratory tract. Concordantly, patients with sIgAD tend to suffer from more severe and

longer-lasting COVID-19 disease[220]. The ongoing development of mucosal vaccines aims to stimulate both mucosal and systemic protective immunity, which cannot be achieved with intramuscular vaccine regimens[221]. To better achieve this goal, it is critical to understand the mucosal immune response to SARS-CoV-2 infection and the viral antagonization mechanisms.

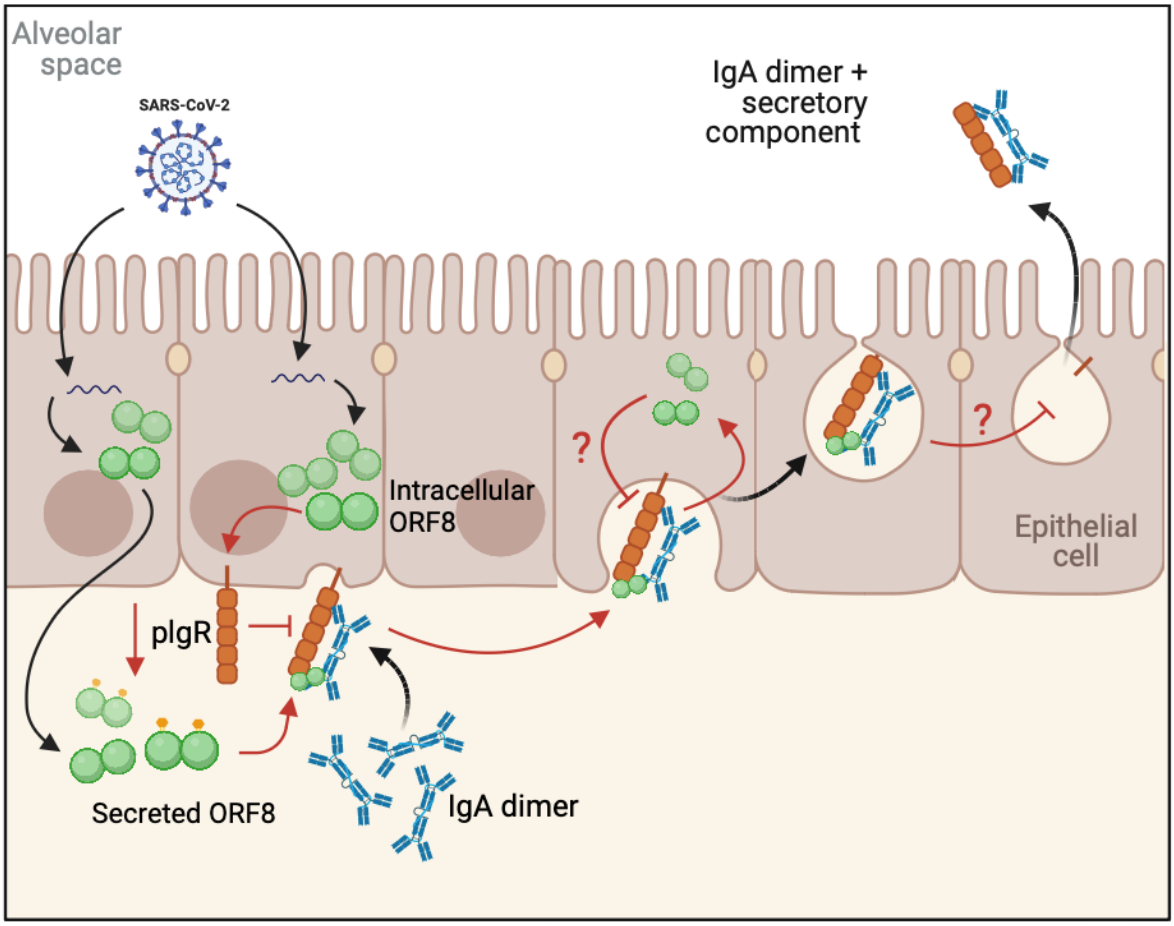

Figure 3. SARS-CoV-2 ORF8 modulates pIgR expression and highjacks the dIgA-pIgR pathway for internalization. Graphical abstract demonstrating the main pathways of pIgR modulation by SARS-COV-2 ORF8. Within cells, ORF8 downregulates pIgR expression, leading to decreased cell-surface dIgA binding. In contrast, soluble ORF8 interacts and highjacks the dIgA-pIgR complex to enter cells. Whether immunomodulation of pIgR by ORF8 leads to an antagonized sIgA response remains to be investigated. Made in biorender.com.

4. Research Objectives and Aims

Given that SARS-CoV-2 infects the respiratory tracts and lungs, mucosal immunity is expected to suppress infection establishment through the transcytosis and secretion of dIgA across lung epithelial cells by pIgR[222]. Loss of this biological function may render the airways more susceptible to SARS-CoV-2 infection, since low pIgR levels have been shown to correlate with COVID-19 disease severity[223,224]. Notably, my preliminary experimental data revealed that SARS-CoV-2 accessory protein ORF8 downregulates pIgR (Fig. 4). This observation, together with the secretory nature of ORF8 and its reported role in modulating host immunity, prompts us to hypothesize that **ORF8 may antagonize dIgA-mediated mucosal immunity by downregulating pIgR and modulating dIgA-pIgR transcytosis, thus facilitating SARS-CoV-2 infection of lung epithelial cells.** Hence, I propose a model where SARS-CoV-2 infection of lung epithelial cells leads to ORF8 expression, which can act intracellularly to decrease pIgR levels and extracellularly to intercept dIgA-pIgR transcytosis (Fig. 3). To test this hypothesis, the following aims were investigated: **(1)** elucidate the molecular mechanism of pIgR downregulation by ORF8 through characterizing their interaction, and **(2)** determining the effect of ORF8 from SARS-CoV-2 and its VOCs on pIgR-mediated dIgA binding and internalization.

4.1. Aim 1: elucidate the molecular mechanism of pIgR downregulation by ORF8 through characterizing their interaction

I have tested a large panel of ORF8 mutants as well as ORF8 from other coronaviruses to determine the key motifs and features of ORF8 underlying its function towards pIgR downregulation, and whether this activity is conserved in SARS-CoV-2 VOCs and in ORF8 of other coronaviruses. I have also designed and performed sequential domain deletions of pIgR ectodomain to determine which domain serves to bind ORF8. Finally, I characterized the

interaction of these ORF8 mutants with pIgR by co-immunoprecipitation and confocal imaging and was able to establish the correlation between ORF8-pIgR interaction and ORF8-mediated downregulation of pIgR. Altogether, I was able to identify ORF8 mutations which modulate its activity against pIgR expression and determine the key domains within pIgR which are responsible for binding to ORF8.

4.2. Aim 2: determine the effect of ORF8 from SARS-CoV-2 and VOCs on pIgR-mediated dIgA binding and internalization

The binding and internalization of the dIgA-pIgR complex initiate the process of transcytosis, rendering these steps indispensable for the secretion of dIgA in the lumen[193]. To study the early transcytosis steps, I used flow cytometry and confocal microscopy to measure the effect of both intracellular and secreted ORF8 on dIgA binding to pIgR and internalization of the dIgA-pIgR complex.

CHAPTER 2: MATERIALS AND METHODS

1. Cell culture

HEK293T kidney epithelial cells (ATCC, cat. CRL-1573) were grown in Dulbecco's Modified Eagle Medium (DMEM; ThermoFisher Scientific, Grand Island, NY) supplemented with 10% fetal bovine serum (FBS; ThermoFisher Scientific), and 1% penicillin and streptomycin (PS; ThermoFisher Scientific). Calu-3 lung epithelial cells (ATCC, cat. HTB-55) were grown in Eagle's Minimum Essential Medium (EMEM; Wisent Bioproducts, St-Jean-Baptiste, Qc) supplemented with 20% FBS and 1% PS. Caco-2 colon epithelial cells (ATCC, HTB-37) were grown in EMEM supplemented with 10% FBS and 1% PS. Cells were passaged every second day or at 90% confluence using 0.05% Trypsin-EDTA (ThermoFisher Scientific, cat. 25300-054).

2. Plasmids and reagents

2.1. Plasmids

The lentiviral mammalian expression vector pLVX-E1alpha-IRES-Puro encoding WT SARS-CoV-2 ORF8 fused to the Strep-II tag (Addgene, cat. 141390) was used as ORF8 expression plasmid. In addition, we used a plasmid containing pIgR fused to the FLAG tag (GenScript, cat. OHu19522D) and the empty vector pQCXIP (Addgene, cat. 631516). We also used transferrin receptor 1 (TFR1) expression plasmid (provided by Dr. Kostas Pantopoulos, McGill University, Qc), as well as M-Cherry-TFR-20 expressing TFR1 fused to the mCherry tag (Addgene, cat.55144). Finally, we used pLVX-EF1alpha-eGFP-2xStrep-IRES-Puro encoding eGFP (Addgene, cat. 141395), pMD2.G (expressing VSV-G; Addgene, cat. 12260), and psPAX2 (lentivirus packaging plasmid; Addgene, cat. 12260).

2.2. Antibodies

Antibodies used in this study were the following: rat monoclonal anti-Strep-II (Abcam, Boston, MA; cat. Ab252885), rabbit SARS-CoV-2 Spike Protein (S1) monoclonal antibody (Cell Signaling Technology, Danvers, MA; cat. 99423S), mouse anti-FLAG (Sigma-Aldrich, Burlington, MA; cat. F1804), mouse anti-tubulin (Santa Cruz Biotechnology, Dallas, TX; cat. SC-23948), rabbit anti-FLAG (Sigma-Aldrich; cat. 7425), rabbit pIgR polyclonal antibody (Thermofisher; cat. PA5-35340), mouse monoclonal anti-hpIgR (R&D Systems, Minneapolis, MA; cat. MAB27172), mouse Transferrin receptor monoclonal antibody (H68.4) (Invitrogen, Carlsbad, CA; cat.13-6800), Zombie Violet (BioLegend, San Diego, CA; cat. 77477), sheep anti-hGM130/GOLGA2 (R&D Systems; cat. AF8199), goat anti-rat IgG-HRP (Invitrogen; cat. 31470), goat anti-mouse IgG-HRP (SeraCare, Milford, MA; cat. 5450-0011), goat anti-rabbit IgG-HRP (SeraCare; cat. 5450-0010), Alexa Fluor 488 donkey anti-rat IgG (H+L) (Invitrogen; cat. A21208), Alexa Fluor 488 goat anti-rat IgG (H+L) (Invitrogen; cat. A11006), Alexa Fluor 594 donkey anti-sheep IgG (H+L) (Invitrogen; cat. A11016), Alexa Fluor 568 goat anti-rabbit IgG (H+L) (Invitrogen; cat. A11011), Alexa Fluor 647 donkey anti-rabbit IgG (H+L) (Invitrogen; cat. A31573), Alexa Fluor 647 donkey anti-mouse IgG (H+L) (Invitrogen; cat. A31571), DAPI (Abcam, cat. Ab228561), Mouse Strep-II-FITC (GenScript; cat. A01736-100), and anti-FLAG-647 (Rockland Scientific, Victoria, BC; cat. 200-343-383).

2.3. Protein and antibody labelling

In this study, we conjugated recombinant SARS-CoV-2 ORF8-His (Invitrogen; cat. RP87666), IgA from human colostrum (Sigma-Aldrich; cat. I2636), and human transferrin (Sigma-Aldrich; cat. T3309) using Alexa Fluor 488 Microscale Protein Labeling Kit (Invitrogen; cat. A30006) and Alexa Fluor 647 Protein Labeling Kit (Invitrogen; A20173). 1 mg/ml – 1.5 mg/ml proteins were

conjugated by incubating with 10% 1M sodium bicarbonate (provided in kit) and incubating with reactive dye for 15 minutes (microscale Alexa Fluor 488 labeling kit) or 1 hour (Alexa Fluor 647 protein labeling kit). Conjugated proteins were purified using spin filters filled with the provided suspended gel resin and spun at 16,000 x g for 1 minute. IgA and transferrin conjugated with the microscale Alexa Fluor 488 labeling kit were not filtered due to a 50 kDa size restriction on the spin filter. Conjugated proteins were stored at 4°C for use.

3. Mutagenesis and plasmid DNA purification

3.1. pIgR domain deletions

To generate pIgR domain deletions, a set of 6 primers was designed to amplify extracellular domain-deleted pIgR sequences (Table 1). Amplification of the pIgR mutants was performed with polymerase chain reaction (PCR) using Accuprime Pfx DNA polymerase (Invitrogen; cat. 12344024). The pIgR vector (pIgR-FLAG) was digested to remove the targeted region of pIgR using restriction enzymes HindIII (New England Biolabs, Burnaby, BC; cat. R0104) and AfeI (New England Biolabs; cat. R0652). To isolate the vector and the amplified mutants, gel electrophoresis was performed, and the DNA was extracted using E.Z.N.A. Gel Extraction Kit (Omega Bio-Tek, Norcross, GA). The extracted vector and amplified PCR products were ligated using T4 ligase (New England Biolabs; cat. M0202).

3.2. Mutant, variant, and animal coronavirus ORF8

The lentiviral mammalian expression vector pLVX-E1alpha-IRES-Puro encoding SARS-CoV-2 ORF8-Strep-II was used as backbone to derive mutant, variant, and animal coronavirus ORF8 by Ariana Arduini (Chen Liang lab). As a control, we also generated an empty vector plasmid from pLVX-E1alpha-IRES-Puro by excising ORF8-Strep-II using EcoRI (New England

Biolabs; cat. R0101) and BamHI (New England Biolabs; cat. R0136). To isolate the empty vector, we performed gel electrophoresis and DNA extraction as described above. DNA Polymerase I, Large (Klenow) Fragment (New England Biolabs; cat. M0210) was used to fill the gap in the empty vector before ligation with T4 ligase.

3.3. Plasmid DNA purification

To expand plasmid stocks, subcloning efficiency DH5α chemically competent cells (Invitrogen; cat. 18265-017) were transformed with 100 ng plasmid DNA (pDNA) and streaked onto LB plates containing either ampicillin (Fresenius Kabi, Bad Homburg, DE; cat. 02227002) or kanamycin (Sigma-Aldrich; cat. K1377-5G), depending on resistance gene expressed by pDNA. Plates were incubated at 37ºC overnight and single colonies were picked and amplified in 3 ml to 50 ml sterile liquid LB containing appropriate antibiotics, as described previously. Tubes or flasks were incubated overnight at 37ºC with shaking at 200 rotations per minute (RPMs). Liquid LB with confluent bacterial growth was used to isolate the expanded plasmid DNA using E.Z.N.A Plasmid DNA Mini/Midi Kit (Omega Bio-Tek). Plasmid sequences were validated using MCLAB sequencing services, and plasmids with verified sequences were stored at -20ºC.

Primer Name	**Primer sequence (5'->3')**	**Tm (ºC)**
Deletion Domain 1 (ΔD1)	cagctaagcttggtaccatgtttgatgtcagcctggaggt	56
Deletion Domain 1-2 (ΔD1-2)	cagcttaagcttggtaccatgctaaagcccgagcccgagct	64
Deletion Domain 1-3 (ΔD1-3)	caattaagcttatgccccgcagccccactgtggt	70
Deletion Domain 1-4 (ΔD1-4)	cagctaagcttggtaccatggaaggagaaccaaacctcaa	53
Deletion Domain 1-5 (ΔD1-5)	cagctaagcttggtaccatggttgaagagaggaaggcagc	57
Primer Name	**Primer sequence (3'->5')**	**Tm (ºC)**
Reverse primer (D5-1)	agaccagcgctctggagcttccaccttgtt	70

Table 1. List of primers for mutagenesis of pIgR extracellular domain deletions. This list includes primers for the deletion of domain 1, deletion of domain 1 through 2, deletion of domain 1 through 3, deletion of domain through 1 through 4, deletion of domain 1 through 5, and a reverse primer flagging the entire extracellular domain of pIgR.

4. Calu-3-ORF8 stable cell line generation

4.1. Generating lentiviral particles expressing ORF8

To generate lentiviral particles expressing ORF8 and its mutants, $4.0x10^6$ HEK293T cells were co-transfected with 500 ng VSV-G, 3000 ng psPAX2, and 4000 ng ORF8 plasmids expressing ORF8 and its mutants, 4000 ng eGFP control plasmid, as well as 2500 ng of the previously described empty lentivirus vector in 10-cm dishes using a 1 ug:3 ul DNA to PEI ratio. Supernatants were collected after 48-hour transfection and filtered through 0.2 μm polyethersulfone sterile membranes (VWR international, Radnor, PA; cat. 514-0073). Sterile conditioned media was aliquoted into ready-for-use 250 μl fractions in 1.5 ml Eppendorf tubes and stored at -80ºC.

4.2 Generating Calu-3 cell-lines which stably express ORF8 and its mutants

Reverse transduction of Calu-3 cells was performed to generate stable cell lines by preparing a 1:2 dilution of lentiviral vector aliquots in EMEM containing 10% FBS and 8 μg/ml hexadimethrine bromide (polybrene; Sigma-Aldrich; cat. H9268-10G). The 1:2 EMEM/lentiviral vector mix was added in a 1:1 volume ratio with $0.5x10^6$ Calu-3 cells in 6-well plates and spinoculated in the centrifuge for 45 minutes at 1800 RPMs. Cells were incubated for 48-72 hours, until sufficient cell growth, and transduced cells were selected and maintained using EMEM containing 10% FBS, 1% PS, and 4 μg/ml puromycin dihydrochloride (Sigma-Aldrich; P8833-25MG). Cells were monitored and media was changed every two days until all control cells were killed, after which confluent cells were expanded to 10-cm dishes and maintained for use in experiments.

4.3. Preparing cell stocks

To prepare stocks of the Calu-3 stable cell lines, $2.0x10^6$ cells were collected in 2 ml Eppendorf tubes and centrifuged for 5 minutes at 1500 RPMs. Cell pellets were decanted and re-

suspended in cold solution constituted of 90% FBS and 10% methyl sulfoxide (DMSO; Sigma-Aldrich; cat. W357520). The cells were placed in an insulated freezing container and stored at -80ºC overnight, after which they were transferred to -135ºC for long-term storage.

5. Western blot analysis

5.1. Western blot of HEK293T cell lysates and conditioned media

$0.6x10^6$ HEK293T cells/well were seeded in a 6-well plate and incubated overnight at 37ºC and 5% CO_2. Cells were co-transfected for 6 hours with 0.1 to 0.5 µg of either SARS-CoV-2 ORF8 or its mutants, variant, and animal CoV ORF8 expression plasmid, 0.5 µg of pIgR, and 0.25 to 0.5 µg of pQCXIP empty vector plasmid using polyethyleneimine (PEI; Sigma-Aldrich; cat. 913375) in a 1 ug:3 ul DNA to PEI ratio. After incubation at 37ºC for 48 hours, cells and conditioned media were harvested using 50 mM Tris HCl, 150 mM NaCl, 1% NP-40, 0.5% Sodium Deoxycholate (SDS), 1 mM EDTA, 0.1% SDS, and 0.01% sodium azide (RIPA) supplemented with complete Mini EDTA-free protease inhibitor cocktail (protease inhibitor; Sigma-Aldrich; cat. 118361700) and stored at -80ºC. 15 µg of lysates and 30 µl of conditioned media were further diluted in 4X Laemmli buffer and treated at 95ºC for 10 minutes. Protein samples were analyzed in a 12% sodium dodecyl-sulfate (SDS; Bioshop, Burlington, ON; cat. SDS001.1) polyacrylamide gel by electrophoresis and transferred on a polyvinylidene difluoride (PVDF) membrane (Sigma-Aldrich; cat. 03010040001).

5.2. Western blot of Calu-3 cell lysates and conditioned media

$3.0x10^6$ Calu-3 and Calu-3 stable cell lines were seeded in a 10-cm dish and incubated at 37ºC and 5% CO_2 until 90% confluence was reached. Cells and conditioned media were harvested on ice using RIPA buffer supplemented with protease inhibitor and stored at -80ºC. 30 µg of lysates and 30 µl of conditioned media were further diluted in 4X Laemmli buffer and boiled at 95ºC for

10 minutes. Protein samples were analyzed in a 12% SDS polyacrylamide gel by electrophoresis and transferred on PVDF membrane.

5.3. Western blot of Caco-2 cell lysates

For electroporation, $1.0x10^6$ Caco-2 cells were centrifuged for 10 minutes at 1200 RPMs and mixed with 5 µg SARS-CoV-2 ORF8, empty vector, or GFP control plasmid, 82 µl cell line nucleofector solution T, 18 µl cell line supplement 1 (Lonza, Walkersville, MD; cat. VCA-1002) and transferred to cuvettes to be electrophoresed using Lonza Amaxa Nucleofactor II Device on Caco-2 program. Following this, cells were incubated at 37ºC and 5% CO_2 in 6-well plates. For transfection, $0.8x10^6$ Caco-2 cells/wells were seeded in a 6-well plate and incubated overnight at 37ºC and 5% CO_2. Cells were co-transfected for 6 hours with 5 µg SARS-CoV-2 ORF8, empty vector, or GFP control plasmid using a ratio of 1:2 DNA to p3000 (Invitrogen; cat. 100022058) and a ratio of 1:3 DNA to lipofectamine (Invitrogen; cat. 100022052). Cells and conditioned media were harvested on ice using RIPA buffer and stored at -80ºC. 30 µg of lysates and 30 µl of conditioned media were further diluted in 4X Laemmli buffer and boiled at 95ºC for 10 minutes. Protein samples were analyzed in a 12% SDS polyacrylamide gel by electrophoresis and transferred on PVDF membrane.

5.4. Western blotting

Membranes were blocked in 5% milk diluted in Dulbecco's phosphate-buffered saline (DPBS) containing 0.1% Tween 20 (PBST; Bioshop; cat. TWN508) at room temperature for 1 hour. The membranes were incubated with primary antibodies rat anti-Strep-II (1:5,000), mouse anti-FLAG (1:5000), mouse anti-tubulin (1:5,000), or rabbit anti-SARS-CoV-2 Spike protein (1:1000) diluted in 2% bovine serum albumin (BSA; BioShop; cat. 9048-46-8) for 2 hours at room temperature, rabbit anti-pIgR (1:1,000) in 2% BSA overnight at 4ºC. After washing with PBST, membranes

were incubated with either HRP-conjugated goat anti-rat (1:10,000), HRP-conjugated goat anti-rabbit (1:5,000), or HRP-conjugated goat anti-mouse (1:5,000) for 1 hour at room temperature, and then exposed to enhanced chemiluminescence (ECL) reagents (PerkinElmer, Waltham, MA; cat. NEL104001EA). Membranes were imaged by exposure to autoradiography films and quantified via ImageJ.

6. Co-immunoprecipitation of HEK293T cell lysates

$4.0x10^6$ HEK293T cells were seeded in 10-cm dishes and incubated overnight at 37ºC and 5% CO_2. Cells were co-transfected for 6 hours with 2.5 μg of either SARS-CoV-2, SARS-CoV, Bat-CoV YNLF_31C, or C20A ORF8 expression plasmids, 5.0 μg of pIgR expression plasmid and 2.5 μg of pQCXIP empty vector plasmid using a 1 ug:3 ul DNA to PEI ratio. After a 48-hour incubation, cells were lysed with RIPA buffer and stored at -80ºC. 1 mg of the whole cell lysates was incubated with 20 μl MagStrep "type 3" XT beads (Strep-II tag beads; IBA-Lifesciences, Gottingen, DE; cat. 2-4090-002) overnight at 4ºC or with 15 μl anti-FLAG M2 Affinity Gel (FLAG tag beads; Sigma-Aldrich; cat. A2220) for 2 hours at 4ºC. Samples incubated with the Strep-II tag beads were placed in a magnetic Eppendorf tray and the supernatant was removed and conserved (flowthrough), while samples incubated with FLAG beads were centrifuged at 6000 RPMs for 5 minutes and the supernatants were removed and conserved (flowthrough). Samples were washed and then precipitated under denaturing condition by adding 30 μl of 1X Laemmli buffer and eluting the samples at 95ºC for 2 minutes. Supernatants were recovered and analyzed together with the whole cell lysates (WCL) via Western blot, as described above.

7. Flow cytometry

7.1. Flow cytometry analysis with HEK293T cells

$0.25x10^6$ HEK293T cells/well were seeded in a 12-well plate and incubated overnight at 37ºC and 5% CO_2. Cells were co-transfected for 6 hours with 0.125 μg of SARS-CoV-2 ORF8, its mutants and variants, or animal CoV ORF8 expression plasmid, 0.25 μg of pIgR and pIgR mutants, and 0.125 μg to 0.25 μg of pQCXIP empty vector plasmid using a 1 ug:3 ul DNA to PEI ratio. After incubation at 37ºC for 48 hours, cells were lifted with 0.1 mM EDTA for 5 minutes at 37ºC. Cells were washed three times in DBPS and stained with cell viability stain Zombie Violet (1:2000) diluted in DBPS for 30 minutes at room temperature. Cells were washed three times with 3% BSA in DPBS and cell surface pIgR was stained with mouse monoclonal anti-hpIgR (1:100) diluted in 3% BSA for 30 minutes at 4ºC. After washing with 3% BSA, cells were stained with Alexa Fluor 647 donkey anti-mouse (3 μg/ml) diluted in 3% BSA for 30 minutes at 4ºC. Cells were washed with 3% BSA in DBPS and fixed with 4% paraformaldehyde (PFA; Bioshop; cat. PAR070.250) in DPBS for 15 minutes at room temperature. Cells were washed three times with 1X BD permeabilizing wash buffer (BD Biosciences, Frankly Lakes, NJ; cat. 51-2091KZ) in distilled H_2O (dH_2O). Cells were stained with either mouse Strep-II-FITC (1:1000) or anti-FLAG-647 (1:1000) for 1 hour at 4ºC. Cells were washed three times with 1X permeabilizing buffer and resuspended in 200 μl mixture of 3% BSA and 1% PFA in DBPS which were stored at 4ºC until analysis on BD LSRFortessa and BD FACSCanto Flow Cytometers.

7.2. Flow cytometry analysis with Calu-3 cells

$0.3x10^6$ Calu-3 cells and ORF8-expressing Calu-3 stable cell lines were seeded per wells of a 12-well plate and incubated for 72 hours at 37ºC and 5% CO_2. Cells were lifted with 0.5 mM EDTA for 15 minutes at 37ºC. Calu-3 ORF8 stable cells lines were stained with anti-Strep-II-488

as described above. Viability staining was not performed for Calu-3 cells. Cells were analyzed using BD LSRFortessa and BD FACSCanto Flow Cytometers

7.3. Flow cytometry analysis with Caco-2 cells

$0.3x10^6$ Caco-2 cells/well were seeded in a 12-well plate and incubated for 72 hours at 37ºC and 5% CO_2. Cells were lifted with 0.5 mM EDTA for 5 minutes at 37ºC. Viability staining was not performed for Caco-2 cells. Cells were analyzed using on BD LSRFortessa and BD FACSCanto Flow Cytometers.

8. Confocal microscopy

8.1. Confocal microscopy analysis of HEK293T cells

$0.1x10^6$ HEK293T cells/well were seeded in a 12-well plate on glass cover slides pre-treated with 10 μg/ml poly-D-lysine hydrobromide (Sigma-Aldrich; cat. P6407-5MG) for 1 hour at 37ºC. Cells were incubated overnight at 37ºC and 5% CO_2 and co-transfected for 6 hours with 0.125 μg of SARS-CoV-2 ORF8, its mutants or variants, and animal CoV ORF8 expression plasmid, 0.25 μg of pIgR, and 0.125 μg to 0.25 μg of pQCXIP empty vector plasmid using a 1 ug:3 ul DNA to PEI ratio. After a 48-hour incubation, cells were fixed with 1 ml 4% PFA for 10 minutes at room temperature. Cells were washed three times with DPBS and permeabilized with 0.1% Triton X-100 in DPBS for 10 minutes at room temperature. After washing, cells were blocked with 3% BSA for 1 hour at room temperature. Cells were then stained with primary antibodies rabbit anti-FLAG (1:200), rabbit pIgR polyclonal antibody (1:50), rat monoclonal anti-Strep-II (1:200), and sheep anti-hGM130/GOLGA2 (1:100) diluted in 0.2% Triton X-100 and 1% BSA in DPBS for 2 hours at room temperature or overnight at 4ºC. After washing cells were stained with secondary antibodies Alexa Fluor 488 donkey anti-rat (1:500), Alexa Fluor 488 goat anti-rat (1:500), Alexa Fluor 594 donkey anti-sheep (1:500), Alexa Fluor 568 goat anti-rabbit (1:500), and

Alexa Fluor 647 donkey anti-rabbit (1:500) diluted in 0.2% Triton X-100 and 1% BSA in DPBS for 1 hour at room temperature protected from light. Cells were washed and finally stained with 1 μg/ml DAPI for 15 minutes at room temperature protected from light. Glass cover slides were mounted onto glass slides using a drop of Immu-mount solution (Epredia, Kalamazoo, MI; cat. 9990402) and stored at 4ºC. Cells were imaged using Zeiss LSM800 laser scanning confocal microscope.

8.2. Confocal microscopy analysis of Calu-3 cells

$0.25x10^6$ Calu-3 cells and Calu-3 cells stably expressing ORF8 and its mutants were seeded in a 12-well plate on non-treated glass cover slides. Cells were incubated at 37ºC and 5% CO_2 for 72 hours. Cells were fixed as described above. Primary antibodies used were rabbit pIgR polyclonal antibody (1:50) and rat monoclonal anti-Strep-II (1:200), while the secondary antibodies used were Fluor 488 donkey anti-rat (1:500), Alexa Fluor 488 goat anti-rat (1:500), Alexa Fluor 568 goat anti-rabbit (1:500), and Alexa Fluor 647 donkey anti-rabbit (1:500). Cells were imaged using Zeiss LSM800 laser scanning confocal microscope.

9. IgA binding and internalization assay

9.1. IgA binding in HEK293T cells for flow cytometry

$0.25x10^6$ HEK293T cells/well were seeded in a 12-well plate and incubated overnight at 37ºC and 5% CO_2. Cells were co-transfected for 6 hours with 0.125 μg of SARS-CoV-2 ORF8, its mutants and variants, and animal CoV ORF8 expression plasmids, 0.25 μg of pIgR and pIgR mutants, and 0.125 μg to 0.25 μg of pQCXIP empty vector plasmid using a 1 ug:3 ul DNA to PEI ratio. After incubation at 37ºC for 48 hours, cells were lifted with 0.1 mM EDTA for 5 minutes at 37ºC. Cells were washed three times in DBPS and stained with cell viability stain Zombie Violet (1:2000) diluted in DBPS for 30 minutes at room temperature. Cells were washed three times with

3% BSA and then incubated with 10 μg/ml IgA-647, 10 μg/ml IgA-488 and/or 10 μg/ml ORF8-488 diluted in 3% BSA for 30 minutes at 4ºC protected from light. Cells were washed three times with 3% BSA and then further stained with either anti-FLAG-647 or anti-Strep-II and analyzed as previously described.

9.2. IgA binding and internalization in HEK293T cells for confocal microscopy

$0.1x10^6$ HEK293T cells/well were seeded in a 12-well plate on glass cover slides pre-treated with 10 μg/ml poly-D-lysine for 1 hour at 37ºC. Cells were incubated overnight at 37ºC and 5% CO_2 and co-transfected for 6 hours with 0.25 μg of pIgR and 0.25μg of pQCXIP empty vector plasmid using a 1 ug:3 ul DNA to PEI ratio. After a 48-hour incubation, two sets of cells were stained with either 10 μg/ml IgA-647, 10 μg/ml ORF8-488, or both for 30 minutes at 4ºC. As a control, cells were pre-treated with 1 ml 10 μM 3-Hydroxynapthalene-2-carboxylix acid-(3,4-dihydroxybenzylidene)-hydrazide (Dynasore; Sigma-Aldrich; cat. 324410) in DMEM with 0.2% FBS for 15 minutes and then incubated with 10 μg/ml IgA-647 for 30 minutes at 4ºC. Cells were washed with DBPS, and the first set was further incubated with 3% BSA at 37ºC for 15 minutes and 30 minutes. After their respective incubations, both sets of cells were fixed with 4% PFA for 10 minutes at room temperature protected from light. Cells were stained with primary antibody rabbit anti-FLAG, and secondary antibodies Alexa Fluor 568 goat anti-rabbit, and DAPI. Samples were mounted and analyzed as previously described.

9.3. IgA binding in Calu-3 cells for flow cytometry

$0.3x10^6$ Calu-3 cells and Calu-3 stable cell lines were seeded per wells of a 12-well plate and incubated for 72 hours at 37ºC and 5% CO_2. Cells were lifted with 0.5 mM EDTA for 15 minutes at 37ºC. Cells were washed three times with 3% BSA and then incubated with 30 μg/ml IgA-647 and/or 10 μg/ml ORF8-488 diluted in 3% BSA for 30 minutes at 4ºC protected from light.

Cells were washed three times with 3% BSA and then further stained with anti-Strep-II and analyzed as previously described.

9.4. IgA binding and internalization in Calu-3 cells for confocal microscopy

$0.25x10^6$ Calu-3 cells/well were seeded in a 12-well plate on non-treated glass cover slides. Cells were incubated at 37ºC and 5% CO_2 for 72 hours. Two sets of cells were stained with either 30 μg/ml IgA-647, 10 μg/ml ORF8-488, or both for 30 minutes at 4ºC. Cells were washed with DBPS, and the first set was further incubated with 3% BSA at 37ºC for 15 minutes. After their respective incubations, both sets of cells were fixed with 4% PFA for 10 minutes at room temperature protected from light. Cells were stained with the primary antibody rabbit anti-pIgR and the secondary antibodies Alexa Fluor 568 goat anti-rabbit and DAPI. Samples were mounted and analyzed as previously described.

10. Chemical inhibition of protein degradation and endocytosis

10.1. Chemical inhibition of protein degradation in HEK293T cells

$0.6x10^6$ HEK293T cells/well were seeded in a 6-well plate and incubated overnight at 37ºC and 5% CO_2. Cells were co-transfected for 6 hours with 0.25 μg SARS-CoV-2 ORF8, 0.5 μg pIgR, and 0.25 μg pQCXIP empty vector plasmid using a 1 ug:3 ul DNA to PEI ratio. After a 48-hour incubation, cells were treated for 4 hours with 50 μM Chloroquine diphosphate salt (CQ; Sigma-Aldrich; cat. C6628), or 10 μg/ml of a 1:1 mixture of (2S,3S)-trans-Epoxysuccinyl-L-leucylamido-3-methylbutane ethyl ester (E64d; Sigma-Aldrich; cat. E8640) and pepstatin (pep; Roche, Idianapolis, IN; cat. 10253286001), and for 6 hours with 10 μM of Z-Leu-Leu-Leu-al (MG132; Sigma-Aldrich; cat. C2211), or 15 μM of N2, N4-dibenzylquinazoline-2,4-diamine (DBeQ; Sigma-Aldrich; cat. SML0031). Cell lysates were harvested, and protein expression was analyzed by Western blot with primary antibodies rat anti-Strep-II (1:5,000), mouse anti-FLAG (1:5000),

mouse anti-tubulin (1:5,000), and with the secondary antibodies HRP-conjugated goat anti-rat (1:10,000), and HRP-conjugated goat anti-mouse (1:5,000) as described above.

10.2 Chemical inhibition of endocytosis in HEK293T cells

$0.6x10^6$ HEK293T cells/well were seeded in a 6-well plate and incubated overnight at 37ºC and 5% CO_2. Cells were co-transfected for 6 hours with 0.25 μg SARS-CoV-2 ORF8, 0.5 μg pIgR, and 0.25 μg pQCXIP empty vector plasmid using a 1 ug:3 ul DNA to PEI ratio. After a 48-hour incubation, cells were treated for 6 hours with 16 μM Dynasore (company). Cell lysates were harvested, and protein expression was analyzed by Western blot with primary antibodies rat anti-Strep-II (1:5,000), mouse anti-FLAG (1:5000), mouse anti-tubulin (1:5,000), and with the secondary antibodies HRP-conjugated goat anti-rat (1:10,000), and HRP-conjugated goat anti-mouse (1:5,000) as described above.

11. Transferrin binding and internalization assay

11.1. Transferrin binding and internalization for Confocal Microscopy

$0.1x10^6$ HEK293T cells/well were seeded in a 12-well plate on glass cover slides pre-treated with 10 μg/ml poly-D-lysine for 1 hour at 37ºC. Cells were incubated overnight at 37ºC and 5% CO_2 and co-transfected for 6 hours with either 0.25 μg of pIgR or 0.25 μg of TFR1 and 0.25μg of pQCXIP empty vector plasmid using a 1 ug:3 ul DNA to PEI ratio. After a 32-hour incubation, cell media was changed, and cells were starved overnight with DMEM containing 0.2% FBS. Two sets of cells were stained with 25 μg/ml pre-conjugated transferrin-488 (Biotium, San Francisco, CA; cat. 00081) diluted in 1% BSA for 90 minutes at 4ºC. As a control, cells were pre-treated with 1 ml 10 μM Dynasore in DMEM with 0.2% FBS for 15 minutes and then incubated with 25 μg/ml pre-conjugated transferrin-488 90 minutes at 4ºC. Cells were washed with DBPS, and the first set was further incubated with 1% BSA at 37ºC for 15 minutes and 30

minutes. After their respective incubations, both sets of cells were fixed with 4% PFA for 10 minutes at room temperature protected from light. Cells were stained with primary antibodies rabbit anti-FLAG (1:200) or mouse transferrin monoclonal antibody (1:250), and secondary antibodies Alexa Fluor 647 donkey anti-rabbit IgG (1:500) or Alexa Fluor 647 donkey anti-mouse (1:500), and DAPI. Confocal microscopy was performed as mentioned above.

11.2. Transferrin binding for flow cytometry in HEK293T cells

$0.25x10^6$ HEK293T cells/well were seeded in a 12-well plate and incubated overnight at 37ºC and 5% CO_2. Cells were transfected for 6 hours with either 0.25 μg of pIgR, 0.25 μg of TFR1, or 0.25 μg TFR1-mCherry, and 0.25μg of pQCXIP empty vector plasmid using a 1 ug:3 ul DNA to PEI ratio. After a 32-hour incubation, cell media was changed, and cells were starved overnight with DMEM containing 0.2% FBS. Cells were lifted with 0.1 mM EDTA for 5 minutes at 37ºC. Cells were washed three times in DBPS and stained with cell viability stain Zombie Violet (1:2000) diluted in DBPS for 30 minutes at room temperature. Cells were washed three times with 3% BSA and then incubated with 25 μg/ml of either pre-conjugated transferrin-488 or our conjugated human transferrin diluted in 1% BSA for 90 minutes at 4ºC protected from light. For competition assays, a titration of pre-conjugated transferrin-488 (6.25 μg/ml, 12.5 μg/ml, 25 μg/ml, 50 μg/ml) was incubated with 10 μg/ml dIgA-647 diluted in 1% BSA for 90 minutes at 4ºC. Alternatively, cells were incubated with 25 ug/ml of our conjugated human transferrin and a titration of unconjugated human transferrin (2 μg/ml, 10 μg/ml, 50 μg/ml, 250 μg/ml) diluted in 1% BSA for 90 minutes at 4ºC. Cells were washed three times with 3% BSA and then further stained with anti-FLAG-647 (1:1000) and analyzed by flow cytometry as previously described.

11.3. Transferrin binding for flow cytometry in Calu-3 cells

$0.3x10^6$ Calu-3 cells and Calu-3 stable cell lines were seeded per wells of a 12-well plate and incubated for 56 hours at 37ºC and 5% CO_2. Cell media was changed, and cells were starved overnight with EMEM containing 0.2% FBS. Cells were lifted with 0.5 mM EDTA for 15 minutes at 37ºC. Cells were washed three times with 3% BSA and then incubated with a titration of pre-conjugated transferrin-488 (50 μg/ml, 100 μg/ml, 200 μg/ml) diluted in 1% BSA for 90 minutes at 4ºC protected from light. Cells were washed three times with 3% BSA and analyzed by flow cytometry as previously described.

12. Bio-layer interferometry (BLI)

BLI protocol was developed and performed by Mehdi Benlarbi from the Dr. Andres Finzi lab at the Centre Hospitalier de l'Université de Montreal (CHUM). Amine reactive second-generation biosensors (AR2G; Sartorius, Gottingen, DE) were hydrated in water for 5 minutes and then activated with 5 mM sulfo-NHS and 10 mM EDC (Sartorius). 12.5 μg/ml unconjugated transferrin, IgA, or IgM were loaded into the A2RG biosensors at 25ºC in 10 mM acetate solution (pH 5) for 10 minutes. The reaction was quenched with 1 M ethanolamine solution (pH 8.5; Sartorius) for 5 minutes. To perform baseline equilibration, the biosensors were incubated with 10X kinetics buffer (Sartorius) for 2 minutes. Association of loaded biosensors with either recombinant pIgR or recombinant TFR1 diluted in 10X kinetics buffer was measured using the Octet RED96e system (ForteBio, Fremont, CA). Association was measured for 3 minutes at various concentrations in a two-fold dilution series ranging from 100 nM to 3.12 nM. Dissociation was then measured for 10 minutes, after which baseline was subtracted prior to data analysis using ForteBio data analysis software.

CHAPTER 3: RESULTS

3.1. SARS-CoV-2 ORF8 potently downregulates pIgR in a dose-dependent manner.

In patients suffering from severe COVID-19 disease, serum and urinary pIgR levels are markedly reduced[223,224]. This highlights a potential mechanism of SARS-CoV-2 in the antagonization of pIgR-mediated mucosal immunity; however, the viral mechanisms behind this effect remain largely unknown. To investigate which viral protein might be responsible for the antagonization of pIgR, we co-transfected HEK293T cells with plasmids expressing pIgR and a panel of SARS-CoV-2 structural, non-structural, and accessory proteins, and assessed the levels of pIgR expression by Western blots. Overall, SARS-CoV-2 proteins had minor up-regulatory and down-regulatory effects on pIgR expression, except for the Spike glycoprotein, NSP1, and ORF8 (Fig. 4A-B). NSP1 exhibited the strongest downregulation of pIgR, due to its previously reported function as a potent inhibitor of both host and viral mRNA translation; yet its intracellular nature makes it unlikely to have systemic effects on pIgR outside infected cells[83,225] (Fig. 4B). Compared to the Spike protein that led to a mean downregulation of pIgR by 40%, we observed a slightly more potent downregulation of 50% by ORF8 (Fig. 4B). Therefore, we decided to focus on studying ORF8 because of its secretion from cells, its capacity to dimerize, its Ig-like fold, as well as its reported antagonization of MHC-I, which together support a potential interaction with Fc receptors, such as pIgR[129,162,163,226].

To further investigate ORF8 downregulation of pIgR, we co-transfected HEK293T cells with a constant amount of pIgR and increasing doses of ORF8 plasmid DNA. We found that ORF8 significantly downregulated pIgR in a dose-dependent manner (Fig. 4C-D). To confirm whether the observed downregulation of pIgR is specific, this experiment was repeated with FcnR (neonatal Fc receptor) as a control Fc receptor. We did not observe any downregulation of FcnR in the

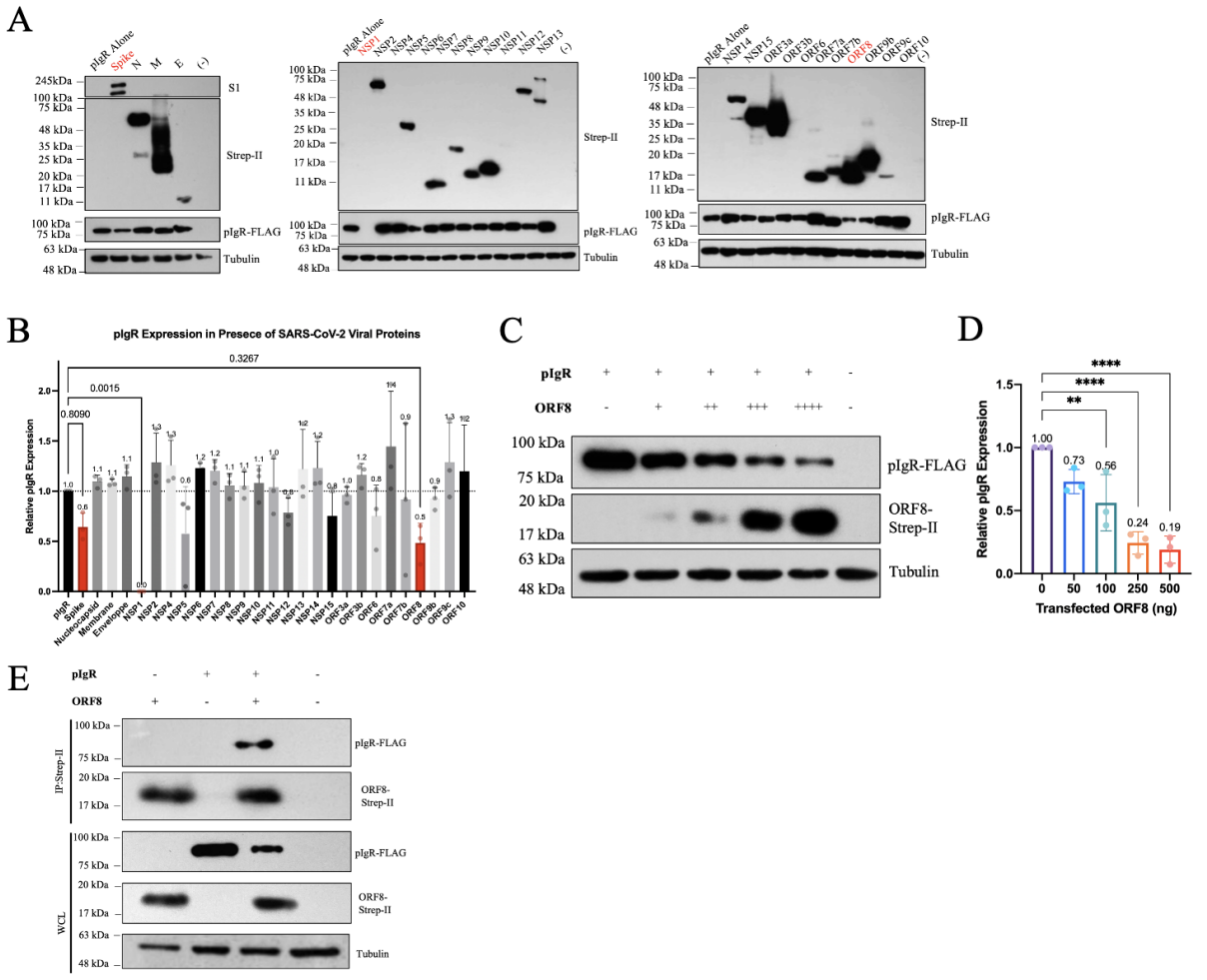

Figure 4. SARS-CoV-2 ORF8 downregulates pIgR in a dose-dependent manner. (**A, B**) HEK293T cells co-transfected with 500 ng pIgR plasmid DNA, 250 ng plasmid DNA expressing SARS-CoV-2 structural, non-structural (nsp), or accessory proteins, and 250 ng QCXIP empty vector. (**C-D**) HEK293T cells co-transfected with 500 ng pIgR plasmid DNA and a titration of SARS-CoV-2 ORF8-Strep-II plasmid DNA (0 ng, 50 ng, 100 ng, 250 ng, 500 ng), and QCXIP DNA. (**F**) HEK293T cells co-transfected with 2500 ng pIgR, 1250 ng ORF8-Strep-II, and 1250 ng QCXIP plasmid DNA. Whole cell lysates were harvested and analyzed for pIgR-FLAG (anti-FLAG), SARS-CoV-2 proteins and ORF8-Strep-II (anti-Strep-II), Spike (anti-Spike), and tubulin (anti-tubulin) by Western blots. Protein expression was quantified using Fiji and analyzed with Prism V9 (statistical significance measured via one-way Anova; * $p \leq 0.05$, ** $p \leq 0.01$, *** $p \leq 0.001$, **** $p \leq 0.0001$).

presence of the highest dose of ORF8, highlighting the specific downregulation of pIgR (data generated by Ariana Arduini, not shown here). We next tested whether ORF8 downregulation of pIgR is a result of an interaction between these two proteins. To examine this, we co-transfected HEK293T cells with plasmids expressing pIgR and ORF8 and performed co-immunoprecipitation using anti-Strep-II magnetic beads (IP:Strep-II). This led to the successful pull-down of pIgR by ORF8, indicating a potential interaction between the two proteins (Fig. 4E). Altogether, these data support the capacity of the SARS-CoV-2 accessory protein ORF8 to interact with and downregulate pIgR.

3.2. ORF8 proteins from SARS-CoV-2 VOCs and VOIs preserve their downregulation of pIgR unlike dimerization deficient ORF8 from mutants and SARS-CoV.

ORF8 is hypervariable within SARS-CoV-2 and across beta-coronaviruses[126,127]. This means that it is readily mutated in variants of concern (VOCs) and interest (VOIs)[127]. In addition, whether its novel capacity to dimerize, a characteristic unique to SARS-CoV-2-like ORF8s, facilitates its immunomodulatory functions against mucosal immunity remains to be investigated[131]. Hence, we first investigated whether the ability of pIgR downregulation is conserved amongst ORF8 across different coronaviruses. Additionally, we sought to assess how dimerization, multimerization, and glycosylation impact ORF8 function by generating a panel of mutants and variants derived from the WT SARS-CoV-2 ORF8 expression plasmid via mutagenesis (Fig. 5A). Mutations C20A, R52A, K53A, and R115A are expected to disrupt ORF8 dimerization, Y73A disrupts multimerization, and N78A impairs glycosylation (Fig. 5A). Moreover, we also cloned the Del119-120 enriched in Delta VOC, T11I in the Iota VOC, E92K in the gamma VOC, and V100L in the Epsilon VOC (Fig. 5A). S24L and S84L were mutated based on their enrichment in SARS-CoV-2 ORF8 in the GSAID database (Fig. 5A). Finally, we also

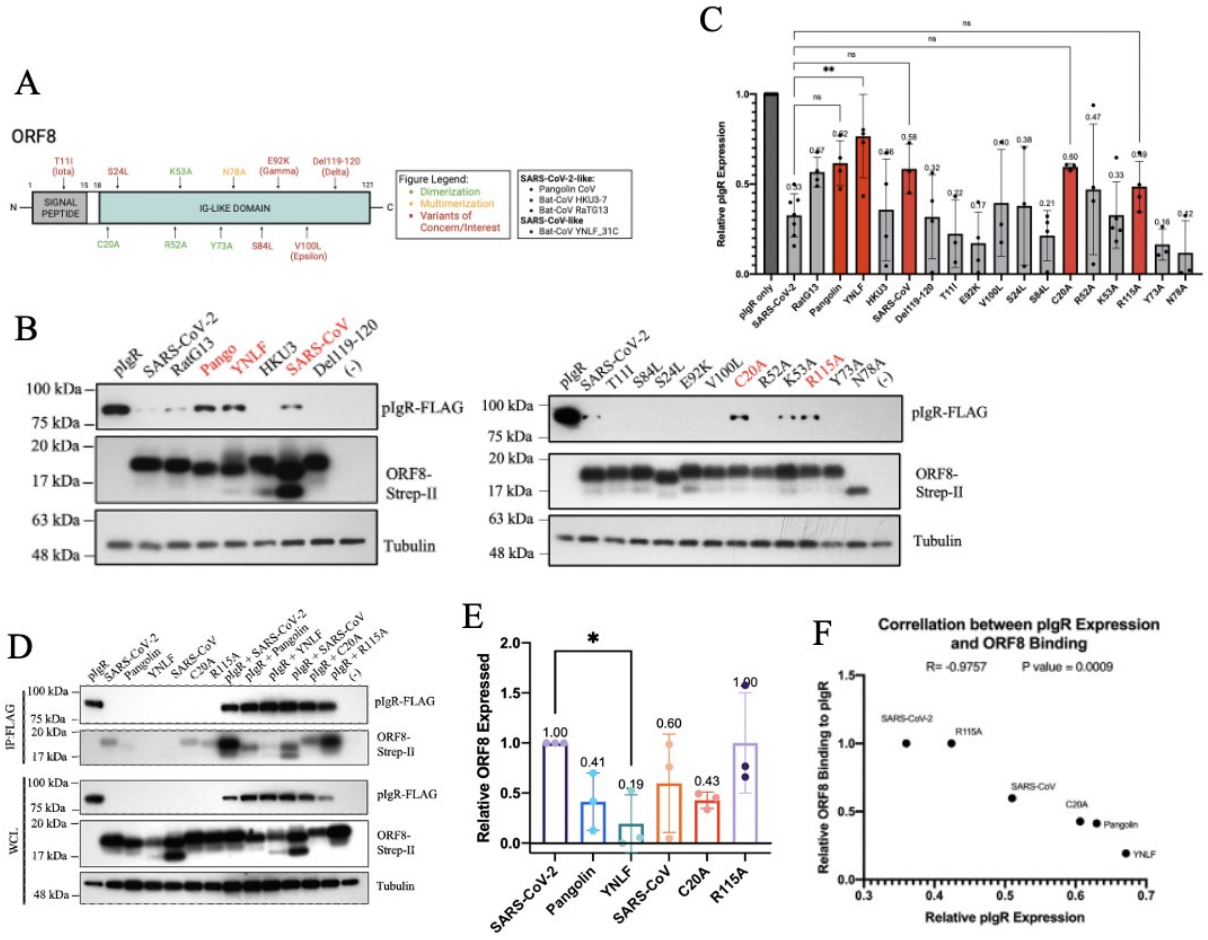

Figure 5. ORF8 from SARS-CoV-2 mutants, variants, and animal CoVs interact differently with pIgR. (**A**) Schematic of ORF8 mutagenesis. (**B-C**) HEK293T co-transfected with 500ng pIgR, 250ng QCXIP, and 250ng mutant, variant, and animal CoV ORF8 proteins. (**D-E**) HEK293T co-transfected with 2500ng pIgR, 1250ng QCXIP, and 1250ng Pangolin, YNLF, SARS-CoV, C20A, and R115A ORF8 proteins. (**F**) Correlation analysis performed on PrismV9. **(B-E)** Protein expression was quantified using Fiji and analyzed with Prism V9 (mean with SD; statistical significance measured via one-way Anova; * $p \leq 0.05$, ** $p \leq 0.01$, *** $p \leq 0.001$, **** $p \leq 0.0001$)

tested the SARS-CoV ORF8, along with ORF8 from SARS-CoV-like bat-CoV YNLF_31C, and the SARS-CoV-2 like pangolin CoV, bat-CoV HKU3-7, and bat-CoV RatG13 (Fig. 5A).

The variant, mutant, and animal CoV ORF8 plasmids were co-transfected into HEK293T cells together with pIgR, and the whole cell lysates were analyzed by Western blots to assess pIgR

expression. ORF8 proteins from RatG13, HKU3-7 (HKU3), Delta, Iota, Gamma, Epsilon, S84L, S24L, R52A, Y73A, and N78A maintained their downregulation of pIgR to levels greater or similar to WT SARS-CoV-2 ORF8 (Fig. 5B-C). Interestingly, ORF8 proteins from pangolin CoV, bat-CoV YNLF_31C, SARS-CoV, C20A, and R115A have a reduced capacity to downregulate pIgR (Fig. 5B-C). More specifically, the WT SARS-CoV-2 ORF8 reduced pIgR expression by 67%, while the pangolin CoV downregulated pIgR expression by 38%, bat-CoV YNLF_31C by 23%, SARS-CoV by 42%, C20A by 40%, and R115A by 51%, (Fig. 5C). These results suggest that dimerization may play a crucial role in ORF8 downregulation of pIgR, since two out of the four dimerization mutants (C20A and R115A), and the monomeric ORF8 proteins of SARS-CoV and bat-CoV YNLF_31C exhibited a weaker downregulation of pIgR (Fig. 5B-C).

3.3. The strength of ORF8 and pIgR interaction correlates with the degree of pIgR downregulation by ORF8.

Since most of the mutants which failed to potently downregulate pIgR are monomeric, we sought to investigate whether pangolin CoV, bat-CoV YNLF_31C, SARS-CoV, C20A, and R115A ORF8 proteins have decreased interaction with pIgR. To this end, HEK293T cells were co-transfected with pIgR and the above mentioned ORF8 proteins. The cell lysates were then co-immunoprecipitated with beads coated with anti-FLAG antibody (IP:FLAG). We observed that pangolin CoV, bat-CoV YNLF_31C, SARS-CoV, and C20A ORF8 proteins have decreased binding to pIgR compared to WT SARS-CoV-2 ORF8 (Fig. 5D-E). In contrast, R115A ORF8 did not show a reduced capacity to interact with pIgR, consistent with its capacity to downregulate pIgR (Fig. 5D-E). A correlation analysis was performed by plotting the relative ORF8 binding to pIgR against the relative pIgR downregulation (Fig. 5F). Mutants which bound pIgR more strongly, such as SARS-CoV-2 and R115A, showed more downregulation of pIgR, while the

opposite was true for mutants which bound pIgR less well, such as C20A, Pangolin, and YNLF ORF8 (Fig. 5A-F). Hence, this indicates a strong negative correlation (R=-0.9757; P=0.0009) between ORF8 binding and pIgR downregulation, suggesting the requirement of a direct ORF8 interaction with pIgR for its downregulation (Fig. 5F).

3.4. ORF8 downregulates endogenous pIgR in Calu-3 cells.

Lung epithelial Calu-3 and intestinal epithelial Caco-2 cells have been commonly used to study SARS-CoV-2 replication, due to their high expression of both ACE2 and TMPRSS2[227,228]. In concordance, SARS-CoV-2 entry in both these cell lines is dominated by the TMPRSS2 pathway, rather than the cathepsin pathway[228]. Due to challenges in expressing ORF8 via transfection in Calu-3 cells, we produced lentiviral vectors which carried puromycin resistance genes, along with either SARS-CoV-2, SARS-CoV, Pangolin, YNLF, R115A, or C20A ORF8 plasmids. These vectors were used to transduce Calu-3 cells and produce cell lines stably expressing ORF8 or its variants. To confirm successful expression of the ORF8 proteins within the stable expression Calu-3 cell lines, we performed flow cytometry where we observed ORF8 expression in around 40%-60% of the cells (Fig. 6B). Altogether these findings suggest that these stable-expression cell lines can be used to study the impact of ORF8 on endogenous pIgR.

To assess whether intracellular ORF8 could downregulate endogenous pIgR, we performed Western blots using cell lysates from the ORF8-expressing Calu-3 cell lines. Similar to exogenous pIgR expression in HEK293T cells, we observed downregulation of endogenous pIgR for all the ORF8 proteins we tested (Fig. 6C-D). However, we found that ORF8 mutants which had the weakest capacity to downregulate pIgR in HEK293T cells, such as C20A and R115A, were more potent at antagonizing endogenous pIgR expression than WT SARS-CoV-2 ORF8 in Calu-3

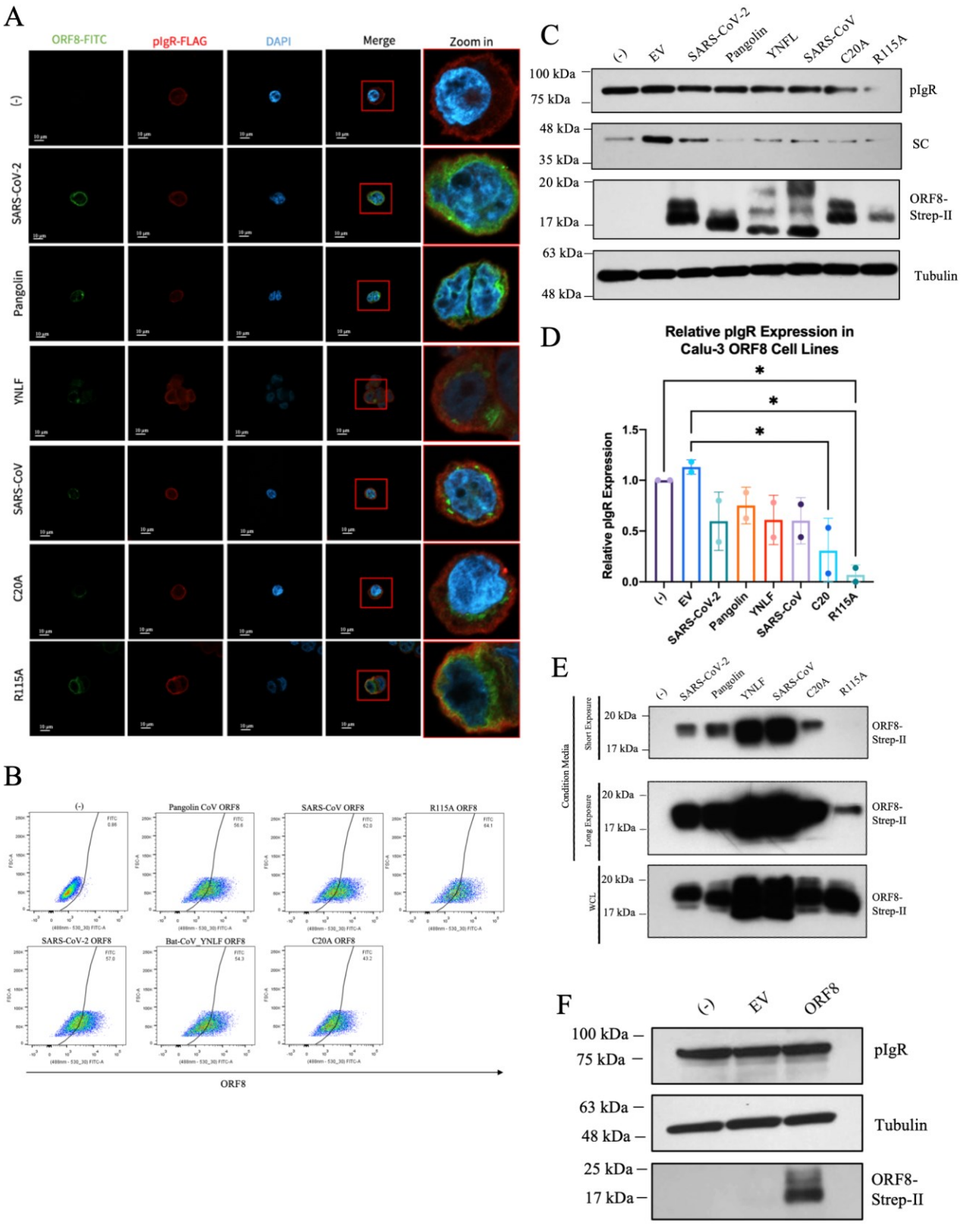
A
ORF8-FITC
pIgR-FLAG
DAPI
Merge
Zoom in
(-)
SARS-CoV-2
Pangolin
YNLF
SARS-CoV
C20A
R115A
B
(-)
Pangolin CoV ORF8
SARS-CoV ORF8
R115A ORF8
SARS-CoV-2 ORF8
Bat-CoV_YNLF ORF8
C20A ORF8
ORF8
C
(-)
EV
SARS-CoV-2
Pangolin
YNFL
SARS-CoV
C20A
R115A
100 kDa
75 kDa
48 kDa
35 kDa
20 kDa
17 kDa
63 kDa
48 kDa
pIgR
SC
ORF8-
Strep-II
Tubulin
D
Relative pIgR Expression in
Calu-3 ORF8 Cell Lines
Relative pIgR Expression
1.5
1.0
0.5
0.0
(-)
EV
SARS-CoV-2
Pangolin
YNLF
SARS-CoV
C20
R115A
E
(-)
SARS-CoV-2
Pangolin
YNLF
SARS-CoV
C20A
R115A
Condition Media
Short Exposure
Long Exposure
WCL
20 kDa
17 kDa
ORF8-
Strep-II
F
(-)
EV
ORF8
100 kDa
75 kDa
63 kDa
48 kDa
25 kDa
17 kDa
pIgR
Tubulin
ORF8-
Strep-II

Figure 6. Calu-3 cell lines express ORF8 stably but fails to observe pIgR downregulation. (**A-D**) Calu-3 cells lines stably expressing SARS-CoV-2 ORF8-Strep-II and its mutants generated via transduction with lentiviral vectors carrying ORF8 expression plasmids. (**A**) Calu-3 cell lines stained for pIgR (anti-pIgR; red), ORF8-Strep-II (anti-Strep-II; green), and DAPI (blue). ORF8 and pIgR cellular localization analyzed by Confocal microscopy. (**B**) Calu-3 cells stained for ORF8-Strep-II (anti-Strep-II-FITC) and analyzed by flow cytometry. (**F**) Calu-3 cells transiently expressing ORF8-Strep-II via lentiviral transduction. Whole cell lysates (**C-F**) and condition media (**E**) were harvested and analyzed for pIgR-FLAG (anti-FLAG), ORF8-Strep-II (anti-Strep-II), and tubulin (anti-tubulin) by Western Blot. Protein expression quantified using Fiji and PrismV9 (mean with SD; statistical significance measured via one-way Anova; * $p \leq 0.05$, ** $p \leq 0.01$, *** $p \leq 0.001$, **** $p \leq 0.0001$).

cells (Fig. 6C-D). To ensure the validity of our findings and that the Calu-3 ORF8 stable cell lines were not becoming tolerant to the constant ORF8 expression, we performed transient transduction of Calu-3 cells using the lentiviral vectors carrying the SARS-CoV-2 ORF8 plasmid. We failed to observe pIgR downregulation in cell lysates by Western blot. However, ORF8 expression was much lower in this transient transduction experiment and required overnight staining to be observed by Western blot (Fig. 6F). This latter result suggests that short transient ORF8 expression (or low ORF8 levels) may not be sufficient to downregulate pIgR, and that SARS-CoV-2-mediated antagonization of pIgR may require high levels or long-lasting stable ORF8 expression in lung-epithelial cells. This further highlights the potential for an equilibrium between short- and long-exposure to ORF8 expression being necessary for potent pIgR downregulation. However, how this translates in the context of SARS-CoV-2 infection in primary lung-epithelial cells requires further investigation.

To confirm these findings, we investigated the expression of SARS-CoV-2 ORF8 on

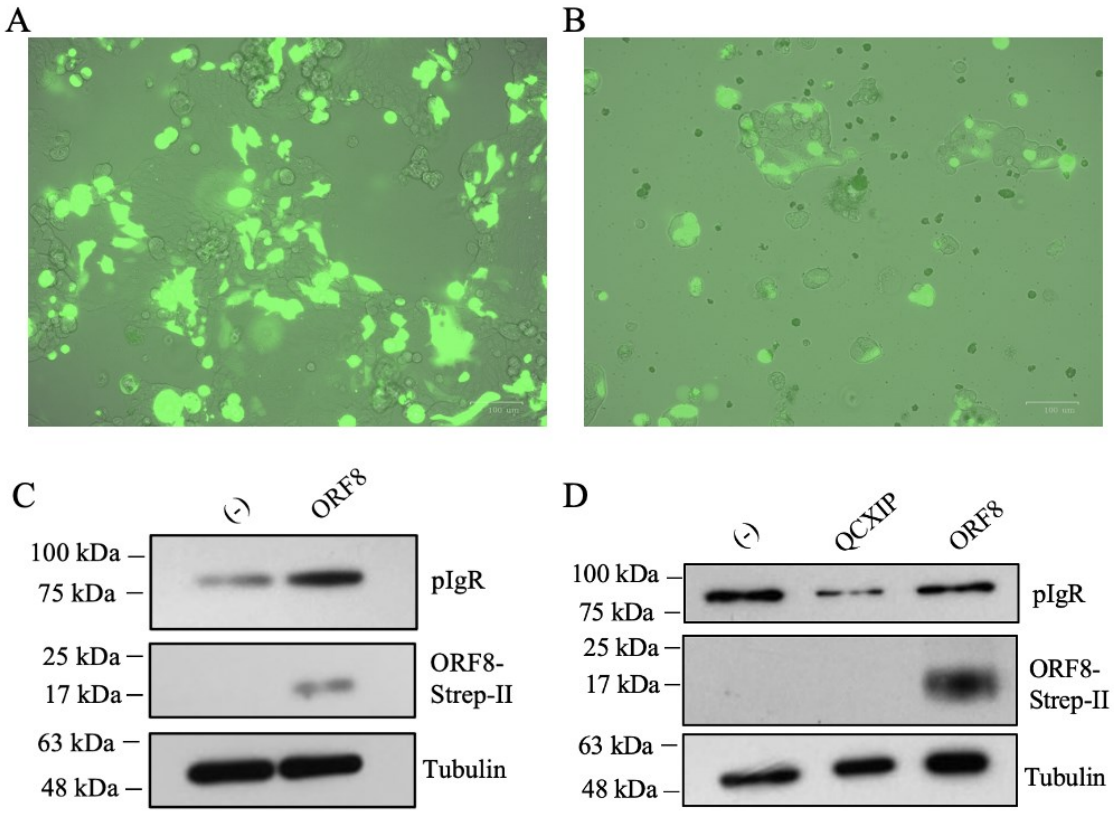

Figure 7. Caco-2 cells express ORF8 difficultly and effect on pIgR expression is inconsistent. (**A**) Caco-2 cells transfected with GFP expression plasmid. (**B**) Caco-2 cells electroporated with GFP expression plasmid. (**A-B**) GFP expression assessed by fluorescence microscopy. (**C-D**) Caco-2 cells electroporated with 5000µg/ml ORF8-Strep-II. Whole cell lysates were harvested and analyzed for pIgR-FLAG (anti-FLAG), ORF8-Strep-II (anti-Strep-II), and tubulin (anti-tubulin) by Western Blot.

endogenous pIgR expression in colorectal adenocarcinoma (intestinal epithelium) Caco-2 cells. Similar to Calu-3 cells, we failed to express ORF8 in Caco-2 cells by transfection, although we were able to successfully transfect and express GFP (Fig. 7A). Overall, we identified challenges in expressing ORF8 across different cell lines, such as Caco-2 and Calu-3 cells, which appear to be non-tolerant of ORF8 but not to other proteins, such as GFP. To mitigate this issue, we proceeded to electroporate Caco-2 cells, which entails the use of high-voltage pulses to

permeabilize cell membranes, allowing plasmids to enter[229]. Using this method, we successfully expressed both GFP and ORF8 (Fig. 7B-C). However, this method led us to observe discrepancies towards the effect of ORF8 on endogenous pIgR expression in Caco-2 cells. We first observed an increase in pIgR in ORF8-electroporated cells when compared to non-electroporated cells, while we later observed a decrease in pIgR expression with the electroporation of both an empty-vector control and ORF8 (Fig. 7C-D). These confounding findings suggest that the stress induced on Caco-2 cells from electroporation may be greater in modulating pIgR expression than the presence of ORF8. However, these results support that transient exposure to low levels of ORF8 may not be sufficient to antagonize endogenous pIgR expression, as observed in Calu-3 cells.

3.5. ORF8 and pIgR modulate each other's subcellular localization.

To further investigate the mechanism behind the downregulation of pIgR by ORF8 from SARS-CoV-2, SARS-CoV, mutants, and SARS-CoV-/CoV-2 like animal CoVs, we co-transfected HEK293T cells with plasmids expressing pIgR and the above-mentioned ORF8 proteins. To assess the cellular localization of these proteins respective of the secretory pathway, we stained the cells with the cis-Golgi marker GM130. In the absence of ORF8, pIgR is seen spread intracellularly and localized to the plasma membrane with no aggregation to the cis-Golgi (Fig. 8A-C). Similarly, when WT SARS-CoV-2, Pangolin, C20A, and R115A are expressed in the absence of pIgR, they are spread intracellularly without aggregation or colocalization with the cis-Golgi (Fig. 8A-B). However, when pIgR is co-expressed with either of these mutants, its localization is modulated into a large punctate which overlaps with the cis-Golgi (Fig. 8A-B). As for the SARS-CoV-2 and its mutant/animal-like ORF8 proteins, there is no striking changes in their cellular localization in the presence of pIgR (Fig. 8A-B). Contrastingly, colocalization of SARS-CoV and YNLF ORF8 with the cis-Golgi is drastically amplified in the presence of pIgR (Fig. 8C). Although SARS-CoV

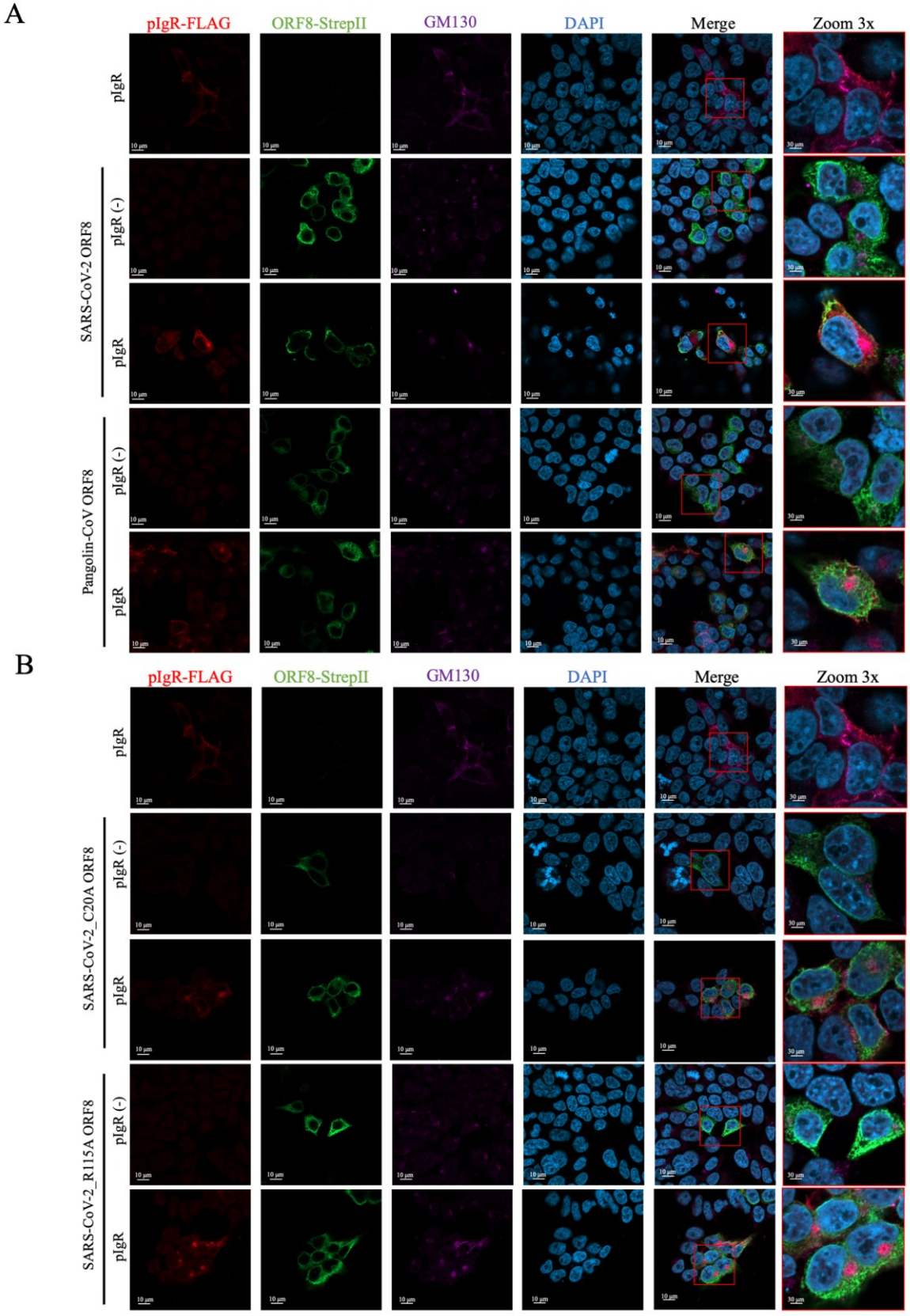
A
pIgR-FLAG
ORF8-StrepII
GM130
DAPI
Merge
Zoom 3x
pIgR
SARS-CoV-2 ORF8
pIgR (-)
pIgR
Pangolin-CoV ORF8
pIgR (-)
pIgR
B
pIgR-FLAG
ORF8-StrepII
GM130
DAPI
Merge
Zoom 3x
pIgR
SARS-CoV-2_C20A ORF8
pIgR (-)
pIgR
SARS-CoV-2_R115A ORF8
pIgR (-)
pIgR

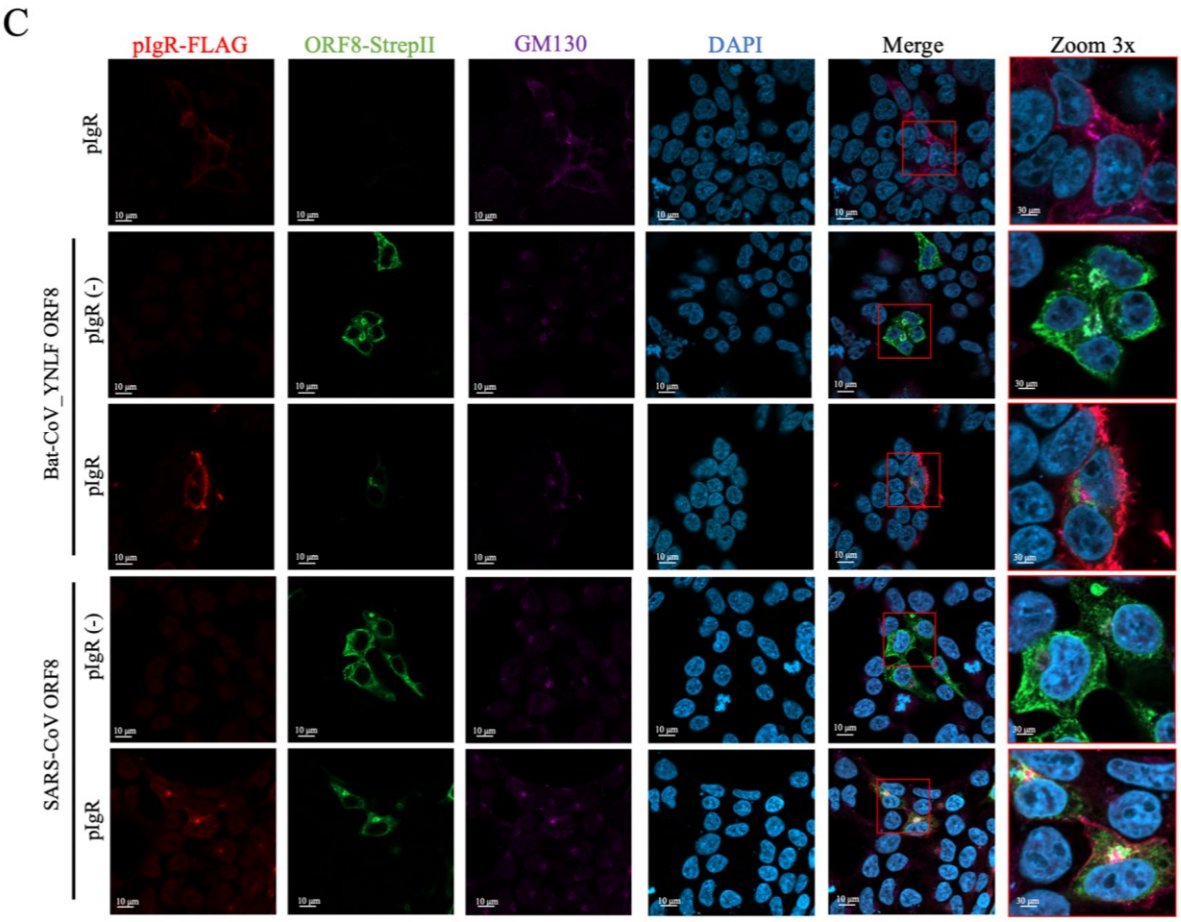
C
pIgR-FLAG
ORF8-StrepII
GM130
DAPI
Merge
Zoom 3x
pIgR
Bat-CoV_YNLF ORF8
pIgR (-)
pIgR
SARS-CoV ORF8
pIgR (-)
pIgR
10 μm
30 μm

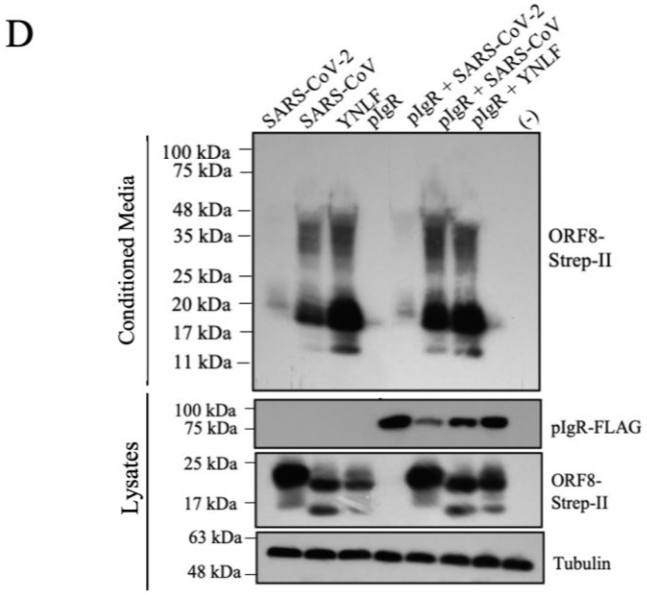
D
SARS-CoV-2
SARS-CoV
YNLF
pIgR
pIgR + SARS-CoV-2
pIgR + SARS-CoV
pIgR + YNLF
(-)
Conditioned Media
100 kDa
75 kDa
48 kDa
35 kDa
25 kDa
20 kDa
17 kDa
11 kDa
ORF8-Strep-II
Lysates
100 kDa
75 kDa
pIgR-FLAG
25 kDa
17 kDa
ORF8-Strep-II
63 kDa
48 kDa
Tubulin

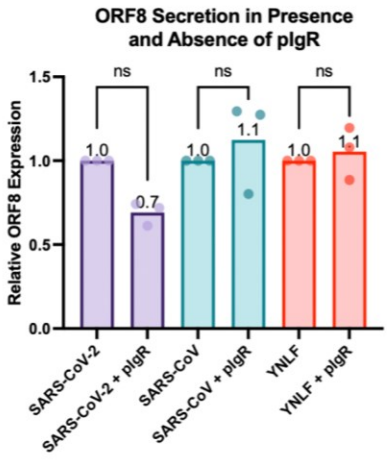
E
ORF8 Secretion in Presence and Absence of pIgR
Relative ORF8 Expression
1.5
1.0
0.5
0.0
ns
ns
ns
1.0
0.7
1.0
1.1
1.0
1.1
SARS-CoV-2
SARS-CoV-2 + pIgR
SARS-CoV
SARS-CoV + pIgR
YNLF
YNLF + pIgR

Figure 8. ORF8 and pIgR modulate each-other's cellular localization. (**A-C**) HEK293T cells co-transfected with 250ng pIgR, 250ng QCXIP, and 500ng SARS-CoV-2 (**A**), Pangolin (**A**), C20A (**B**), R115A (**B**), YNLF (**C**), and SARS-CoV ORF8 (**C**). Cells stained with anti-FLAG (red), anti-Strep-II (green), anti-GM130 (purple), and DAPI (blue), and analyzed by Confocal microscopy. (**D-E**) HEK293T cells co-transfected with and without 250ng pIgR, 250ng QCXIP, and 500ng SARS-CoV-2, Pangolin, YNLF, SARS-CoV, C20A, and R115A ORF8. Whole cell lysates and conditioned media were harvested and analyzed for pIgR-FLAG (anti-FLAG), ORF8-Strep-II (anti-Strep-II), and tubulin (anti-tubulin) by Western Blot. Protein expression quantified using Fiji and PrismV9 (statistical significance measured via one-way Anova; * $p \leq 0.05$, ** $p \leq 0.01$, *** $p \leq 0.001$, **** $p \leq 0.0001$).

---

and YNLF ORF8 also promote accumulation and co-localization of pIgR to the cis-Golgi, it does so less potently that SARS-CoV-2 and does not restrain pIgR expression to the plasma membrane (Fig. 8C).

The subcellular localization of these ORF8 proteins is consistent with expression of endogenous pIgR in Calu-3 cells, where SARS-CoV-2, Pangolin, and R115A ORF8 are spread intracellularly, while SARS-CoV and YNLF ORF8 form perinuclear punctates (Fig. 6A). However, a major difference resides within the cellular localization of C20A which is seen to form perinuclear punctates in Calu-3 cells rather than being spread intracellularly, as seen in HEK293T cells (Fig. 6A). In addition, pIgR cellular location did not seem to be affected by the presence of any of the ORF8 proteins (Fig. 6A). These finding confirm that ORF8 cellular localization is not cell-type dependent, however it may indicate differences between its interaction with endogenous and exogenous pIgR. Overall, we believe that the increased cellular localization of the SARS-CoV-like ORF8 proteins to the cis-Golgi in both HEK293T and Calu-3 cells could indicate increased activity of the secretory pathway.

Furthermore, our previous data highlighted a strong interaction between SARS-CoV-2

ORF8 and pIgR; however, we observed marginal co-localization of ORF8 with pIgR in confocal microscopy (Fig. 8A-C). We worked to optimize co-localization analysis using Fiji with the help of the imaging core manager at the Lady Davis Institute for medical research (LDI), but we were unable to measure co-localization within our samples. This is consistent with imaging data in Calu-3 cells, where distinct signals can be observed for SARS-CoV-2 ORF8 and pIgR, with no apparent presence of co-localization (Fig. 6A). Although this may indicate that interaction with pIgR might be mediated by secreted ORF8 binding to cell-surface pIgR, the discrepancy between the co-immunoprecitation and imaging data merits further investigation.

To investigate whether pIgR may influence the secretion of SARS-CoV-like ORF8 proteins by promoting an increased activity of the secretory pathway, we co-transfected HEK293T cells with and without SARS-CoV-2, SARS-CoV, and YNLF ORF8 plasmids, and then assessed protein expression in both the cell lysates and conditioned media by Western blots. In the absence of pIgR, we noticed that both SARS-CoV and YNLF ORF8 are more secreted than SARS-COV-2 ORF8 (Fig. 8D). This may be explained by the localization of SARS-CoV and YNLF ORF8 to the cis-Golgi in the absence of pIgR. However, in the presence of pIgR, we only observed a mild decrease of 30% in SARS-CoV-2 ORF8 secretion, and an increase of 10% in the secretion for both SARS-CoV and YNLF ORF8, although not statistically significant (Fig. 8D-E).

Concordantly, we found that SARS-CoV-2, Pangolin, and C20A ORF8 proteins were well secreted in Calu-3 cells and correlated with increased cellular expression (Fig. 6E). However, we did observe very low secretion of the dimerization mutant R115A, albeit similar cellular expression to SARS-CoV-2, Pangolin, and C20A ORF8 proteins (Fig. 6E). These results are consistent with previous findings in literature which reported that disruption of ORF8 dimerization at C20 was not sufficient to interrupt secretion, and highlight the importance of other intermolecular associations

between ORF8 monomers for dimer stability and secretion[157,230]. Additionally, these results highlight that ORF8 expression and secretion does not differ between cell types, as both secretion and expression are similar between HEK293T cells and Calu-3 cells. Altogether, these results suggest that, although pIgR modulation of ORF8 cellular localization may influence secretion, its role in doing so is not significant.

3.6. SARS-CoV-2 ORF8 does not downregulate pIgR via protein degradation or endocytosis pathways.

In other studies, it was found that SARS-CoV-2 ORF8 downregulates MHC-I via lysosomal degradation and autophagy[162]. To investigate whether ORF8 employed this pathway for pIgR downregulation, HEK293T cells co-expressing pIgR and ORF8 plasmids were treated with

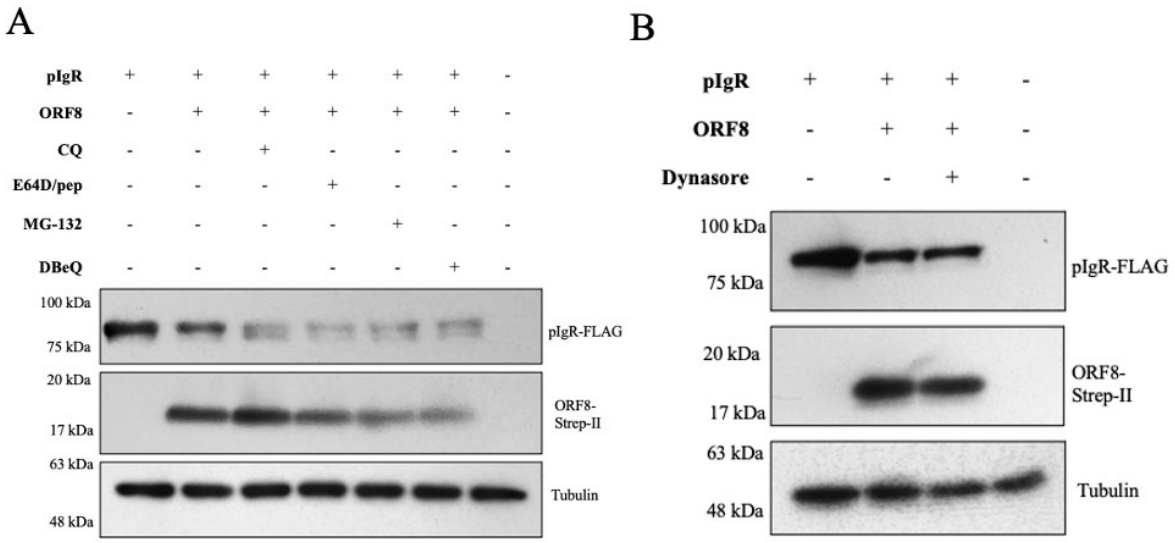

Figure 9. ORF8 does not downregulate pIgR via degradation or endocytosis pathways. (**A-B**) HEK293T cells co-transfected with 500ng pIgR, 250ng QCXIP, and 250ng SARS-CoV-2 ORF8. (**A**) Cells treated with CQ (50 μM; 4 hours), E64d/pepstatin (10 μg/ml; 4 hours), MG-132 (10 μM; 6 hours), and DBeQ (15 μM; 6 hours). (**B**) Cells treated with 16μM Dynasore for 6 hours. (**A-B**) Whole cell lysates were harvested and analyzed for pIgR-FLAG (anti-FLAG), ORF8-Strep-II (anti-Strep-II), and tubulin (anti-tubulin) by Western Blot.

chloroquine (CQ), E64d/pepstatin (E64D/pep), MG-132, or DBeQ, which respectively inhibits lysosomal (CQ & E64d/pep), proteasomal (MG-132), and ER-associated degradation (DBeQ)[162]. We failed to see any of these drugs recover pIgR expression in the presence of ORF8, indicating lysosomal, proteasomal or ER-associated pathways are not employed to downregulate pIgR (Fig. 9A). This led us to believe the possibility that ORF8 may be promoting an increased internalization of pIgR endocytosis which may lead to the accumulation of intracellular pIgR and then promote its downregulation. Hence, HEK293T cells co-expressing pIgR and ORF8 were treated with Dynasore, an inhibitor of clathrin-mediated endocytosis. Again, we did not observe a recovery of pIgR expression with the inhibition of endocytosis, suggesting that ORF8 does not downregulate pIgR via increased internalization of the receptor (Fig. 9B).

In support of our findings, lysosomal degradation of MHC-I has been contested and groups have rather suggested that MHC-I downregulation by ORF8 is dependent on the antagonization of MHC-I activators, such as NLRC5[163]. Therefore, SARS-CoV-2 ORF8 may antagonize pIgR by targeting steps upstream of its expression, such as through the inhibition of NF-kB signalling, which is known to increase pIgR expression[231]. This is in concurrence by the fact that SARS-CoV-2 is known to antagonize IFN-I antiviral responses, including the induction of NF-kB[99,232]. However, whether the antagonization of the IFN-I response by SARS-CoV-2 ORF8 directly leads to the downregulation of pIgR requires further investigation.

3.7. SARS-CoV-2 ORF8 interacts with the extracellular D1 of pIgR

To further investigate how ORF8 interacts with pIgR and whether this may affect pIgR's capacity to bind and transcytoses dIgA, we performed mutagenesis to generate a panel of extracellular domain deletions in pIgR (Fig. 10A). We did not perform deletions of the intracellular or transmembrane domains, since we expected ORF8 to engage with pIgR extracellular domains

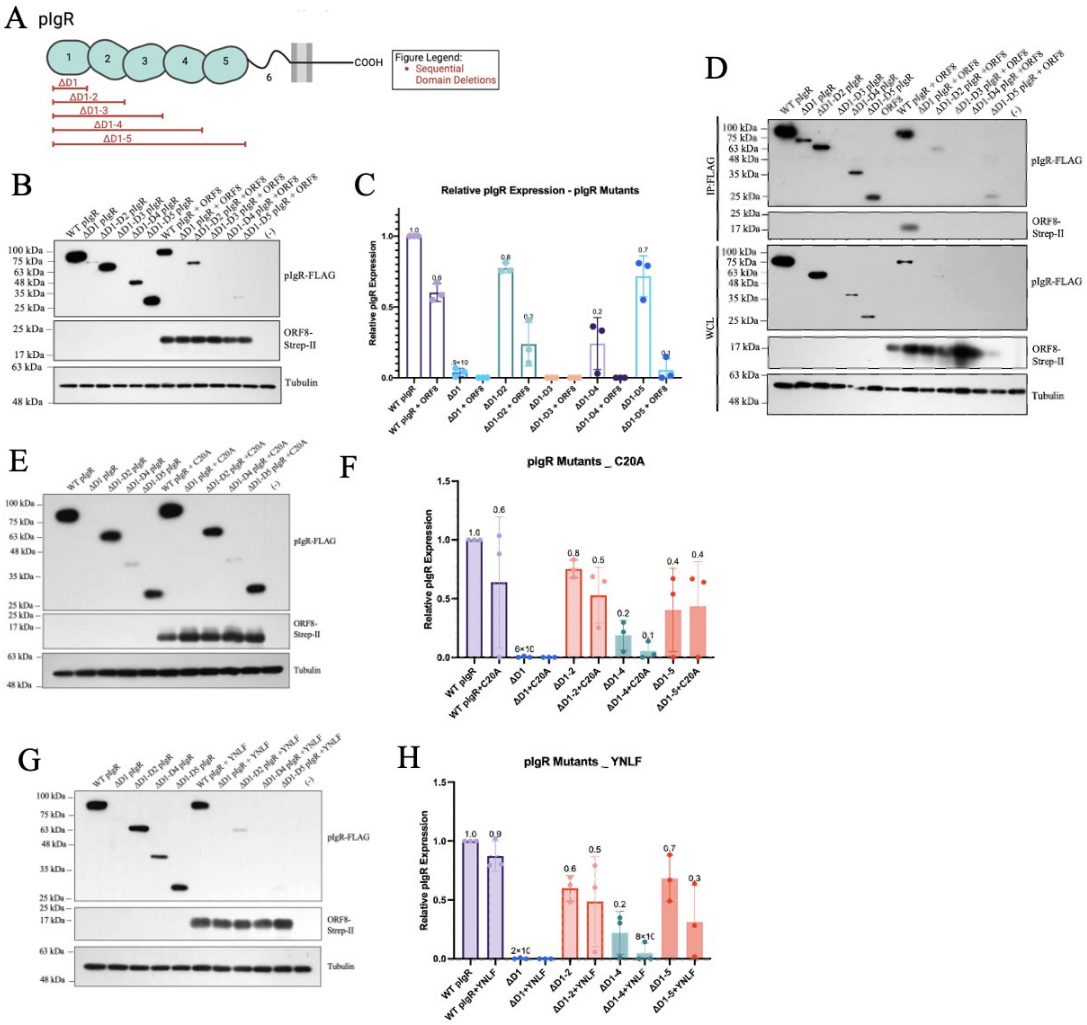

Figure 10. Intracellular ORF8 downregulates pIgR mutants. (**A**) Schematic of pIgR mutagenesis. (**B-C**) HEK293T cells co-transfected with 500ng pIgR or pIgR mutants, 250ng ORF8, and 250ng QCXIP. (**D**) HEK293T cells co-transfected with 2500ng pIgR or pIgR mutants, 1250ng ORF8, and 1250ng QCXIP. Protein expression quantified using Fiji and PrismV9. (**E-H**) HEK293T co-transfected with 500ng pIgR or pIgR mutants, 250ng QCXIP, and 250ng either C20A ORF8 (**E-F**) or R115A ORF8 (**G-H**). (**B-H**) Whole cell lysates were harvested and analyzed for pIgR-FLAG (anti-FLAG), ORF8-Strep-II (anti-Strep-II), and tubulin (anti-tubulin) by Western Blot. Protein expression was quantified using Fiji and analyzed with Prism V9 (mean with SD; statistical significance measured via one-way Anova; * $p \leq 0.05$, ** $p \leq 0.01$, *** $p \leq 0.001$, **** $p \leq 0.0001$).

due to being both luminal and secreted[142,151,157]. The mutant panel included deletions of domain 1 (ΔD1), domains 1 through 2 (ΔD1-2), domains 1 through 3 (ΔD1-3), domains 1 through 4 (ΔD1-4), and domains 1 through 5 (ΔD1-5) (Fig. 10A). We employed these mutants to further elucidate ORF8-pIgR interactions and investigate similarities and differences between dIgA and ORF8 binding to pIgR.

3.7.1. Intracellular ORF8 downregulates pIgR mutants similarly to full-length pIgR.

To understand whether any of the pIgR mutants were resistant to antagonization by ORF8, we co-transfected HEK293T cells with pIgR mutants and ORF8 plasmids and analyzed pIgR levels by Western blots. Unexpectedly, we found that all pIgR mutants were capable of being downregulated by ORF8, if not at higher degrees than WT pIgR (Fig. 10B-C). This could also be explained by the decreased stability observed for some of these mutants, most notably ΔD1, ΔD1-3, and ΔD1-4 (Fig. 10B-C). Additionally, co-immunoprecipitation of these mutants using anti-FLAG beads on HEK293T co-transfected cell lysates failed to highlight any interactions between ORF8 and the pIgR mutants due to the low expression and poor stability of the pIgR mutants (Fig. 10D).

To confirm this observation, we decided to see how some of the ORF8 mutants, C20A and YNLF), which demonstrated poor antagonization of pIgR expression due to low interaction, would affect the pIgR mutants; and whether this could confirm if the previously described downregulation of the pIgR mutants was ORF8-specific or rather due to the low stability. In HEK293T cells co-transfected with the pIgR mutants and C20A ORF8 plasmids, we observed a similar downregulation of WT pIgR (40%) as previously mentioned (Fig. 10E-F). Furthermore, we failed to observe more than 30% downregulation of the pIgR mutants, with ΔD1-5 being unaffected by the presence of C20A ORF8 (Fig. 10E-F). Contrastingly, in HEK293T cells co-

transfected with the pIgR mutants and YNLF ORF8 plasmids, we observed only a 10% downregulation of WT pIgR, and downregulation of the pIgR mutants did not exceed 15%, except for ΔD1-5 which displayed a 40% downregulation when co-expressed with YNLF ORF8 (Fig. 8G-H). Overall, we observed that ORF8 mutants, which do not bind pIgR potently, tend to exert lower downregulation of the pIgR mutants (C20A average of 13.4% downregulation across pIgR mutants; YNLF average of 20.7% downregulation across pIgR mutants; Fig. 10E-H) when compared to WT ORF8 (average of 40% downregulation across pIgR mutants; Fig. 5B-C). This highlights the importance of ORF8 binding mediated by dimerization in contribution to pIgR downregulation. Regarding discrepancies in the downregulation of ΔD1-5 by C20A and YNLF, this may be due to the stability of this mutant. However, whether this may also indicate a possible binding site for YNLF outside of pIgR ectodomain, which might not be accessible when WT pIgR is folded, requires further investigation.

3.7.2 Secretory ORF8 and dIgA interact mainly with D1 of pIgR.

Since ORF8 co-expression potently downregulated the pIgR mutants and made it difficult to detect pIgR mutants in the co-IP study, we sought to investigate binding of soluble ORF8 to the pIgR mutants. To assess expression of these mutants, we expressed pIgR mutants in HEK293T cells which were stained and analyzed by flow cytometry. In agreement with previous data, we observed low expression for the pIgR mutants ΔD1, ΔD1-3, and ΔD1-4 (Fig. 11A-B). This potentially highlights the importance of extracellular D1, D3, and D4 at maintaining the stability of pIgR structure. In fact, *in silico* and *in vitro* analyses have described the main structural interactions between pIgR to be found between the binding of D1 to D2, D4, and D5, and the bindings of D2 and D3, as well as D4 and D5[195].

To investigate which extracellular domain is important for ORF8 binding to pIgR, we

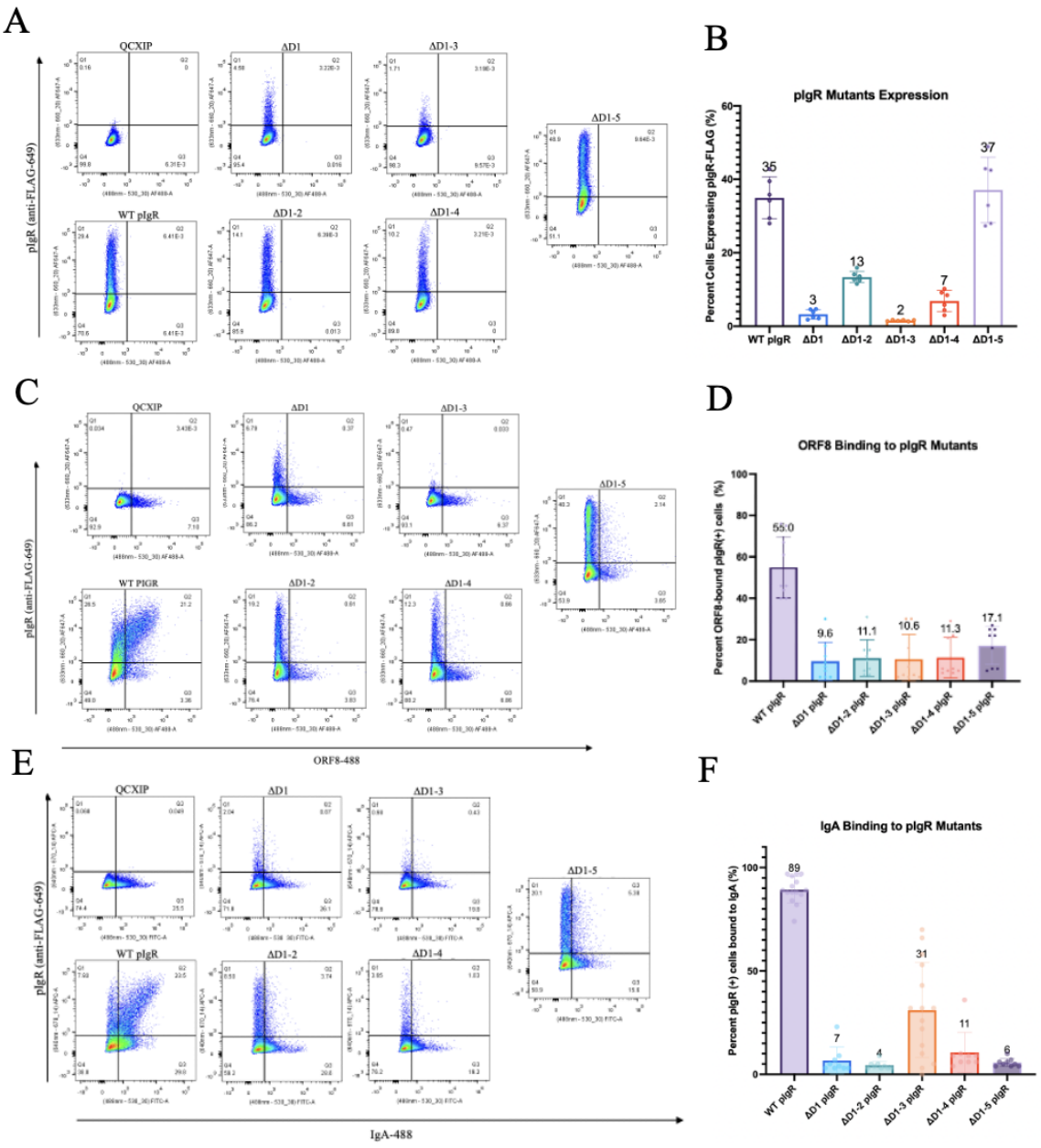

Figure 11. Secretory ORF8 and dIgA interact with D1 of pIgR. (A-F) HEK293T cells transfected with 250ng pIgR or pIgR mutants and (**A-F**) treated with 10µg/ml ORF-488 (**C-D**) or 10µg/ml IgA-488 (**E-F**) for 30 minutes on ice. Cells stained with anti-FLAG (pIgR) and ORF8 and IgA binding analyzed by flow cytometry. Data analyzed by PrismV9 (mean with SD; statistical significance measured via one-way Anova; * $p \leq 0.05$, ** $p \leq 0.01$, *** $p \leq 0.001$, **** $p \leq 0.0001$).

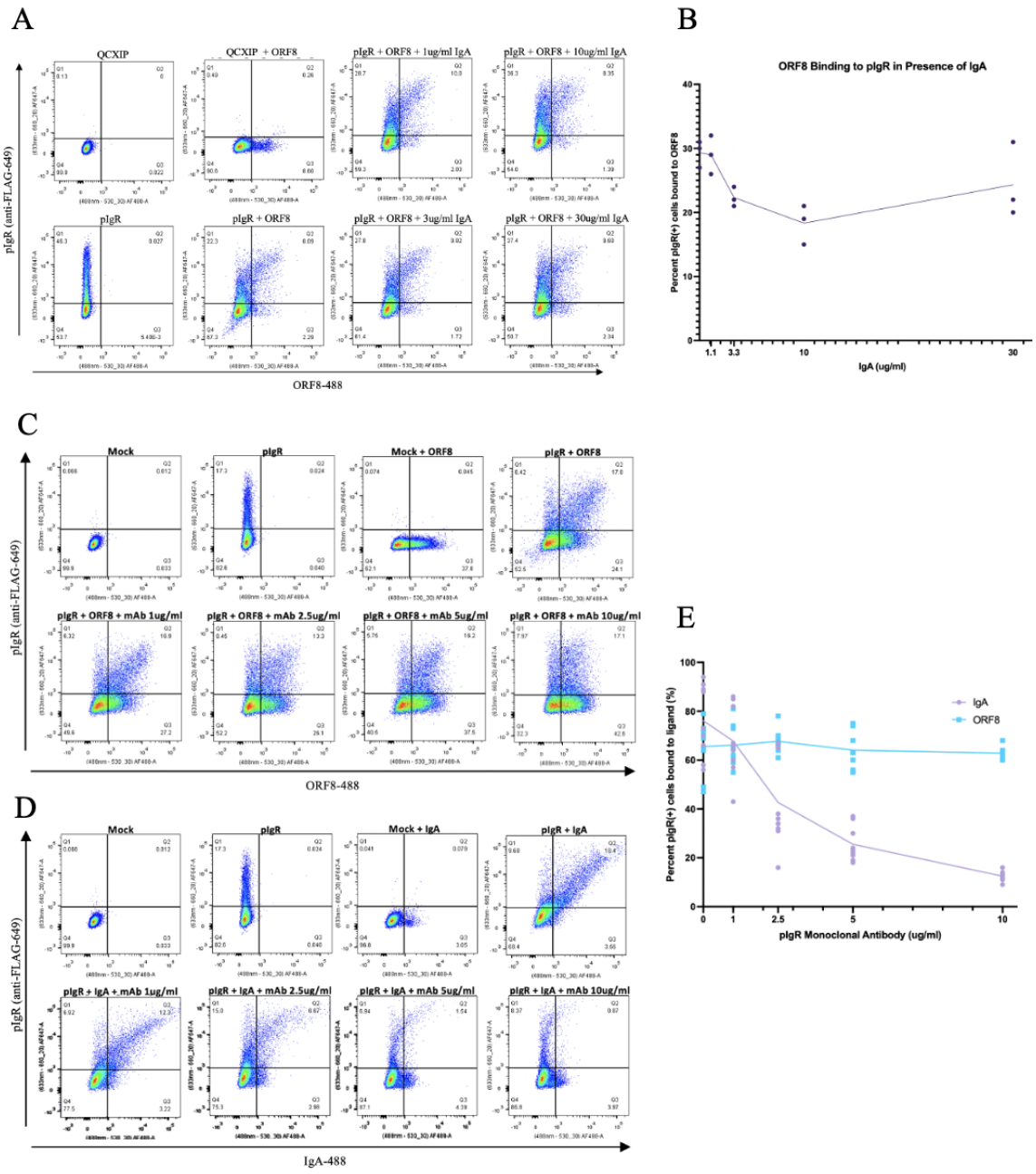

Figure 12. SARS-CoV-2 ORF8 does not compete with IgA for binding to pIgR. (**A-B**) HEK293T cells transfected with 250ng pIgR and QCXIP and treated with 10µg/ml ORF8-488 and a titration of IgA (1µg/ml, 3µg/ml, 10µg/ml, 30µg/ml) for 30 minutes on ice. (**B**) ORF8 binding to pIgR-positive cells analyzed with PrismV9. (**C-E**) HEK293T cells transfected with 250ng pIgR and QCXIP and treated with either 10µg/ml ORF8-488 (**C**) or 10µg/ml IgA-488 (**D**) and a titration of anti-pIgR monoclonal blocking antibody (1µg/ml, 2.5µg/ml, 5µg/ml, 10µg/ml). (**E**) ORF8 and IgA binding to pIgR-positive cells analyzed with PrismV9.

transfected HEK293T cells with WT and mutant pIgR plasmids and treated the cells with soluble ORF8 for 30 minutes at 4°C. We observed strong binding of soluble ORF8 to WT pIgR, but not to any of the pIgR mutants (Fig. 11C-D). This indicated that the main interaction site for secretory ORF8 likely resides within pIgR extracellular D1. To compare whether this overlapped with the binding site for dIgA, we repeated the experiment but incubated the cells with dIgA for 30 minutes at 4°C instead of ORF8. Similarly, we observed strong binding of dIgA to WT pIgR, but not to the other pIgR mutants (Fig. 11E-F). Of note, quantification revealed strong binding of dIgA to the pIgR mutant ΔD1-3, but this may be a result of the low stability and expression of this mutant skewing the quantification (Fig. 11E-F). Overall, these data suggest that the primary binding sites for both ORF8 and dIgA most likely reside within the extracellular D1 of pIgR.

3.7.3 Secreted ORF8 and dIgA bind independently to pIgR.

To investigate whether ORF8 and dIgA binding to the same domain of pIgR could lead to competition, we transfected HEK293T cells with WT pIgR plasmid and then incubated the cells with soluble ORF8 and a titration of dIgA at 4°C. We found that, even at the highest dose of IgA, ORF8 binding to pIgR was not blocked (Fig. 12A-B). This leads to two main hypotheses, the first being that ORF8 and dIgA bind to different sites on domain 1 of pIgR, and the second that ORF8 may be small enough to bind pIgR without disrupting dIgA binding. To test these hypotheses, we repeated the experiment but this time using a titration of pIgR monoclonal blocking antibody to block either ORF8 or dIgA binding. Although we observed effective blocking of dIgA binding to pIgR, the blocking antibody only promoted minimal antagonization against ORF8 binding (Fig. 12C-E). Altogether, these findings further support our previous hypotheses and highlight that both ORF8 and dIgA maintain interactions with the extracellular domain 1 of pIgR independently of

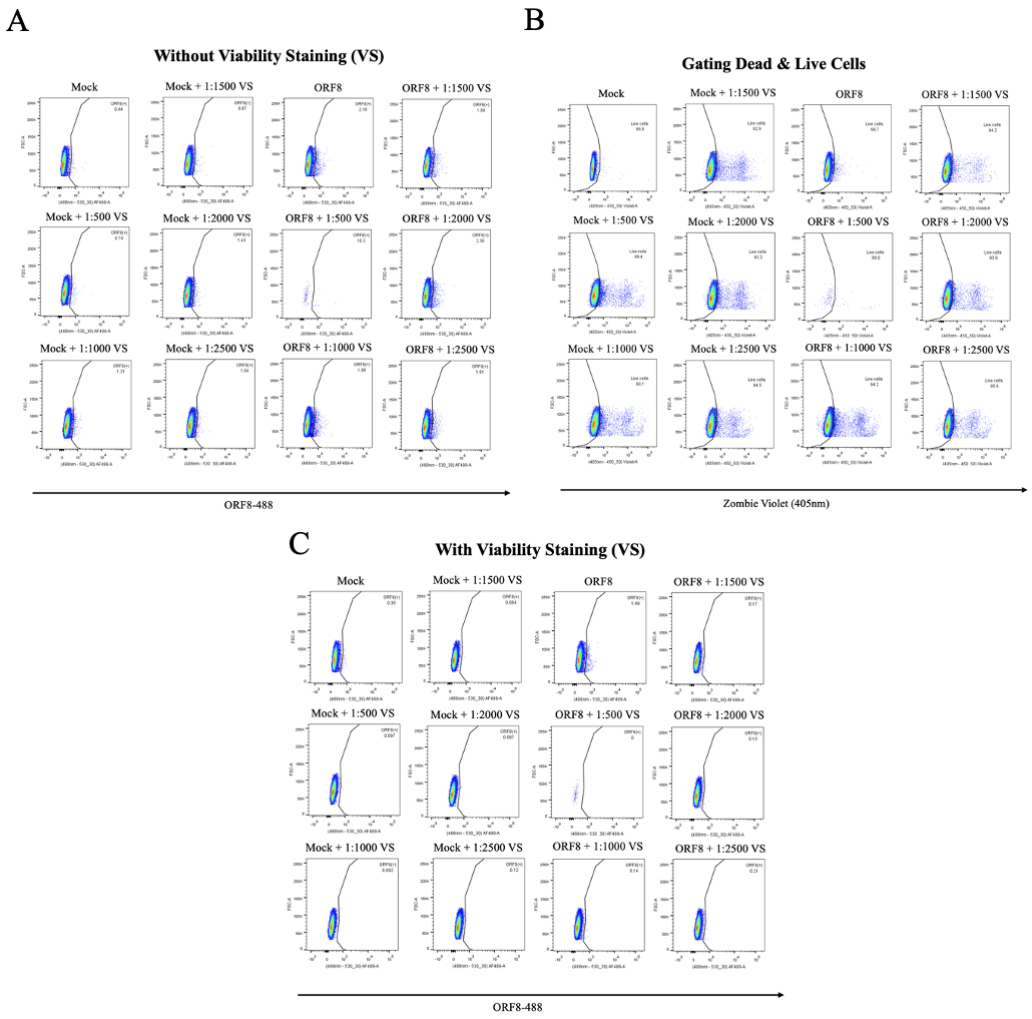

Figure 13. Optimizing flow cytometry staining to remove background ORF8 binding. (**A-C**) HEK293T cells transfected with 250ng pIgR and 250ng QCXIP, incubated with 10µg/ml ORF8-488 for 30 minutes on ice and stained with titrations of viability staining (zombie violet; 1:500, 1:1000, 1:1500, 1:2000, 1:2500). (**A**) ORF8 binding before applying viability staining gating strategy. (**B**) Viability staining gating. (**C**) ORF8 binding after applying viability staining gating strategy.

one another.

To ensure specificity of ORF8 and dIgA binding to pIgR, we sought to optimize our flow cytometry assay to remove background binding observed in Figures 11-12. In other experiments, my colleague, Qinghua Pan, had noticed low ORF8 binding to cells stained with Annexin V, a cell

viability marker[233]. However, due to my experimental limitations requiring staining to be performed prior to fixation, we could not use annexin V[233]. To mitigate this issue, we transfected HEK293T cells with pQCXIP mock plasmid and treated the cells with soluble ORF8 and a titration of Zombie Violet stain, a cell viability marker which can be used on live cells. Using this marker, we noticed a marked reduction in background binding of ORF8 to mock-transfected cells when compared to cells (Fig. 13A-C). Hence, we incorporated this staining in all following flow cytometry experiments with HEK293T cells.

To confirm the lack of competition between dIgA and ORF8 observed in HEK293T cells, we sought to investigate this relationship in the context of endogenous pIgR expression. To establish a functioning cellular system for a dIgA binding and internalization assay using endogenous pIgR, we optimized dIgA binding to Calu-3 and Caco-2 cells. In Caco-2 cells, binding was saturated at 30 μg/ml dIgA, while Calu-3 cells saturated at 100 μg/ml dIgA and incubation with 30 μg/ml led to around 70% dIgA binding (Fig. 14A). Hence, we decided to use 30 μg/ml dIgA when using Calu-3 cells as saturation may render competition with weaker ligands more difficult to observe. We proceeded to incubate Calu-3 cells with an increasing titration of dIgA and a constant dose of soluble ORF8. At the lowest dose of dIgA, we did not observe the capacity of secreted ORF8 to antagonize dIgA binding (Fig. 14B-C). Altogether, these results suggest a lack of competition between IgA and ORF8, as similarly observed in HEK293T cells. However, in a repeat of this assay, this time using a constant dose of dIgA, we observed dIgA binding decreased from around 23.3% to 4.8% in the presence of soluble ORF8 (Fig. 14E). These confounding findings could be a result of external factors, such as differences reagent lots or cell age, which may have affected the health of the cells and subsequently the stability of pIgR expression. Altogether, our data have suggested that ORF8 cannot compete against dIgA binding to either

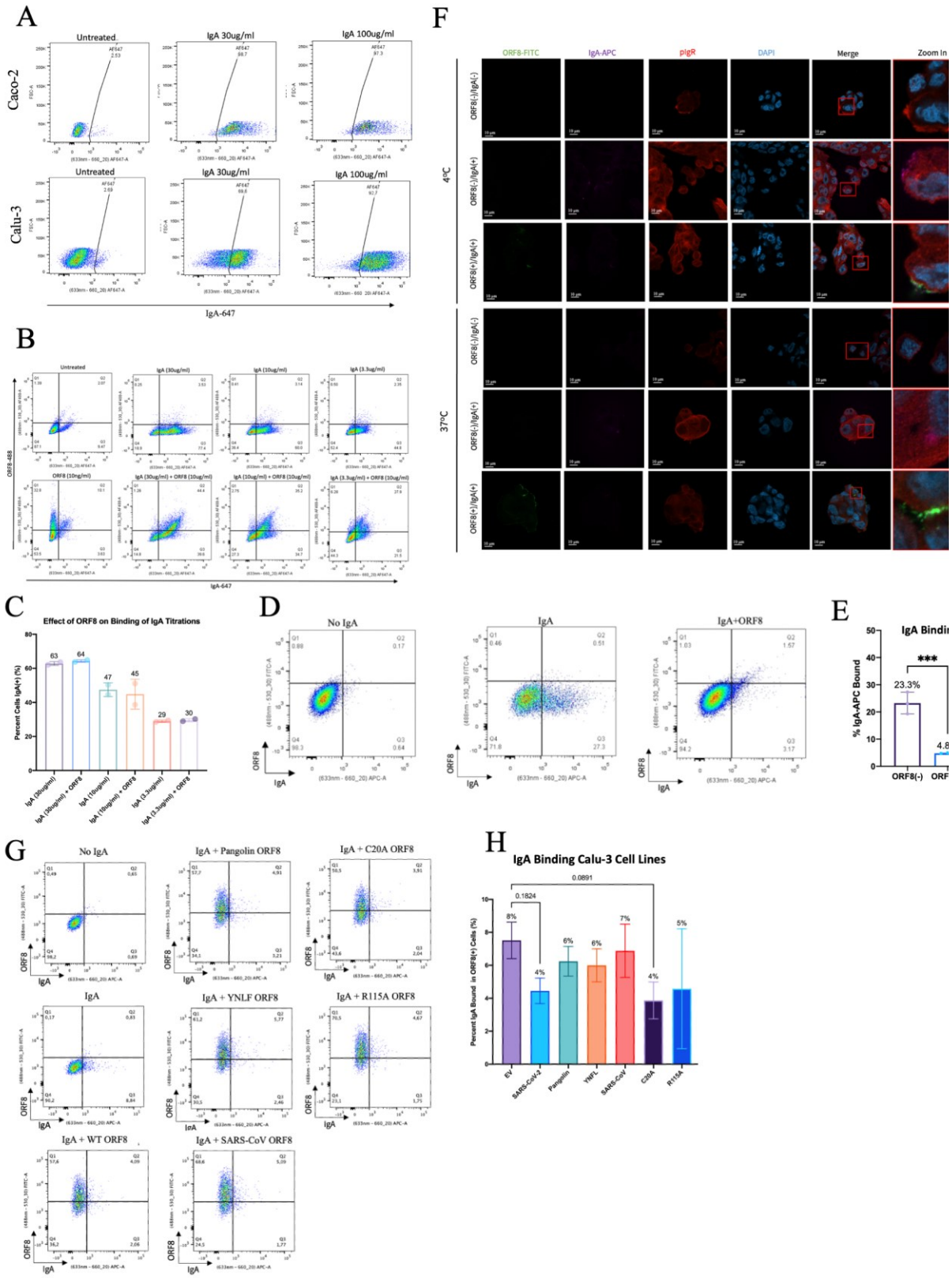
A
Untreated
IgA 30ug/ml
IgA 100ug/ml
Caco-2
Calu-3
IgA-647
B
Untreated
IgA (30ug/ml)
IgA (10ug/ml)
IgA (3.3ug/ml)
ORF8 (10ng/ml)
IgA (30ug/ml) + ORF8 (10ug/ml)
IgA (10ug/ml) + ORF8 (10ug/ml)
IgA (3.3ug/ml) + ORF8 (10ug/ml)
ORF8-488
IgA-647
C
Effect of ORF8 on Binding of IgA Titrations
Percent Cells IgA(+) (%)
63
64
47
45
29
30
IgA (30ug/ml)
IgA (30ug/ml) + ORF8
IgA (10ug/ml)
IgA (10ug/ml) + ORF8
IgA (3.3ug/ml)
IgA (3.3ug/ml) + ORF8
D
No IgA
IgA
IgA+ORF8
ORF8
IgA
E
IgA Bindi
% IgA-APC Bound
***
23.3%
ORF8(-)
F
ORF8-FITC
IgA-APC
pIgR
DAPI
Merge
Zoom In
4°C
37°C
ORF8(-)/IgA(-)
ORF8(-)/IgA(+)
ORF8(+)/IgA(+)
G
No IgA
IgA + Pangolin ORF8
IgA + C20A ORF8
IgA
IgA + YNLF ORF8
IgA + R115A ORF8
IgA + WT ORF8
IgA + SARS-CoV ORF8
H
IgA Binding Calu-3 Cell Lines
0.0891
0.1824
Percent IgA Bound in ORF8(+) Cells (%)
8%
4%
6%
6%
7%
4%
5%
EV
SARS-CoV-2
Pangolin
YNFL
SARS-CoV
C20A
R115A

Figure 14. ORF8 appears to prevent IgA internalization but not binding in Calu-3 cells. (**A**) Calu-3 and Caco-2 cells incubated with a titration of IgA-647 (30µg/ml, 100µg/ml) on ice for 30 minutes and analyzed by flow cytometry. (**B-C**) Calu-3 cells incubated with a titration of IgA-647 (3.3µg/ml, 10µg/ml, 30µg/ml) and 10µg/ml ORF8-488 for 30 minutes ice, followed by flow cytometry analysis. (**D-E**) Calu-3 cells incubated with 30µg/ml IgA-647 and 10µg/ml ORF8-488 for 30 minutes ice, followed by flow cytometry analysis. (**G-H**) Calu-3 cells lines expressing ORF8, and its mutants incubated with 30µg/ml IgA-647 for 30 minutes ice, followed by flow cytometry analysis. (**F**) Calu-3 cells incubated with 30µg/ml IgA-647 (purple) and 10µg/ml ORF8-488 (green) for 30 minutes ice, followed by pIgR staining (rabbit anti-pIgR; anti-rabbit-568; red). Immunofluorescence assessed by confocal microscopy. Data analyzed with Prism V9 (mean with SD; statistical significance measured via one-way Anova; * $p \leq 0.05$, ** $p \leq 0.01$, *** $p \leq 0.001$, **** $p \leq 0.0001$).

---

endogenous or exogenous pIgR.

3.8. Intracellular SARS-CoV-2 ORF8 antagonizes IgA binding to pIgR.

The transcytosis and secretion of dIgA across epithelial cells consists one of the first adaptive immune responses against incoming pathogens[197]. The initiating steps of transcytosis involve the engagement of pIgR D1 and D5, which leads to a conformational change within pIgR and opens the receptor, exposing binding motifs in D1, D4 and D5 that engage with dIgA into its final binding state[195]. Subsequently, the pIgR-dIgA complex undergoes clathrin-dependent internalization where it traverses to basolateral early endosomes and is assisted by Rab11 proteins to complete its transcytosis towards to apical pole of epithelial cells, allowing the complex to be cleaved and released as sIgA [193,234].

To assess the functional effect of ORF8 downregulation of pIgR, we decided to focus on the initiating steps of pIgR-dIgA transcytosis, binding, and internalization. Since previous experiments had determined a lack of competition between secretory ORF8 and dIgA (Fig. 11A-B), we sought to investigate whether intracellular ORF8 had the capacity to antagonize IgA binding

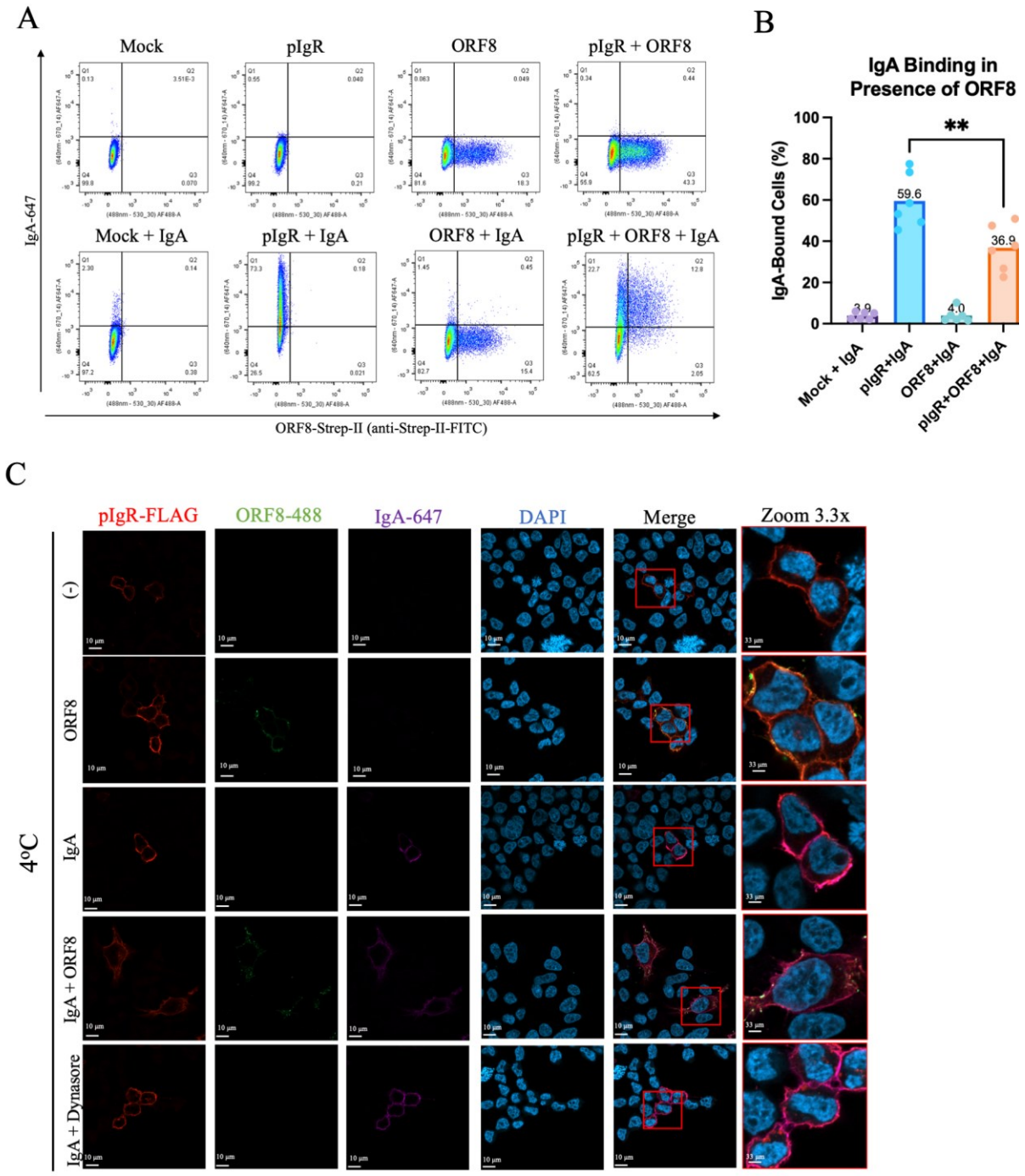
A
Mock
pIgR
ORF8
pIgR + ORF8
Mock + IgA
pIgR + IgA
ORF8 + IgA
pIgR + ORF8 + IgA
IgA-647
ORF8-Strep-II (anti-Strep-II-FITC)
B
IgA Binding in Presence of ORF8
IgA-Bound Cells (%)
**
59.6
36.9
4.0
3.9
Mock + IgA
pIgR+IgA
ORF8+IgA
pIgR+ORF8+IgA
C
pIgR-FLAG
ORF8-488
IgA-647
DAPI
Merge
Zoom 3.3x
4°C
(-)
ORF8
IgA
IgA + ORF8
IgA + Dynasore

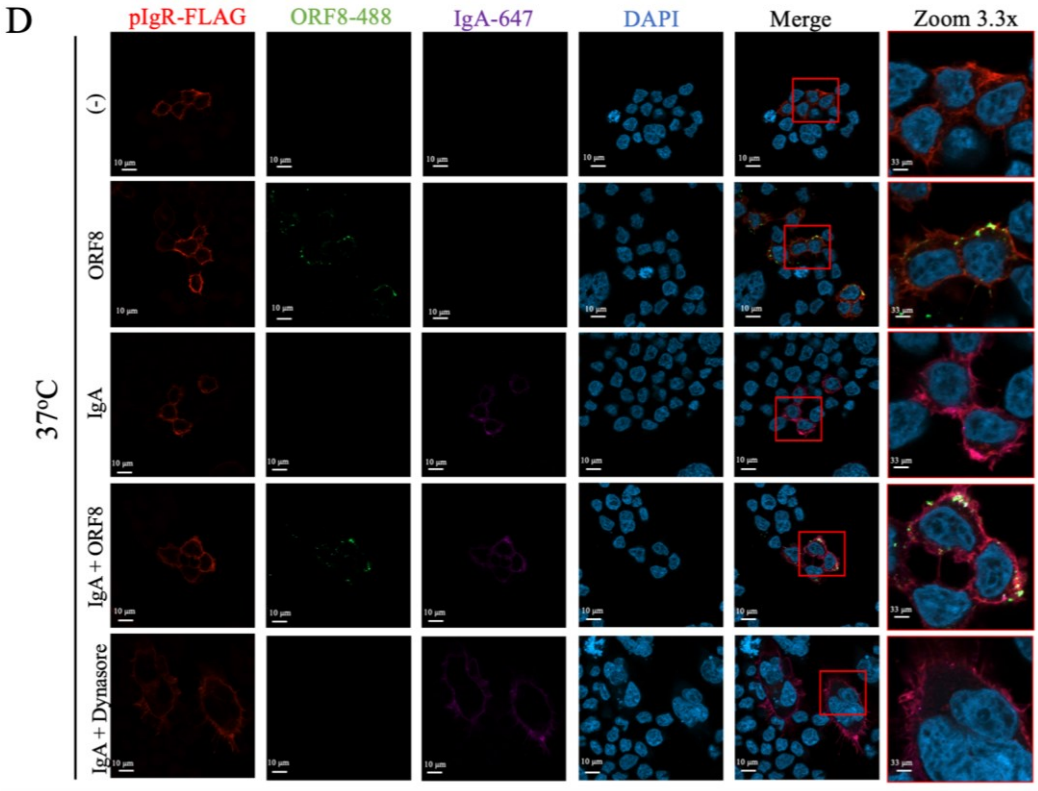
D
pIgR-FLAG
ORF8-488
IgA-647
DAPI
Merge
Zoom 3.3x
37°C
(-)
ORF8
IgA
IgA + ORF8
IgA + Dynasore

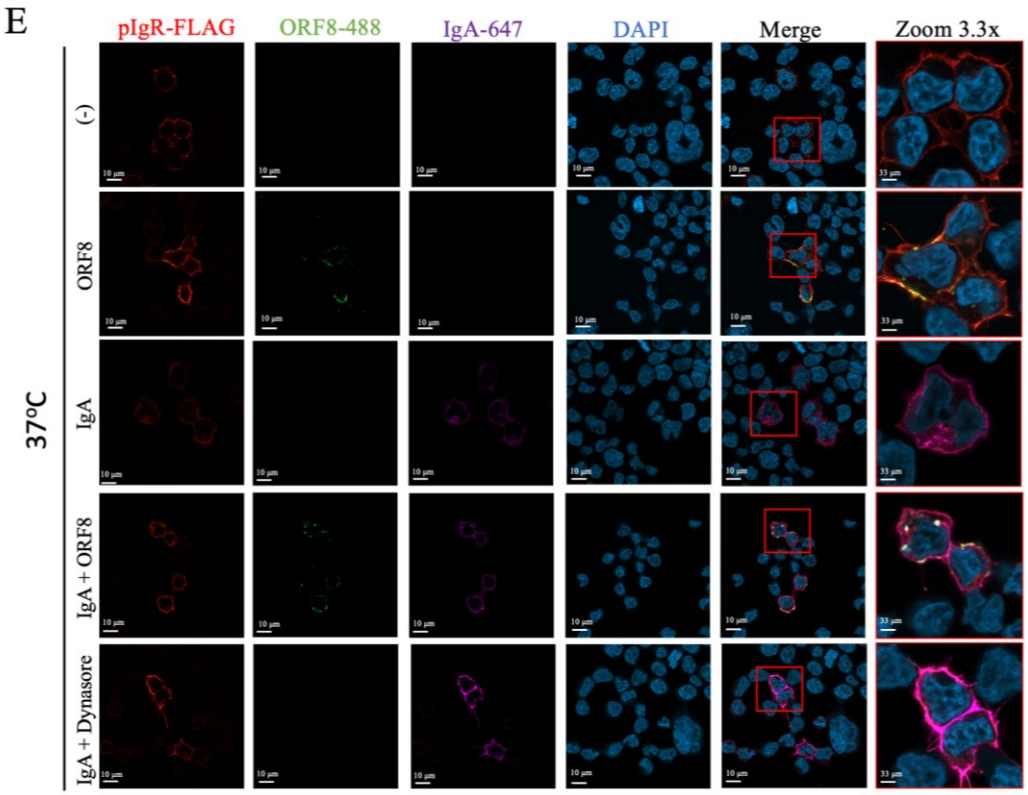
E
pIgR-FLAG
ORF8-488
IgA-647
DAPI
Merge
Zoom 3.3x
37°C
(-)
ORF8
IgA
IgA + ORF8
IgA + Dynasore

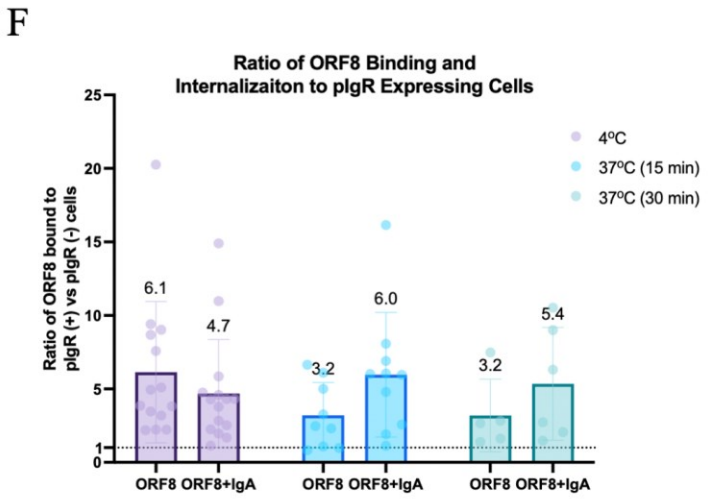

Figure 15. Intracellular ORF8 antagonizes IgA binding while secreted ORF8 exploits the pIgR-endocytosis pathway. (**A-B**) HEK293T cells co-transfected with 250ng pIgR, 250ng QCXIP, and 500ng SARS-CoV-2 ORF8 expression plasmids. Cells incubated with 10µg/ml IgA-647 for 30 minutes on ice and stained for ORF8-Strep-II (anti-Strep-II-FITC). IgA binding assessed by flow cytometry. (**C-F**) HEK293T cells co-transfected with 250ng pIgR and 250ng QCXIP expression plasmids, then treated with 10µg/ml IgA-647 (purple) and/or 10µg/ml ORF8-488 (green) for 30 minutes on ice. Cells washed and incubated at 37ºC for 15 and 30 minutes. Cells stained for pIgR-FLAG (anti-FLAG; red), and DAPI (blue). Cellular localization visualized by confocal microscopy. (**F**) Macro developed by Mathew Duguay on Fiji to analyze and quantify ratio of ORF8 bound and internalized to pIgR expressing vs. pIgR naïve cells. Data analyzed with Prism V9 (mean with SD; statistical significance measured via one-way Anova; * $p \leq 0.05$, ** $p \leq 0.01$, *** $p \leq 0.001$, **** $p \leq 0.0001$).

---

due to the downregulation of pIgR expression. Hence, we incubated HEK293T cells co-expressing pIgR and ORF8 with dIgA and assessed binding by flow cytometry. Concordantly, we found that intracellular ORF8 antagonized total dIgA binding to pIgR-expressing cells (Fig. 15A-B). Specifically, the mean dIgA binding to pIgR-expressing cells was of 59.6%, but it dropped to

36.9% in the presence of ORF8 (Fig. 15B). This suggests the capacity of intracellular ORF8 to antagonize the early steps of transcytosis by interfering with the binding of dIgA to pIgR. Interestingly, we observed an increase in intracellular ORF8 expression when co-expressed with pIgR (Fig. 12A). This increase was not observed in previous assays where pIgR and ORF8 were co-expressed (Fig. 10D-E; Fig. 11E-H), but we believe this could be a result of secreted ORF8 getting internalized by surrounding pIgR-expressing cells leading to accumulation in non-ORF8-expressing cells, although this needs to be further investigated.

To investigate whether the decrease in dIgA binding in the presence of intracellular ORF8 was due to decreased cell-surface pIgR expression, we optimized our staining protocol for cell-surface pIgR. Using the pIgR blocking antibody, we successfully stained cell-surface pIgR with little to no background staining of mock-transfected and ORF8-treated cells (Supp. Fig. 1A). We did notice that pIgR levels (~85%) seemed to be much higher than those detected with the anti-FLAG antibody in previous experiments (~50%) (Fig. 9A). Whether this could be due to the blocking antibody having a greater sensitivity to pIgR remains to be investigated. Using this staining method, we unexpectedly observed a slight increase in the mean cell-surface pIgR expression in the presence of ORF8 from 73.8% to 84.9% (Fig. 16C). This could indicate that ORF8 may antagonize dIgA binding by an alternate mechanism than decreasing pIgR cell-surface expression, but whether this perceived increase is due to a lack of optimization of our staining methods cannot be excluded.

To understand whether antagonization of IgA binding by intracellular ORF8 was ubiquitous to both exogenously and endogenously expressed pIgR, we incubated the Calu-3 cell lines stably expressing SARS-CoV-2 ORF8 or its mutants with dIgA to assess binding. Although we did observe a mild decrease in dIgA binding in cells expressing SARS-CoV-2 and C20A ORF8,

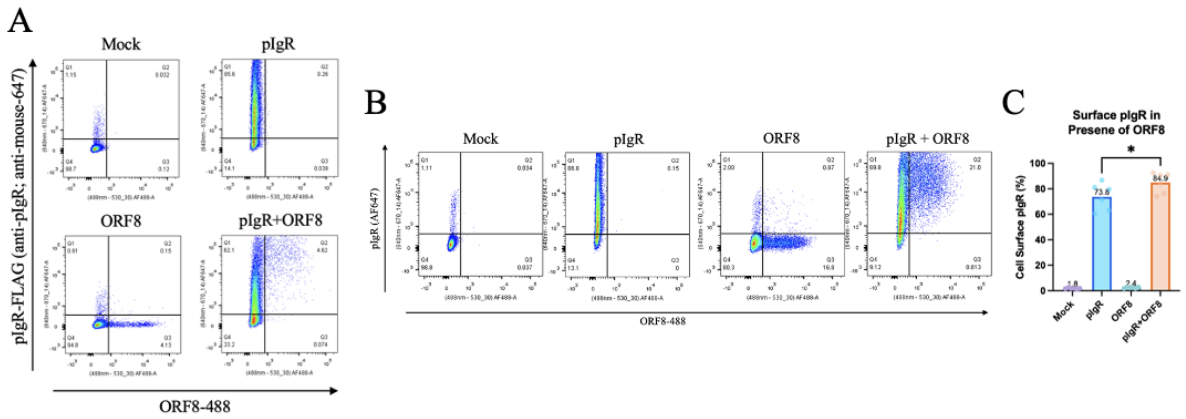

Figure 16. Optimizing cell-surface binding of pIgR. (**A-C**) HEK293T cells co-transfected with 250ng pIgR, 250ng QCXIP. Cells stained with mouse anti-pIgR monoclonal antibody (1:1000), followed by anti-mouse-647 (3µg/ml). Staining analyzed by flow cytometry. (**A**) Cells incubated with 10µg/ml ORF8-488. (**B-C**) Cells transfected with ORF8-Strep-II and stained with anti-Strep-II-FITC. Data analyzed with Prism V9 (mean with SD; statistical significance measured via one-way Anova; * $p \leq 0.05$, ** $p \leq 0.01$, *** $p \leq 0.001$, **** $p \leq 0.0001$).

---

we did not observe any statistically significant decreases (Fig. 14G-H). However, control binding of IgA to ORF8-naïve cells was very low (8%), so although binding dropped by half in the presence of SARS-CoV-2 and C20A ORF8 (4%), it is difficult to conclude on the importance of this finding within the context of infection. Altogether, we observed intracellular ORF8 expression to modulate pIgR and lead to a decrease in dIgA binding.

3.9. Secretory ORF8 exploits the pIgR-endocytosis pathway to potentially dampen mucosal immunity and promote early SARS-CoV-2 infection.

The secretory nature of ORF8 makes it a protein of interest due to its capacity to act systemically in the context of SARS-CoV-2 infection by potentially priming its surrounding environment to increase infection susceptibility. To assess this, we treated HEK293T cells expressing pIgR with either dIgA, soluble ORF8, or both at different temperatures to promote

either binding or internalization. At 4ºC, we observed both ORF8 and dIgA individually binding to cell-surface pIgR, and their co-incubation did not affect the binding of either protein (Fig. 15C). Furthermore, we observed that co-localization between ORF8 and dIgA binding occurred at pIgR-rich regions at the cell surface (Fig. 15C).

At 37ºC for 15 minutes, ORF8 and dIgA were individually localized close to the plasma membrane, but their signals had agglomerated together (Fig. 15D). Similarly, co-incubation of ORF8 and dIgA led to large punctates near the plasma membrane, likely indicating the localization of both proteins to the same pIgR-rich regions in preparation for internalization (Fig. 15D). This is in agreement with early studies which proposed that binding of dIgA to pIgR may induce homotypic dimerization of pIgR, which facilitates internalization of the dIgA-pIgR complex, although these findings have not been further investigated and corroborated[235]. However, our observations suggest a clustering event of pIgR in response to dIgA binding, supported by the hypothesized homodimerization of pIgR.

Further incubation at 37ºC for 30 minutes reveals little to no internalization of soluble ORF8 alone by pIgR (Fig. 15 E). As for dIgA, we observed clear internalization represented by multiple small intracellular punctates overlapping with pIgR signals (Fig. 15E). Interestingly, when ORF8 is co-incubated with dIgA, we observed the internalization of large punctates containing ORF8, dIgA, and pIgR (Fig. 15E). This finding suggests that secreted ORF8 may be dependent on dIgA for internalization by pIgR. Of note, we did observe ORF8 binding to non-pIgR expressing cells in all our imaging. However, through analysis of these images using Fiji, we confirmed that ORF8 was 3-6 times more likely to bind pIgR-expressing cells (Fig. 15F). Altogether, these results suggest the dependence of ORF8 on the pIgR-dIgA complex for internalization into cells. This further highlights a mechanism by which secreted ORF8 produced

by SARS-CoV-2 infected cells may enter naïve-uninfected cells to exert its known immunomodulatory functions and render these cells more permissive to infection, hence exacerbating disease severity.

However, we observed that secreted ORF8 behaved differently in the presence of endogenous pIgR expressed by Calu-3 cells. In similar conditions to HEK293T cells, we found that ORF8 binds to the same regions on the surface of Calu-3 cells as dIgA without disrupting binding; however, ORF8 appears to aggregate and retain dIgA near the cell membrane, indicating the capacity of ORF8 to potentially prevent internalization of dIgA by pIgR (Fig. 14). These findings contrast with our observations in HEK293T cells, where we found that ORF8 was dependent on the pIgR-dIgA complex for internalization. Whether this could be due to differences in the internalization of the pIgR-dIgA across different cell lines or the use of endogenous versus exogenous pIgR merits further investigation.

3.10. Transferrin may use pIgR for internalization in cells expressing low levels of transferrin receptor 1.

When performing our binding and internalization assay using dIgA and ORF8, we sought to introduce a control for internalization. Since all nucleated cells can uptake transferrin, we used conjugated transferrin as our internalization control. We found that mock-transfected HEK293T cells were unable to uptake significant amounts of transferrin (data not shown), which could be a result of low transferrin receptor 1 (TFR1) expression[236,237]. We proceeded to transfect HEK293T cells with TFR1 and incubated cells at 4ºC with conjugated transferrin and followed with either a 15-minute or 30-minute incubation at 37ºC to assess internalization. This assay allowed to confirm successful internalization of transferrin at both 15-minutes and 30-minute in TFR1-expressing HEK293T cells (Fig. 17A). We had initially performed this experiment with pIgR as our control

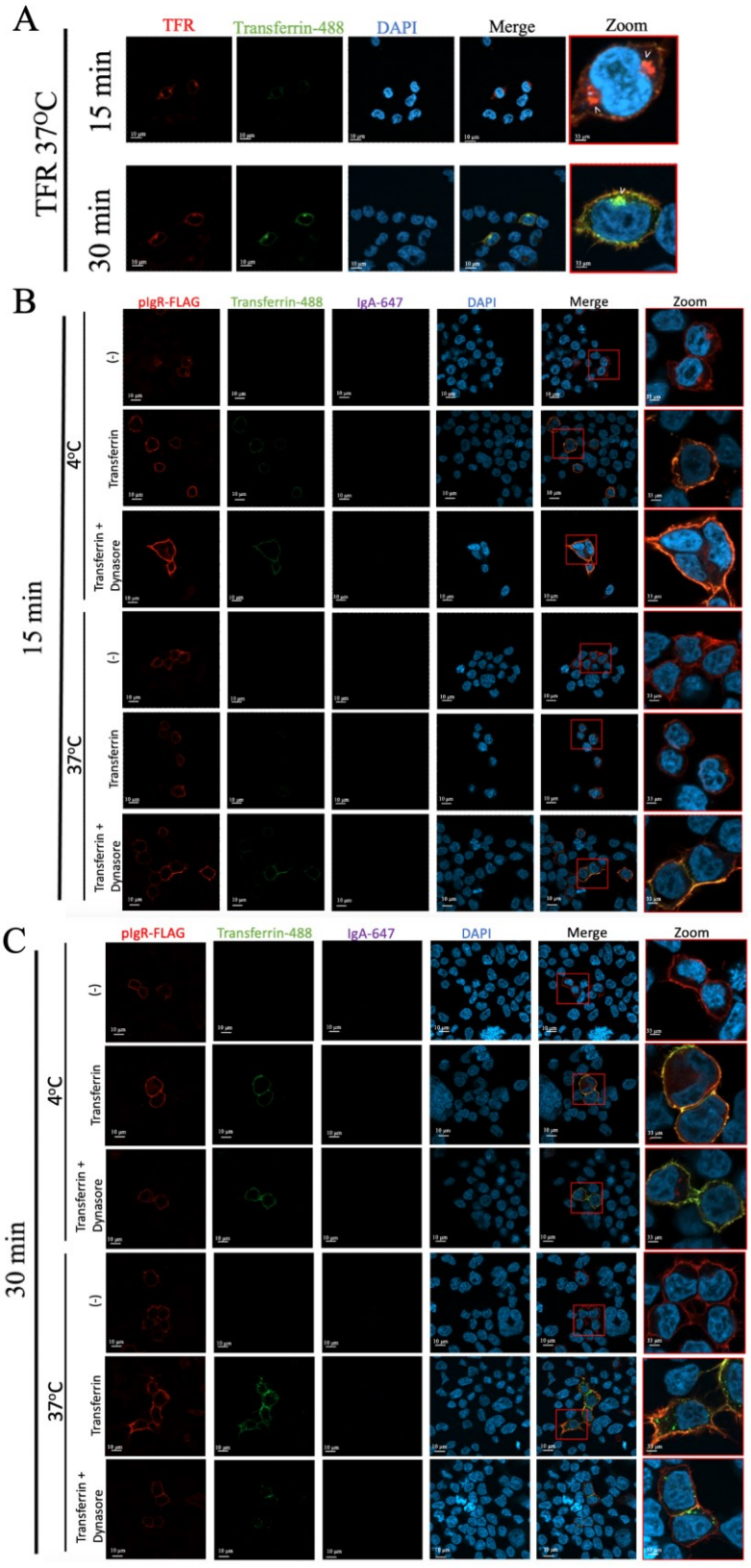
A
TFR
Transferrin-488
DAPI
Merge
Zoom
TFR 37°C
15 min
30 min
B
pIgR-FLAG
Transferrin-488
IgA-647
DAPI
Merge
Zoom
15 min
4°C
37°C
(-)
Transferrin
Transferrin + Dynasore
C
pIgR-FLAG
Transferrin-488
IgA-647
DAPI
Merge
Zoom
30 min
4°C
37°C
(-)
Transferrin
Transferrin + Dynasore

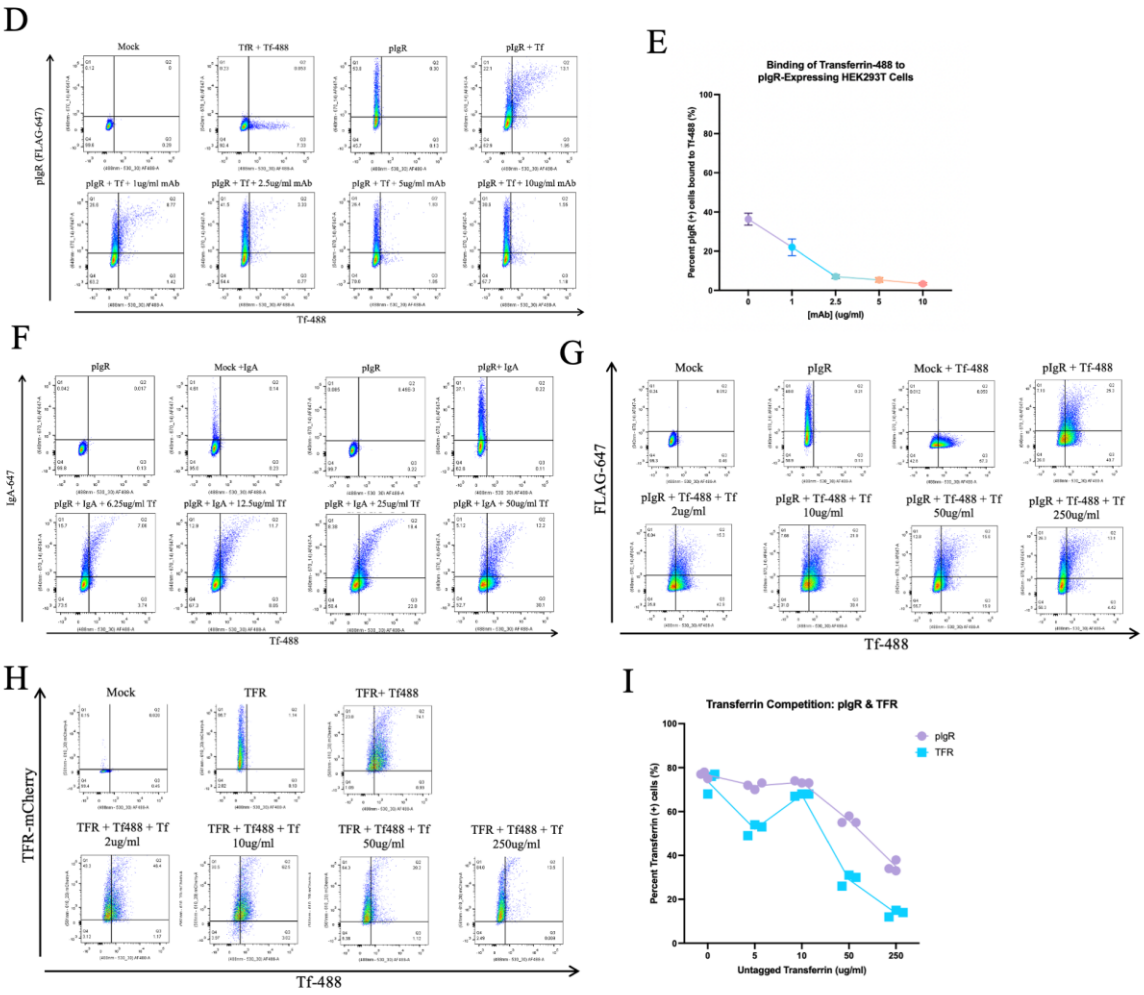

Figure 17. pIgR binds and internalizes transferrin. (**A**) HEK293T cells transfected with TFR1 (Dr. Kostas Pantapoulous) and incubated with 25µg/ml for 90 minutes at 4ºC, and then incubated at 37ºC for 15 minutes and 30 minutes. (**B-C**) HEK293T cells transfected with pIgR and incubated with 25µg/ml for 90 minutes at 4ºC, and then incubated at 37ºC for 15 minutes (**B**) and 30 minutes (**C**)**.** (**A-C**) Cells stained and analyzed by confocal microscopy. (**D-E**) HEK293T cells transfected with pIgR and incubated with 25µg/ml transferrin-488 and a titration of pIgR mAb (1µg/ml, 2.5µg/ml, 5µg/ml, 10µg/ml) for 90 minutes at 4ºC. (**F**) HEK293T cells transfected with pIgR and incubated with a titration of transferrin-488 (6.25µg/ml, 12.5µg/ml, 25µg/ml, 50µg/ml) and 10µg/ml IgA-647 for 90 minutes at 4ºC. (**G-I**) HEK293T cells transfected with either pIgR or TFR1-mCherry and incubated with 25µg/ml serum transferrin-488 and a titration of unconjugated serum transferrin (2µg/ml, 10µg/ml, 50µg/ml, 250µg/ml) for 90 minutes at 4ºC. (**D-I**) Cells quantified analyzed by flow cytometry and analyzed using PrismV9.

for internalization in our previous binding and internalization assay, where we had interestingly observed that transferrin was bound to pIgR-expressing cells when incubated at 4ºC (Fig. 17B-C). We further observed transferrin internalization by pIgR when incubated for 30 minutes at 37ºC (Fig. 17B-C). These results led us to hypothesize that pIgR may act as a novel receptor for transferrin uptake in cells which express low levels of TFR1. However, it is interesting to note that internalization of transferrin by pIgR appears to be slower and less potent than with TFR1, as we saw little to no internalization after a 15-minute incubation at 37ºC (Fig. 17B). Overall, these results suggest the potential of pIgR to act as a novel receptor for transferrin endocytosis.

Iron is an essential micronutrient found primarily within hemoglobin of red blood cells (RBCs)[238]. Due to the low availability of biologically active iron, reticuloendothelial macrophages and liver hepatocytes will not only serve as major storing sites for the micronutrient, but also contribute heavily towards its recycling from RBCs[238]. Circulating Iron is found bound to transferrin, which has the capacity to bind and maintain 2 iron molecules in their redox inert state. Transferrin will deliver iron to different tissues mainly through the ubiquitously expressed transferrin receptor 1 (TFR1) and its homologue transferrin receptor 2 (TFR2) found on hepatocytes and erythrocytes[238–241]. Internalization into endosomes is triggered through binding of differic transferrin on the plasma membrane to TFR1, where acidification and ferriductases will allow the release and reduction of iron, which will be exported into the cytoplasm by the divalent metal transporter 1 (DMT1) and stored as ferritin[238,242–244]. Meanwhile, TFR1 will be recycled to the plasma membrane for further transferrin uptake[238]. In the case of excess cellular iron, ferroportin 1 (FPN1) meditates the secretion of iron, which is regulated by the release of liver-derived hepcidin which can bind and downregulate FPN1 when body iron levels are sufficient[238,245,246]. Iron homeostasis plays an important role towards immune responses, as an iron

deplete state can lead to immune dysfunctions including decreased neutrophil recruitment, natural killer (NK) cell dysfunction, decreased T cell proliferation, and antagonized antibody responses[247].

Although circulating iron is mainly found under the form of transferrin, two other members of the transferrin family proteins, notably lactoferrin and melanotransferrin, are also known to bind and transport ferric ions[248]. Lactoferrin is mainly found in secreted fluids which include milk, tears, saliva and bile, while melanotransferrin is rather expressed on salivary glands, skin and kidney[248,249]. Iron transporters of the transferrin protein family have been characterized for their critical role towards innate immunity. For instance, transferrin is known to sequester iron from pathogenic bacteria, hence promoting nutrient deficiencies to halt infection[248,250]. On the other hand, lactoferrin is less sensible to pH than transferrin, allowing it to sequester iron over a broad pH range[248]. Furthermore, lactoferrin possesses immunomodulatory properties as it is able to modulate the secretion of dIgA and pIgM, maturation of B- and T- lymphocytes, cytokine secretion, etc. in favour of pathogen clearance [251]. It has been further investigated for its antiviral properties, as it is believed to have broad activity against both enveloped RNA and DNA viruses by antagonizing different steps of the viral life cycle against viruses including Avian flu (H5N1), Hepatitis B virus (HBV), Human papillomavirus (HPV), Herpes simplex virus 1 and 2 (HSV-1, HSV-2), Human immunodeficiency virus (HIV), etc [251,252].

Of interest are recent studies which have highlighted lactoferrin having antiviral functions against SARS-CoV-2[252]. *In silico* and *in vitro* studies have suggested that lactoferrin and bovine lactoferrin, which share high homology, can compete with SARS-CoV-2 Spike binding to ACE2 and target the RNA-dependent RNA polymerase (RdRp) complex leading to effective antagonization of SARS-CoV-2 infection[252–257]. These findings are supported by clinical trial findings which have demonstrated that bovine lactoferrin supplementation can lead from mild to

moderate symptom improvement in COVID-19-infected patients[252,258,259].

Furthermore, iron homeostasis has been demonstrated to be critical during SARS-CoV-2 infection, such that hyperferritinemia (high levels of ferritin – iron stores – within cells) is common amongst patients admitted with severe COVID-19 and tends to be a clinical predictor of disease outcome[260,261]. Due to the large involvement of iron homeostasis towards immune responses during viral infections, the known existence of alternate iron receptors outside of TFR1 and TFR2, and our preliminary data demonstrating an interaction between transferrin and pIgR, we hypothesized that transferrin can use pIgR as an alternate receptor for cellular entry into lung epithelial cells[262]. To assess our hypothesis, we aimed to elucidate the molecular mechanism of transferrin binding to pIgR by characterizing its role in binding, internalization, and secretion.

To confirm whether the previously described transferrin binding and internalization was pIgR-dependent, transfected HEK293T cells with pIgR expression plasmid and incubated cells with transferrin and a titration of pIgR monoclonal blocking antibody. We found that the pIgR blocking antibody was effective in blocking transferrin binding to pIgR, with little to no background binding to HEK293T cells (Fig. 17D-E). This suggests that binding of transferrin to pIgR is specific and likely does not involve the binding of other surface receptors. This finding led us to question whether transferrin may have the capacity to compete with dIgA for binding to pIgR. However, when incubating pIgR-transfected HEK293T cells with dIgA and a titration of transferrin we did not observe a decrease in dIgA binding (Fig. 17F). Since we did not observe any competition between dIgA and transferrin, we incubated TFR1- and pIgR-transfected HEK293T cells with conjugated transferrin and a titration of unconjugated transferrin. With both TFR1 and pIgR, we observed the antagonization of conjugated transferrin by increased doses of unconjugated transferrin (Fig. 17G-H). These results confirmed that transferrin is binding both TFR1 and pIgR.

A

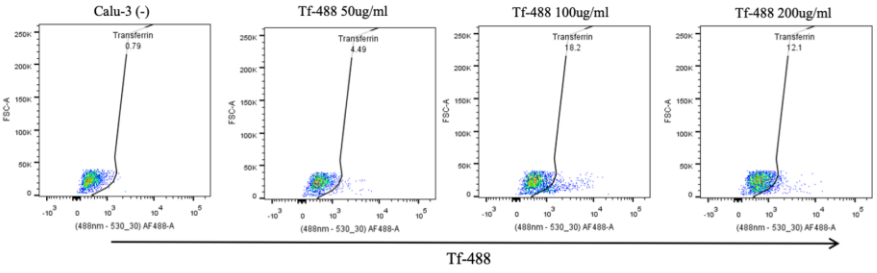

B

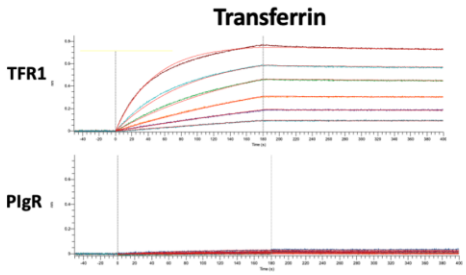

C

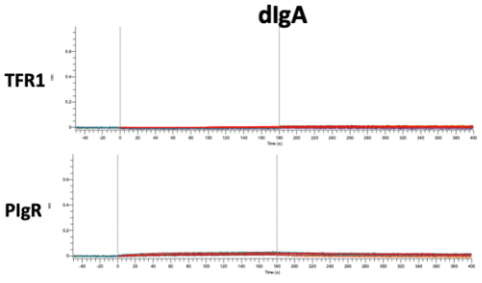

D

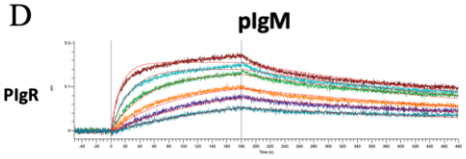

E

Receptor	Loading Sample	KD (M)
pIgR	Transferrin	-
	dIgA	-
	pIgM	$2.62x10^{-9} \pm 1.54x10^{-11}$
TFR1	Transferrin	$6.13x10^{-10} \pm 8.29x10^{-12}$
	dIgA	-

F

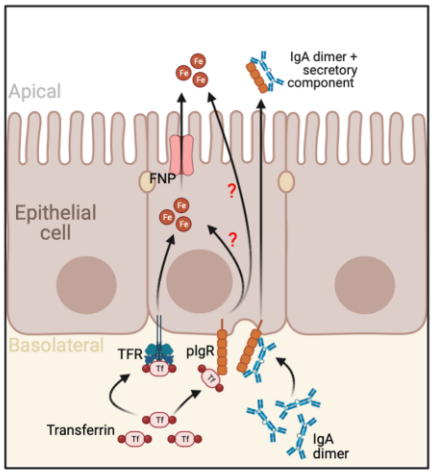

Figure 18. Transferrin and dIgA do not bind recombinant pIgR. (**A**) Calu-3 cells incubated with a titration of transferrin conjugated to Alexa fluor 488 (50µg/ml, 100µg/ml, 200µg/ml) for 30 minutes at 4ºC. Binding analyzed by flow cytometry. (**B-D**) Bio-layer interferometry (BLI) performed using recombinant pIgR (**B-D**) and recombinant TFR1 (**B-C**) as receptors, and transferrin (**B**), dIgA (**C**), and pIgM (**D**) as ligands (Mehdi Benlarbi, Dr. Andres Finzi lab). (**E**) Table of ligand bindings to pIgR and TFR1. (**F**) Graphical abstract describing transferrin binding to pIgR, leading to internalization.

Altogether, these results support the potential of pIgR as a novel receptor for pIgR.

To further test transferrin binding to endogenous pIgR, we incubated Calu-3 cells with a transferrin titration and found that Calu-3 cells were capable of binding transferrin at concentrations of 100 μg/ml and higher (Fig. 18A). However, lack of controls such as the use of pIgR blocking antibody or the knockdown of pIgR renders it difficult to conclude endogenous pIgR specificity. Hence, we sought to investigate whether we could confirm pIgR specificity through binding of transferrin to both recombinant TFR1 (rTFR1) and recombinant pIgR (rpIgR). In collaboration with the Dr. Andres Finzi lab at the Centre Hospitalier de l'Université de Montreal (CHUM), Mehdi Benlarbi performed bio-layer interferometry (BLI) to assess the binding of rTFR1 and rpIgR to transferrin, dIgA, and pIgM (Fig. 18B-E). In contrast to our previous data, there was no binding between rpIgR and transferrin (Fig. 18B). However, strong binding was observed for transferrin and rTFR1, with a KD of around 0.6 nM, similar to what has been recorded in literature (Fig. 18B, E)[239]. Interestingly, we did not observe any binding for dIgA to rpIgR, but we did observe binding of pIgM to rpIgR at a KD of 2.62 nM (Fig. 18C-E). The lack of binding of both transferrin and dIgA to rpIgR questions our previous findings where we observe both dIgA and transferrin to bind exogenous and endogenous pIgR. Overall, our findings suggest the potential of a novel mechanism for transferrin endocytosis, where transferrin can bind cell surface pIgR and get internalized (Fig. 18F). However, further experiments are required to confirm our findings.

CHAPTER 4: DISCUSSION

4.1. Main Findings

Albeit the high effectivity of intramuscular vaccines against SARS-CoV-2, lack of sterilizing immunity allows for continued viral transmission and the possible emergence of highly pathogenic VOIs and VOCs [221]. The current development of mucosal vaccines is promising, as stimulation of potent mucosal immune responses could promote sterilizing immunity. However, viral mechanisms employed by SARS-CoV-2 to evade mucosal immunity remain understudied and must be considered for both therapeutic development and pandemic preparedness. To this end, we have identified ORF8 as a pivotal antagonist of dIgA-mediated immunity.

Our study demonstrates that SARS-CoV-2 ORF8 can specifically modulate pIgR expression and function via two distinct pathways: intracellular and secretory expression of ORF8. Within cells, we showed that SARS-CoV-2 ORF8 can bind and downregulate pIgR in a dose-dependent manner, resulting in decreased dIgA binding. More specifically, we observed a trend where dimerization-deficient ORF8 proteins (SARS-CoV, YNLF, C20A, and R115A) were less efficient in downregulating pIgR in correlation with their binding capacities. These results highlighted a dependency on ORF8's dimer structure to mediate potent binding and downregulation with pIgR.

As a secretory protein, we observed ORF8 binding to D1 of pIgR without disrupting dIgA binding. In contrast, we observed a capacity for unglycosylated, soluble ORF8 to modulate and hijack the endocytosis of the dIgA-pIgR complex to promote its internalization within cells. We propose a model where SARS-CoV-2 infected cells produce ORF8 which will act on pIgR intracellularly to antagonize dIgA, and ORF8 secretion will lead to its internalization in uninfected cells via binding to the dIgA-pIgR complex (Fig. 3). Finally, we highlighted a potentially novel

function of pIgR as a receptor for transferrin internalization.

4.2. Modulation of pIgR across microbial infections: a double-edged sword

By mediating the transcytosis of sIgA, pIgR plays a crucial role in maintaining mucosal immune homeostasis. Although its role can be protective against incoming pathogens, many microbes have adapted to exploit pIgR to their own advantage[197]. Examples of pIgR's protective role are highlighted during chlamydial infections, which are linked with increased expression of pIgR that correlate with high levels of sIgA, required to clear infection [263,264]. In contrast, increased pIgR expression subsequent to infection has also been shown to contribute towards inflammation, as is the case for herpes simplex virus 2 (HSV-2) and porcine epidemic diarrhea virus (PEDV)[197,265]. Similarly, enteric viruses, such as norovirus and reovirus, have been found to be reliant on pIgR-mediated sIg sensing for infection, such that decreased pIgR levels leads to reduced viral titres *in vivo*[266]. Overall, whether pIgR and sIg responses are beneficial or detrimental for pathogen clearance appears to vary. However, multiple pathways of pIgR modulation have been identified for a broad range of pathogens, indicating a complex relationship between mucosal pathogen persistence and clearance.

Other well-characterized examples of pathogens modulating or exploiting pIgR for its gain is *Streptococcus pneumoniae.* This bacterium invades the brain through the blood-brain barrier (BBB) to cause meningitis by using pIgR expressed on endothelial cells as a receptor for its adhesins[267,268]. Its further been shown to subvert pIgR function by promoting reverse transcytosis to enter nose epithelial cells[269]. Additionally, the fungus *Candida albicans* can otherwise bind free SC to promote its attachment to mucosal epithelial cells[197,270]. As for viruses, Epstein-Barr virus (EBV) has been shown to expands its cellular tropism by binding and exploiting anti-EBV sIgA bound to pIgR, allowing its entry into otherwise non-permissive epithelial cells [197,271,272]. Other

viruses, such as simian immunodeficiency virus (SIV) and chimeric simian/human immunodeficiency virus (S/HIV) mediate mucosal immune evasion by downregulating pIgR expression in the lungs and gut[273,274]. The mechanisms that govern pathogen exploitation of pIgR are broad, but some of these mechanisms seem to be conserved and shared by SARS-CoV-2.

In the context of SARS-CoV-2, clinical data correlates the importance of sIgA for SARS-CoV-2 neutralization yet no direct link has been made between pIgR expression, IgA secretion, and viral clearance [216,219]. We identified two possible pathways by which SARS-CoV-2 may both modulate and exploit pIgR to evade mucosal immunity and promote its replication. Similarly to SIV and S/HIV, SARS-CoV-2 ORF8 is capable of potently downregulating pIgR expression. In contrast, secreted ORF8 may mimic mechanisms seen in EBV and *S. pneumoniae* by its capacity to exploit and seemingly highjack the dIgA-pIgR complex for internalization in cells. This could highlight adaptation of SARS-CoV-2 for distinct early- and late-infection immune evasion mechanisms. However, our findings are limited due to the lack of confirmation of this effect in the context of SARS-CoV-2 infection in lung epithelial cells. Interestingly, we also observed downregulation of pIgR by spike glycoprotein which may parallel *S. pneumoniae'*s capacity to mediate adhesin binding via pIgR. Hence, whether SARS-CoV-2 virions could exploit pIgR for entry or to expand its cellular tropism, like EBV, merits further investigation.

4.3. Lung and gut epithelial cell lines to study pIgR transcytosis in the context of viral infection

Due to pIgR transcytosis being an understudied field, many challenges arise when translating key assays used in the study of transcytosis for diseases such as cancer, COPD, asthma, and allergy to viral infections. What is termed the "pIgR transcytosis assay" has become a standard for studying sIgA secretion under different physiological conditions. In short, this assay employs polarized cells which express human pIgR, either endogenously or exogenously, and the addition

of dIgA in the basolateral pole of a transwell insert will allow to measure the rate of pIgR-mediated transcytosis via the measurement of sIgA in the apical pole after a set incubation time (typically around 48 hours)[275]. However, the use of specific cell lines and particular conditions can challenge the study of viral infection.

One of the first cell lines optimized for this assay was the use of polarized Madin-Darby canine kidney (MDCK) cells expressing human pIgR[276]. Although this system can efficiently promote transcytosis of dIgA, this cell line is limited as it does not always represent an appropriate physiological environment for viral infection[277,278]. However, it remains a useful tool to study the biology and dynamics of dIgA transcytosis[196,279,280].

Another commonly used cell line for the establishment of a transcytosis assay are Calu-3 cells. Notably, their expression of endogenous pIgR and their nature as lung epithelial cells leads to a more accurate system for the study of pulmonary disease[275]. They have been used to study transcytosis in the context of cystic fibrosis and pulmonary drug delivery[275,281–283]. Although characterization of polarized Calu-3 cells under air-liquid interface (ALI) reveals a representative morphology of airway epithelium, the nature of a transcytosis assay requires liquid-covered culture (LCC)[275,282]. In regards to SARS-CoV-2 infection, Calu-3 cells have been used in cell culture to study mechanics of SARS-CoV-2 entry and replication, making them a potential cell line for studying the impact of SARS-CoV-2 infection on dIgA transcytosis by pIgR[227,228].

Finally, recent research has focused on using relevant primary epithelial cell lines, such as primary human bronchial epithelial cells (HBECs), to study sIgA secretion in the context of asthma and cystic fibrosis[210,281]. These cell lines offer the advantage of polarizing into mucociliated tissue under ALI culture in supplement growth media[284]. Furthermore, the endogenous expression of ACE2, TMPRSS2, and pIgR highlight the potential of the cells in the study of dIgA transcytosis

modulation by SARS-CoV-2[285,286]. This is supported by the use of HBECs for the study of drug discovery against SARS-CoV-2 infection[285,286]. However, the short lifespan and limited replication ability of primary cell lines can become challenging when designing and optimizing such experiments[287].

Aside from the use of various cell lines with their own advantage and disadvantages, pIgR transcytosis assays are limited by experimental conditions which poorly reflect physiological conditions. In MDCK cells, dIgA transcytosis by pIgR is determined by pulse chase assay of radioactively labelled IgA, requiring shorter incubation times and smaller antibody titres (around 0.1mg/ml dIgA)[276,280]. However, likely due to lower pIgR levels expressed in Calu-3 cells and HBECs, these cell lines otherwise require higher dIgA concentrations of around 1 mg/ml and longer incubation times raging from 48 to 72 hours[210,281]. Clinically, sIgA are commonly tested in the saliva, where normal levels can range anywhere between 0.0159 to 0.6 mg/L with a secretion rate of 0.0072 to 0.235 mg/min[288]. Although initial dIgA concentrations produced by local ASCs have yet to be determined clinically, it is likely that experimental conditions used for dIgA transcytosis in Calu-3 cells and HBECs are not representative of actual physiological conditions. This is further amplified by the long incubation time required for the detection of sIgA in the apical pole which contrast with the rapid clinical sIgA secretion rates.

In our hands, we have tried to polarize Calu-3 cells under LCC culture, but we were unsuccessful in measuring trans-epithelial electrical resistance (TEER) of 1000 Ωxcm^2 required for tight junctions to form between the cells (data not shown)[275]. We further tried to perform the transcytosis assay using polarized HBECs, however we failed to detect sIgA in the apical pole by ELISA likely due to using insufficient quantities of dIgA (around 0.2 mg/ml) in the basolateral pole (data not shown). Lack of published articles studying pIgR transcytosis and sIgA secretion in

the context of pulmonary viral infections renders optimization a challenge. Our current study is limited by our capacity to mainly investigate transcytosis at its initiating steps (binding and internalization), however we plan to continue optimizing our protocol for Calu-3 polarization to study the impact of ORF8 on dIgA transcytosis by pIgR in the context of SARS-CoV-2 infection.

4.4. Endogenous vs exogenous pIgR expression: optimization to study impact of viral infections on IgA-mediated mucosal immunity

When setting up our assays, we sought to confirm our findings from HEK293T-pIgR expressing cells against cell lines which endogenously expressed pIgR. Due to their use in the study of SARS-CoV-2, we settled in optimizing our assays in Calu-3 (lung epithelial) and Caco-2 (gut epithelial) cells[286]. In both cell lines we experienced challenges in the transient expression of SARS-CoV-2 ORF8 as we tested methods ranging from transfection, electroporation, to transduction. For Caco-2 cells, electroporation was successful in promoting transient ORF8 expression. However, we noticed that the process of electroporation itself appeared to modulate pIgR expression. This is agreement with findings highlighting a decrease in gut sIgA in the presence of cellular stress[289].

As for Calu-3 cells, we were able to induce ORF8 expression through the development of Calu-3 selective cell lines stably expressing ORF8 via lentiviral transduction. However, our results suggest some minor discrepancies with results generated in HEK293T cells expressing pIgR, notably for the effect of some of the ORF8 dimerization mutants (C20A and R115A). Whether this might be a result of cellular adaptation of Calu-3 cell to the constant ORF8 expression merits further investigation. Altogether, studying impacts of viral infection on dIgA-mediated mucosal immunity through pIgR remains a challenge due to lack of standardized and optimized protocols.

4.5. Study of pIgR transcytosis in vivo: murine models and their challenges

Although studies of pIgR *in vivo* are limited, their use has considerably contributed to our understanding of mucosal immunity regulation. While germ-free mice allowed to establish a link between the presence of gut commensal bacteria and the modulation of pIgR expression, other models have been used to demonstrate that the application of mild physiological stress, such as exercise and heat acclimatization, leads to and upregulation in pIgR and IgA secretion[193,290–292]. In the late 90s, pIgR knockout ($pIgR^{-/-}$) mice were developed and have since been heavily used to study the role of pIgR and IgA secretion deficiencies in disease pathology[193]. As previously described, these mice models allowed to successfully identify an increased occurrence of auto-immune and inflammatory diseases, such as IBD, in response to altered gut microbiota due to the impaired gut mucosal immune response[193,201].

Conversely, while humans have two IgA subtypes, IgA1 and IgA2, mice only have one IgA subtype which more closely resembles human IgA2[193]. However, this difference does not affect the capacity of murine models to effectively transcytose and secrete IgA to mucosal surfaces via pIgR [193]. In fact, *in vitro* primary murine epithelial models have been successfully developed to facilitate the study of IgA transcytosis by pIgR[293].

On the other hand, studying COVID-19 in mice is a challenge since these rodents are not naturally permissive to SARS-CoV-2 due to their lack of endogenous ACE2 expression[294]. To circumvent this issue, ACE2 transgenic mice have been frequently used to study SARS-CoV-2, however, whether exogenous ACE2 expression can modulate pIgR expression or IgA secretion has not been investigated[294]. Regardless these mice models offer an opportunity to easily study the impact of SARS-CoV-2 infection on pIgR expression and IgA secretion.

4.6. Transferrin binding to pIgR: divergence between experimental conditions

An interesting finding we made while conducting our study was the potential novel function of pIgR as a receptor for transferrin. Although this was surprising, iron has been known to use receptors outside of TFR1 and TFR2, such as zinc transporter 8 (ZIP8) and 14, for internalization[262]. However, we were unable to confirm our findings using recombinant pIgR (rpIgR) and transferrin by BLI. Of note, we also failed to see any interaction between dIgA and rpIgR and were only able to see strong interactions between pIgM and rpIgR. These findings challenge our study design, by which we saw strong binding of both transferrin and dIgA to Calu-3 cells and HEK293T cells expressing pIgR.

In respect to our transferrin study, we observed additional discrepancies between experiments depending on the origin of the transferrin used. In assays using pre-conjugated holo-transferrin, we observed no binding and internalization by mock-transfected HEK293T cells and high pIgR-specificity for binding and internalization (Fig. 17A-E). In contrast, in assays where we used human transferrin, with unspecified contents and production (proprietary protocols), we noticed high background binding to mock-transfected HEK293T cells, indicating low specificity for pIgR (Fig. 17F-I). This may be a result in differences in apo- and holo-transferrin ratios present in this transferrin sample. In fact, apo-transferrin is the iron-free version of transferrin while holo-transferrin is iron-bound[295]. Although holo-transferrin binds TFR1 with higher affinity, apo-transferrin remains capable of binding TFR1 non-competitively[239]. Due to apo-transferrin's lower affinity to TFR1 than holo-transferrin, we expect differences in ratios of the two proteins to be insufficient at generating the discrepancies we observed in background binding in Figure 12.

Another possibility for the high background binding could be related to our conjugation protocol. In fact, the conjugation kit we use comes with purification columns with protein

molecular weight restrictions of 50 KDa. Due to transferrin being around 80 KDa, we were unable to purify our conjugation product using the provided column. This may have resulted in the presence of free fluorophore in our conjugated-transferrin sample which may have further contributed to the background binding observed in Figure 12. Altogether, the presence of discrepancies across our data needs to be further investigated to conclude on the role of pIgR in transferrin internalization.

4.7. Binding of dIgA to rpIgR: implications for pIgM

In our study, we found that dIgA was capable of binding pIgR-expressing HEK293T cells and Calu-3 cells. However, the BLI assay refuted our findings, as no binding was observed between rpIgR and dIgA. In contrast, strong binding was observed between pIgM and rpIgR. A possible reason for this could be our dIgA source. We had previously tried our assays using serum IgA, however, due to serum IgA being primarily comprised of monomeric IgA, we did not observe significant binding to pIgR-expressing cells (data not shown)[296]. Since dIgA is mainly produced by tissue-resident plasma B cells, we struggled to acquire human dIgA[188]. To circumvent this issue, we decided to use IgA isolated from human colostrum, which is the first form of breastmilk produced and known to be rich in sIgs[297]. However, this implies that the IgA isolated would be under the form of sIgA, which is dIgA bound to SC. Although we saw binding of this IgA in our cell-based assays, the presence of SC on the dIgA moiety could explain why there was no binding observed in the BLI.

In addition, binding of dIgA to pIgR involves a conformational change within pIgR[192,195]. Since rpIgR is not membrane-bound, it is unknown whether it would be capable of undergoing the conformational changes required for dIgA binding. Further supporting this, we observed discrepancies between ORF8 binding to membrane-bound and soluble pIgR. In fact, in data not

shown, we found that rpIgR could bind secreted SARS-CoV, but not SARS-CoV-2, ORF8 (data not shown). This contrasts with our findings where we observed membrane-bound pIgR to exert stronger interactions with SARS-CoV-2 than SARS-CoV ORF8. However, the lack of binding of dIgA to rpIgR in the BLI questions the validity of our findings regarding the effect of SARS-CoV-2 ORF8 on dIgA binding and internalization.

Unlike dIgA, IgM is found as a pentamer in serum, rendering its acquisition easier[298]. To mediate the inconsistencies regarding dIgA, we plan to repeat key experiments using pIgM. In doing so, we will be able to confirm whether SARS-CoV-2 ORF8's antagonization of pIgR ligand binding is conserved with pIgM or whether this effect may dIgA-specific. Altogether, we expect to highlight SARS-CoV-2 ORF8 as an antagonist of pIgR-mediated mucosal immunity, independently of its ligand interaction.

4.8. Conclusions and future work

Overall, pathogens have evolved an array of mechanisms to modulate mucosal immunity to their advantage. Although whether SARS-CoV-2 employs mechanism to evade mucosal immunity remains poorly understood, sIgs have been highlighted in playing a pivotal role during early infection. To this end, we have provided insight into the antagonization of IgA-mediated mucosal immunity by SARS-CoV-2. Specifically, we identified the accessory protein ORF8 as having the capacity to potently downregulate pIgR through interactions mediated in part by its novel capacity to dimerize. Furthermore, we highlighted that intracellular ORF8 can disrupt dIgA binding to pIgR, while soluble, secreted ORF8 rather hijacks the dIgA-pIgR complex for internalization. Finally, we highlighted a potential novel function of pIgR as a receptor for transferrin uptake.

While we demonstrated the role of ORF8 against the initiating steps of dIgA-pIgR

transcytosis, whether ORF8 affects dIgA secretion remains to be investigated via the development of a functional transcytosis assay. Live infection of primary human airway epithelial cells to compare wild-type and ORF8-deleted SARS-CoV-2 viruses would further inform whether dIgA antagonization is specific to SARS-CoV-2 ORF8, and whether other SARS-CoV-2 viral proteins contribute towards impaired mucosal immunity and enhanced establishment of viral infection in lung epithelial cells. Moreover, this work demonstrates that SARS-CoV-2 ORF8 is a key viral antagonist of protective mucosal immunity that merits consideration when developing novel antiviral therapies fortifying local mucosal immunity, such as mucosal vaccines. Furthering our understanding of immune escape mechanisms associated with proteins of SARS-CoV-2 and its VOCs, such as ORF8, will contribute to future pandemic preparedness.

REFERENCES

1. Corman, V. M., Muth, D., Niemeyer, D. & Drosten, C. Hosts and Sources of Endemic Human Coronaviruses. *Adv Virus Res* **100**, 163–188 (2018).
2. Grellet, E., L'Hôte, I., Goulet, A. & Imbert, I. Replication of the coronavirus genome: A paradox among positive-strand RNA viruses. *J Biol Chem* **298**, 101923 (2022).
3. Forni, D., Cagliani, R., Clerici, M. & Sironi, M. Molecular Evolution of Human Coronavirus Genomes. *Trends Microbiol* **25**, 35–48 (2017).
4. Wertheim, J. O., Chu, D. K. W., Peiris, J. S. M., Kosakovsky Pond, S. L. & Poon, L. L. M. A Case for the Ancient Origin of Coronaviruses. *J Virol* **87**, 7039–7045 (2013).
5. Blair, J. E. & Hedges, S. B. Molecular phylogeny and divergence times of deuterostome animals. *Mol Biol Evol* **22**, 2275–2284 (2005).
6. Saif, L. J. Animal coronaviruses: what can they teach us about the severe acute respiratory syndrome? *Rev Sci Tech* **23**, 643–660 (2004).
7. Schalk, A. F., Hawn, M. C., Schalk, A. F. & Hawn, M. C. An Apparently New Respiratory Disease of Baby Chicks. *J. Amer. Vet. Med. Ass* **78**, 413–423 (1931).
8. Hamre, D. & Procknow, J. J. A new virus isolated from the human respiratory tract. *Proc Soc Exp Biol Med* **121**, 190–193 (1966).
9. Ye, Z.-W. *et al.* Zoonotic origins of human coronaviruses. *Int J Biol Sci* **16**, 1686–1697 (2020).
10. McIntosh, K., Dees, J. H., Becker, W. B., Kapikian, A. Z. & Chanock, R. M. Recovery in tracheal organ cultures of novel viruses from patients with respiratory disease. *Proc Natl Acad Sci U S A* **57**, 933–940 (1967).
11. Peiris, J. S. M. *et al.* Coronavirus as a possible cause of severe acute respiratory syndrome. *Lancet* **361**, 1319–1325 (2003).

12. van der Hoek, L. *et al.* Identification of a new human coronavirus. *Nat Med* **10**, 368–373 (2004).

13. Woo, P. C. Y. *et al.* Characterization and complete genome sequence of a novel coronavirus, coronavirus HKU1, from patients with pneumonia. *J Virol* **79**, 884–895 (2005).

14. Zaki, A. M., van Boheemen, S., Bestebroer, T. M., Osterhaus, A. D. M. E. & Fouchier, R. A. M. Isolation of a novel coronavirus from a man with pneumonia in Saudi Arabia. *N Engl J Med* **367**, 1814–1820 (2012).

15. Zhu, N. *et al.* A Novel Coronavirus from Patients with Pneumonia in China, 2019. *New England Journal of Medicine* **382**, 727–733 (2020).

16. Huynh, J. *et al.* Evidence supporting a zoonotic origin of human coronavirus strain NL63. *J Virol* **86**, 12816–12825 (2012).

17. Corman, V. M. *et al.* Evidence for an Ancestral Association of Human Coronavirus 229E with Bats. *J Virol* **89**, 11858–11870 (2015).

18. Lau, S. K. P. *et al.* Discovery of a novel coronavirus, China Rattus coronavirus HKU24, from Norway rats supports the murine origin of Betacoronavirus 1 and has implications for the ancestor of Betacoronavirus lineage A. *J Virol* **89**, 3076–3092 (2015).

19. Wang, W. *et al.* Discovery, diversity and evolution of novel coronaviruses sampled from rodents in China. *Virology* **474**, 19–27 (2015).

20. Xiong, Q. *et al.* Close relatives of MERS-CoV in bats use ACE2 as their functional receptors. *Nature* **612**, 748–757 (2022).

21. Li, W. *et al.* Bats are natural reservoirs of SARS-like coronaviruses. *Science* **310**, 676–679 (2005).

22. Zhou, H. *et al.* Identification of novel bat coronaviruses sheds light on the evolutionary origins of SARS-CoV-2 and related viruses. *Cell* **184**, 4380-4391.e14 (2021).

23. Eckerle, L. D. *et al.* Infidelity of SARS-CoV Nsp14-Exonuclease Mutant Virus Replication Is Revealed by Complete Genome Sequencing. *PLoS Pathog* **6**, e1000896 (2010).

24. Yin, X., Popa, H., Stapon, A., Bouda, E. & Garcia-Diaz, M. Fidelity of Ribonucleotide Incorporation by the SARS-CoV-2 Replication Complex. *J Mol Biol* **435**, 167973 (2023).

25. Castro, C., Arnold, J. J. & Cameron, C. E. Incorporation fidelity of the viral RNA-dependent RNA polymerase: a kinetic, thermodynamic and structural perspective. *Virus Res* **107**, 141–149 (2005).

26. Montoya, V., McLaughlin, A., Mordecai, G. J., Miller, R. L. & Joy, J. B. Variable routes to genomic and host adaptation among coronaviruses. *Journal of Evolutionary Biology* **34**, 924–936 (2021).

27. Ruiz-Aravena, M. *et al.* Ecology, evolution and spillover of coronaviruses from bats. *Nat Rev Microbiol* **20**, 299–314 (2022).

28. Plowright, R. K. *et al.* Pathways to zoonotic spillover. *Nat Rev Microbiol* **15**, 502–510 (2017).

29. Rabaan, A. A. *et al.* SARS-CoV-2, SARS-CoV, and MERS-CoV: a comparative overview.

30. Zhang, Y.-Z. & Holmes, E. C. A Genomic Perspective on the Origin and Emergence of SARS-CoV-2. *Cell* **181**, 223–227 (2020).

31. Abdelrahman, Z., Li, M. & Wang, X. Comparative Review of SARS-CoV-2, SARS-CoV, MERS-CoV, and Influenza A Respiratory Viruses. *Frontiers in Immunology* **11**, (2020).

32. Kirtipal, N., Bharadwaj, S. & Kang, S. G. From SARS to SARS-CoV-2, insights on structure, pathogenicity and immunity aspects of pandemic human coronaviruses. *Infection, Genetics and Evolution* **85**, 104502 (2020).

33. Xu, R.-H. *et al.* Epidemiologic Clues to SARS Origin in China. *Emerg Infect Dis* **10**, 1030–1037 (2004).

34. Centers for Disease Control and Prevention (CDC). Prevalence of IgG antibody to SARS-associated coronavirus in animal traders--Guangdong Province, China, 2003. *MMWR Morb Mortal Wkly Rep* **52**, 986–987 (2003).

35. Guan, Y. *et al.* Isolation and characterization of viruses related to the SARS coronavirus from animals in southern China. *Science* **302**, 276–278 (2003).

36. Kan, B. *et al.* Molecular Evolution Analysis and Geographic Investigation of Severe Acute Respiratory Syndrome Coronavirus-Like Virus in Palm Civets at an Animal Market and on Farms. *Journal of Virology* **79**, 11892–11900 (2005).

37. Poon, L. L. M. *et al.* Identification of a Novel Coronavirus in Bats. *Journal of Virology* **79**, 2001–2009 (2005).

38. Wang, L.-F. & Eaton, B. T. Bats, Civets and the Emergence of SARS. in *Wildlife and Emerging Zoonotic Diseases: The Biology, Circumstances and Consequences of Cross-Species Transmission* (eds. Childs, J. E., Mackenzie, J. S. & Richt, J. A.) 325–344 (Springer, Berlin, Heidelberg, 2007). doi:10.1007/978-3-540-70962-6_13.

39. HUI, D. S., WONG, P. & WANG, C. SARS: clinical features and diagnosis. *Respirology* **8**, S20–S24 (2003).

40. Janice Oh, H.-L., Ken-En Gan, S., Bertoletti, A. & Tan, Y.-J. Understanding the T cell immune response in SARS coronavirus infection. *Emerg Microbes Infect* **1**, e23 (2012).

41. Hsueh, P.-R., Huang, L.-M., Chen, P.-J., Kao, C.-L. & Yang, P.-C. Chronological evolution of IgM, IgA, IgG and neutralisation antibodies after infection with SARS-associated coronavirus. *Clin Microbiol Infect* **10**, 1062–1066 (2004).

42. Channappanavar, R., Fett, C., Zhao, J., Meyerholz, D. K. & Perlman, S. Virus-specific memory CD8 T cells provide substantial protection from lethal severe acute respiratory syndrome coronavirus infection. *J Virol* **88**, 11034–11044 (2014).

43. Zhao, J., Zhao, J. & Perlman, S. T cell responses are required for protection from clinical disease and for virus clearance in severe acute respiratory syndrome coronavirus-infected mice. *J Virol* **84**, 9318–9325 (2010).

44. He, Z. *et al.* Effects of severe acute respiratory syndrome (SARS) coronavirus infection on peripheral blood lymphocytes and their subsets. *International Journal of Infectious Diseases* **9**, 323–330 (2005).

45. Chen, J. & Subbarao, K. The Immunobiology of SARS*. *Annu Rev Immunol* **25**, 443–472 (2007).

46. Jiang, Y. *et al.* Characterization of Cytokine/Chemokine Profiles of Severe Acute Respiratory Syndrome. *Am J Respir Crit Care Med* **171**, 850–857 (2005).

47. Huang, K.-J. *et al.* An interferon-γ-related cytokine storm in SARS patients. *Journal of Medical Virology* **75**, 185–194 (2005).

48. Lee, C.-H. *et al.* Altered p38 Mitogen-Activated Protein Kinase Expression in Different Leukocytes with Increment of Immunosuppressive Mediators in Patients with Severe Acute Respiratory Syndrome1. *The Journal of Immunology* **172**, 7841–7847 (2004).

49. Zhang, Y. *et al.* Analysis of Serum Cytokines in Patients with Severe Acute Respiratory Syndrome. *Infection and Immunity* **72**, 4410–4415 (2004).

50. Zhao, J., Zhao, J., Van Rooijen, N. & Perlman, S. Evasion by Stealth: Inefficient Immune Activation Underlies Poor T Cell Response and Severe Disease in SARS-CoV-Infected Mice. *PLoS Pathog* **5**, e1000636 (2009).

51. Baric, R. S. SARS-CoV: Lessons for global health. *Virus Research* **133**, 1–3 (2008).

52. Umakanthan, S. *et al.* Origin, transmission, diagnosis and management of coronavirus disease 2019 (COVID-19). *Postgrad Med J* **96**, 753–758 (2020).

53. COVID-19 deaths | WHO COVID-19 dashboard. *datadot* https://data.who.int/dashboards/covid19/cases.

54. Zhou, P. *et al.* A pneumonia outbreak associated with a new coronavirus of probable bat origin. *Nature* **579**, 270–273 (2020).

55. Klestova, Z. Possible spread of SARS-CoV-2 in domestic and wild animals and body temperature role. *Virus Res* **327**, 199066 (2023).

56. Pizzato, M. *et al.* SARS-CoV-2 and the Host Cell: A Tale of Interactions. *Frontiers in Virology* **1**, (2022).

57. Zhang, S. *et al.* Bat and pangolin coronavirus spike glycoprotein structures provide insights into SARS-CoV-2 evolution. *Nat Commun* **12**, 1607 (2021).

58. Niu, S. *et al.* Molecular basis of cross-species ACE2 interactions with SARS-CoV-2-like viruses of pangolin origin. *EMBO J* **40**, e107786 (2021).

59. Schindell, B. G., Allardice, M., McBride, J. A. M., Dennehy, B. & Kindrachuk, J. SARS-CoV-2 and the Missing Link of Intermediate Hosts in Viral Emergence - What We Can Learn From Other Betacoronaviruses. *Frontiers in Virology* **2**, (2022).

60. Araf, Y., Faruqui, N. A., Anwar, S. & Hosen, M. J. SARS-CoV-2: a new dimension to our understanding of coronaviruses. *Int Microbiol* **24**, 19–24 (2021).

61. Sanyaolu, A. *et al.* The emerging SARS-CoV-2 variants of concern. *Ther Adv Infect Dis* **8**, 20499361211024372 (2021).

62. Anka, A. U. *et al.* Coronavirus disease 2019 (COVID-19): An overview of the immunopathology, serological diagnosis and management. *Scand J Immunol* **93**, e12998 (2021).

63. Muralidar, S., Ambi, S. V., Sekaran, S. & Krishnan, U. M. The emergence of COVID-19 as a global pandemic: Understanding the epidemiology, immune response and potential therapeutic targets of SARS-CoV-2. *Biochimie* **179**, 85–100 (2020).

64. Le Bert, N. *et al.* Highly functional virus-specific cellular immune response in asymptomatic SARS-CoV-2 infection. *J Exp Med* **218**, e20202617 (2021).

65. Yu, L. *et al.* Immunodepletion with Hypoxemia: A Potential High Risk Subtype of Coronavirus Disease 2019. 2020.03.03.20030650 Preprint at https://doi.org/10.1101/2020.03.03.20030650 (2020).

66. Hu, B., Guo, H., Zhou, P. & Shi, Z.-L. Characteristics of SARS-CoV-2 and COVID-19. *Nat Rev Microbiol* **19**, 141–154 (2021).

67. Gustine, J. N. & Jones, D. Immunopathology of Hyperinflammation in COVID-19. *Am J Pathol* **191**, 4–17 (2021).

68. Boechat, J. L., Chora, I., Morais, A. & Delgado, L. The immune response to SARS-CoV-2 and COVID-19 immunopathology - Current perspectives. *Pulmonology* **27**, 423–437 (2021).

69. COVID-19: immunopathogenesis and Immunotherapeutics | Signal Transduction and Targeted Therapy. https://www.nature.com/articles/s41392-020-00243-2.

70. V'kovski, P., Kratzel, A., Steiner, S., Stalder, H. & Thiel, V. Coronavirus biology and replication: implications for SARS-CoV-2. *Nat Rev Microbiol* **19**, 155–170 (2021).

71. Hamming, I. *et al.* Tissue distribution of ACE2 protein, the functional receptor for SARS coronavirus. A first step in understanding SARS pathogenesis. *J Pathol* **203**, 631–637 (2004).

72. Salamanna, F., Maglio, M., Landini, M. P. & Fini, M. Body Localization of ACE-2: On the Trail of the Keyhole of SARS-CoV-2. *Frontiers in Medicine* **7**, (2020).

73. Bestle, D. *et al.* TMPRSS2 and furin are both essential for proteolytic activation of SARS-CoV-2 in human airway cells. *Life Sci Alliance* **3**, e202000786 (2020).

74. Xia, S. *et al.* Inhibition of SARS-CoV-2 (previously 2019-nCoV) infection by a highly potent pan-coronavirus fusion inhibitor targeting its spike protein that harbors a high capacity to mediate membrane fusion. *Cell Res* **30**, 343–355 (2020).

75. Li, X., Yuan, H., Li, X. & Wang, H. Spike protein mediated membrane fusion during SARS-CoV-2 infection. *J Med Virol* **95**, e28212 (2023).

76. Jackson, C. B., Farzan, M., Chen, B. & Choe, H. Mechanisms of SARS-CoV-2 entry into cells. *Nat Rev Mol Cell Biol* **23**, 3–20 (2022).

77. Bayati, A., Kumar, R., Francis, V. & McPherson, P. S. SARS-CoV-2 infects cells after viral entry via clathrin-mediated endocytosis. *J Biol Chem* **296**, 100306 (2021).

78. Zhang, Q. *et al.* Molecular mechanism of interaction between SARS-CoV-2 and host cells and interventional therapy. *Signal Transduct Target Ther* **6**, 233 (2021).

79. Ou, T. *et al.* Hydroxychloroquine-mediated inhibition of SARS-CoV-2 entry is attenuated by TMPRSS2. *PLoS Pathog* **17**, e1009212 (2021).

80. Arya, R. *et al.* Structural insights into SARS-CoV-2 proteins. *J Mol Biol* **433**, 166725 (2021).

81. Osipiuk, J. *et al.* Structure of papain-like protease from SARS-CoV-2 and its complexes with non-covalent inhibitors. *Nat Commun* **12**, 743 (2021).

82. Yan, W., Zheng, Y., Zeng, X., He, B. & Cheng, W. Structural biology of SARS-CoV-2: open the door for novel therapies. *Sig Transduct Target Ther* **7**, 1–28 (2022).

83. Schubert, K. *et al.* SARS-CoV-2 Nsp1 binds the ribosomal mRNA channel to inhibit translation. *Nat Struct Mol Biol* **27**, 959–966 (2020).

84. Tardivat, Y. *et al.* SARS-CoV-2 NSP1 induces mRNA cleavages on the ribosome. *Nucleic Acids Res* **51**, 8677–8690 (2023).

85. Hackstadt, T. *et al.* Disruption of the Golgi Apparatus and Contribution of the Endoplasmic Reticulum to the SARS-CoV-2 Replication Complex. *Viruses* **13**, 1798 (2021).

86. Zimmermann, L. *et al.* SARS-CoV-2 nsp3 and nsp4 are minimal constituents of a pore spanning replication organelle. *Nat Commun* **14**, 7894 (2023).

87. Ricciardi, S. *et al.* The role of NSP6 in the biogenesis of the SARS-CoV-2 replication organelle. *Nature* **606**, 761–768 (2022).

88. Biswal, M. *et al.* Two conserved oligomer interfaces of NSP7 and NSP8 underpin the dynamic assembly of SARS-CoV-2 RdRP. *Nucleic Acids Res* **49**, 5956–5966 (2021).

89. Ma, Y. *et al.* Structural basis and functional analysis of the SARS coronavirus nsp14-nsp10 complex. *Proc Natl Acad Sci U S A* **112**, 9436–9441 (2015).

90. Romano, M., Ruggiero, A., Squeglia, F., Maga, G. & Berisio, R. A Structural View of SARS-CoV-2 RNA Replication Machinery: RNA Synthesis, Proofreading and Final Capping. *Cells* **9**, 1267 (2020).

91. Otter, C. J. *et al.* SARS-CoV-2 nsp15 endoribonuclease antagonizes dsRNA-induced antiviral signalling. *bioRxiv* 2023.11.15.566945 (2023) doi:10.1101/2023.11.15.566945.

92. Zandi, M. *et al.* The role of SARS-CoV-2 accessory proteins in immune evasion. *Biomed Pharmacother* **156**, 113889 (2022).

93. Wang, R. *et al.* ORF3a Protein of Severe Acute Respiratory Syndrome Coronavirus 2 Inhibits Interferon-Activated Janus Kinase/Signal Transducer and Activator of Transcription

Signaling via Elevating Suppressor of Cytokine Signaling 1. *Front Microbiol* **12**, 752597 (2021).

94. Konno, Y. *et al.* SARS-CoV-2 ORF3b Is a Potent Interferon Antagonist Whose Activity Is Increased by a Naturally Occurring Elongation Variant. *Cell Rep* **32**, 108185 (2020).
95. Miorin, L. *et al.* SARS-CoV-2 Orf6 hijacks Nup98 to block STAT nuclear import and antagonize interferon signalling. *Proceedings of the National Academy of Sciences* **117**, 28344–28354 (2020).
96. Kimura, I. *et al.* Sarbecovirus ORF6 proteins hamper induction of interferon signalling. *Cell Rep* **34**, 108916 (2021).
97. Cao, Z. *et al.* Ubiquitination of SARS-CoV-2 ORF7a promotes antagonism of interferon response. *Cell Mol Immunol* **18**, 746–748 (2021).
98. Xia, H. *et al.* Evasion of Type I Interferon by SARS-CoV-2. *Cell Rep* **33**, 108234 (2020).
99. Chen, J. *et al.* Severe Acute Respiratory Syndrome Coronavirus 2 ORF8 Protein Inhibits Type I Interferon Production by Targeting HSP90B1 Signaling. *Front Cell Infect Microbiol* **12**, 899546 (2022).
100. Jiang, H.-W. *et al.* SARS-CoV-2 Orf9b suppresses type I interferon responses by targeting TOM70. *Cell Mol Immunol* **17**, 998–1000 (2020).
101. Li, X. *et al.* SARS-CoV-2 ORF10 suppresses the antiviral innate immune response by degrading MAVS through mitophagy. *Cell Mol Immunol* **19**, 67–78 (2022).
102. Gordon, D. E. *et al.* A SARS-CoV-2 protein interaction map reveals targets for drug repurposing. *Nature* **583**, 459–468 (2020).

103. Bracquemond, D. & Muriaux, D. Betacoronavirus Assembly: Clues and Perspectives for Elucidating SARS-CoV-2 Particle Formation and Egress. *mBio* **12**, 10.1128/mbio.02371-21 (2021).

104. Tugaeva, K. V. *et al.* The Mechanism of SARS-CoV-2 Nucleocapsid Protein Recognition by the Human 14-3-3 Proteins. *Journal of Molecular Biology* **433**, 166875 (2021).

105. Perdikari, T. M. *et al.* SARS-CoV-2 nucleocapsid protein undergoes liquid-liquid phase separation stimulated by RNA and partitions into phases of human ribonucleoproteins. 2020.06.09.141101 Preprint at https://doi.org/10.1101/2020.06.09.141101 (2020).

106. Arndt, A. L., Larson, B. J. & Hogue, B. G. A conserved domain in the coronavirus membrane protein tail is important for virus assembly. *J Virol* **84**, 11418–11428 (2010).

107. Neuman, B. W. *et al.* A structural analysis of M protein in coronavirus assembly and morphology. *J Struct Biol* **174**, 11–22 (2011).

108. Boson, B. *et al.* The SARS-CoV-2 envelope and membrane proteins modulate maturation and retention of the spike protein, allowing assembly of virus-like particles. *J Biol Chem* **296**, 100111 (2021).

109. Ghosh, S. *et al.* β-Coronaviruses Use Lysosomes for Egress Instead of the Biosynthetic Secretory Pathway. *Cell* **183**, 1520-1535.e14 (2020).

110. Chen, D. *et al.* ORF3a of SARS-CoV-2 promotes lysosomal exocytosis-mediated viral egress. *Dev Cell* **56**, 3250-3263.e5 (2021).

111. Diamond, M. S. & Kanneganti, T.-D. Innate immunity: the first line of defence against SARS-CoV-2. *Nat Immunol* **23**, 165–176 (2022).

112. Zheng, M. *et al.* TLR2 senses the SARS-CoV-2 envelope protein to produce inflammatory cytokines. *Nat Immunol* **22**, 829–838 (2021).

113. Choudhury, A. & Mukherjee, S. In silico studies on the comparative characterization of the interactions of SARS-CoV-2 spike glycoprotein with ACE-2 receptor homologs and human TLRs. *J Med Virol* **92**, 2105–2113 (2020).

114. Thorne, L. G. *et al.* SARS-CoV-2 sensing by RIG-I and MDA5 links epithelial infection to macrophage inflammation. *EMBO J* **40**, e107826 (2021).

115. Zhao, X. *et al.* LY6E Restricts Entry of Human Coronaviruses, Including Currently Pandemic SARS-CoV-2. *J Virol* **94**, e00562-20 (2020).

116. Martin-Sancho, L. *et al.* Functional landscape of SARS-CoV-2 cellular restriction. *Mol Cell* **81**, 2656-2668.e8 (2021).

117. Campbell, G. R., To, R. K., Hanna, J. & Spector, S. A. SARS-CoV-2, SARS-CoV-1, and HIV-1 derived ssRNA sequences activate the NLRP3 inflammasome in human macrophages through a non-classical pathway. *iScience* **24**, 102295 (2021).

118. Domizio, J. D. *et al.* The cGAS-STING pathway drives type I IFN immunopathology in COVID-19. *Nature* **603**, 145–151 (2022).

119. Silva, M. J. A., Ribeiro, L. R., Lima, K. V. B. & Lima, L. N. G. C. Adaptive immunity to SARS-CoV-2 infection: A systematic review. *Frontiers in Immunology* **13**, (2022).

120. Kalfaoglu, B., Almeida-Santos, J., Tye, C. A., Satou, Y. & Ono, M. T-cell dysregulation in COVID-19. *Biochemical and Biophysical Research Communications* **538**, 204–210 (2021).

121. Karki, R. *et al.* Synergism of TNF-α and IFN-γ Triggers Inflammatory Cell Death, Tissue Damage, and Mortality in SARS-CoV-2 Infection and Cytokine Shock Syndromes. *Cell* **184**, 149-168.e17 (2021).

122. Minkoff, J. M. & tenOever, B. Innate immune evasion strategies of SARS-CoV-2. *Nat Rev Microbiol* **21**, 178–194 (2023).

123. Kasuga, Y., Zhu, B., Jang, K.-J. & Yoo, J.-S. Innate immune sensing of coronavirus and viral evasion strategies. *Exp Mol Med* **53**, 723–736 (2021).

124. Arduini, A., Laprise, F. & Liang, C. SARS-CoV-2 ORF8: A Rapidly Evolving Immune and Viral Modulator in COVID-19. *Viruses* **15**, 871 (2023).

125. Chen, S. *et al.* Extended ORF8 Gene Region Is Valuable in the Epidemiological Investigation of Severe Acute Respiratory Syndrome-Similar Coronavirus. *J Infect Dis* **222**, 223–233 (2020).

126. Tan, Y., Schneider, T., Leong, M., Aravind, L. & Zhang, D. Novel Immunoglobulin Domain Proteins Provide Insights into Evolution and Pathogenesis of SARS-CoV-2-Related Viruses. *mBio* **11**, (2020).

127. Badua, C. L. D. C., Baldo, K. A. T. & Medina, P. M. B. Genomic and proteomic mutation landscapes of SARS-CoV-2. *J Med Virol* **93**, 1702–1721 (2021).

128. Hassan, S. S. *et al.* A unique view of SARS-COV-2 through the lens of ORF8 protein. *Comput Biol Med* **133**, 104380 (2021).

129. Chen, X. *et al.* Crystal Structures of Bat and Human Coronavirus ORF8 Protein Ig-Like Domain Provide Insights Into the Diversity of Immune Responses. *Frontiers in Immunology* **12**, (2021).

130. Valcarcel, A., Bensussen, A., Álvarez-Buylla, E. R. & Díaz, J. Structural Analysis of SARS-CoV-2 ORF8 Protein: Pathogenic and Therapeutic Implications. *Front. Genet.* **12**, 693227 (2021).

131. Flower, T. G. *et al.* Structure of SARS-CoV-2 ORF8, a rapidly evolving immune evasion protein. *Proc Natl Acad Sci U S A* **118**, e2021785118 (2021).

132. Brandt, D. *et al.* Multiple Occurrences of a 168-Nucleotide Deletion in SARS-CoV-2 ORF8, Unnoticed by Standard Amplicon Sequencing and Variant Calling Pipelines. *Viruses* **13**, 1870 (2021).

133. Chaudhari, A. M., Singh, I., Joshi, M., Patel, A. & Joshi, C. Defective ORF8 dimerization in SARS-CoV-2 delta variant leads to a better adaptive immune response due to abrogation of ORF8-MHC1 interaction. *Mol Divers* (2022) doi:10.1007/s11030-022-10405-9.

134. Tang, X. *et al.* On the origin and continuing evolution of SARS-CoV-2. *National Science Review* **7**, 1012–1023 (2020).

135. Alanagreh, L., Alzoughool, F. & Atoum, M. The Human Coronavirus Disease COVID-19: Its Origin, Characteristics, and Insights into Potential Drugs and Its Mechanisms. *Pathogens* **9**, (2020).

136. Alkhansa, A., Lakkis, G. & El Zein, L. Mutational analysis of SARS-CoV-2 ORF8 during six months of COVID-19 pandemic. *Gene Rep* **23**, 101024 (2021).

137. Koyama, T., Platt, D. & Parida, L. Variant analysis of SARS-CoV-2 genomes. *Bull World Health Organ* **98**, 495–504 (2020).

138. Islam, M. R. *et al.* Genome-wide analysis of SARS-CoV-2 virus strains circulating worldwide implicates heterogeneity. *Sci Rep* **10**, 14004 (2020).

139. Pereira, F. SARS-CoV-2 variants combining spike mutations and the absence of ORF8 may be more transmissible and require close monitoring. *Biochem Biophys Res Commun* **550**, 8–14 (2021).

140. Shiehzadegan, S., Alaghemand, N., Fox, M. & Venketaraman, V. Analysis of the Delta Variant B.1.617.2 COVID-19. *Clin Pract* **11**, 778–784 (2021).

141. Chou, J.-M. *et al.* The ORF8 Protein of SARS-CoV-2 Modulates the Spike Protein and Its Implications in Viral Transmission. *Frontiers in Microbiology* **13**, (2022).

142. Kim, I.-J. *et al.* SARS-CoV-2 protein ORF8 limits expression levels of Spike antigen and facilitates immune evasion of infected host cells. *J Biol Chem* **299**, 104955 (2023).

143. Rodriguez-Rodriguez, B. A. *et al.* A neonatal mouse model characterizes transmissibility of SARS-CoV-2 variants and reveals a role for ORF8. *bioRxiv* 2022.10.04.510658 (2023) doi:10.1101/2022.10.04.510658.

144. Wang, X. *et al.* Accurate Diagnosis of COVID-19 by a Novel Immunogenic Secreted SARS-CoV-2 orf8 Protein. *mBio* **11**, (2020).

145. Wu, X. *et al.* Secreted ORF8 is a pathogenic cause of severe Covid-19 and potentially targetable with select NLRP3 inhibitors. 2021.12.02.470978 Preprint at https://doi.org/10.1101/2021.12.02.470978 (2021).

146. Fong, S.-W. *et al.* Robust Virus-Specific Adaptive Immunity in COVID-19 Patients with SARS-CoV-2 Δ382 Variant Infection. *J Clin Immunol* **42**, 214–229 (2022).

147. Su, Y. C. F. *et al.* Discovery and Genomic Characterization of a 382-Nucleotide Deletion in ORF7b and ORF8 during the Early Evolution of SARS-CoV-2. *mBio* **11**, e01610-20 (2020).

148. Bazykin, G. *et al.* Emergence of Y453F and Δ69-70HV mutations in a lymphoma patient with long-term COVID-19. *virological.org* https://virological.org/t/emergence-of-y453f-and-69-70hv-mutations-in-a-lymphoma-patient-with-long-term-covid-19/580.

149. Oostra, M., de Haan, C. A. M. & Rottier, P. J. M. The 29-nucleotide deletion present in human but not in animal severe acute respiratory syndrome coronaviruses disrupts the functional expression of open reading frame 8. *J Virol* **81**, 13876–13888 (2007).

150. Chiu, R. W. K. *et al.* Tracing SARS-coronavirus variant with large genomic deletion. *Emerg Infect Dis* **11**, 168–170 (2005).

151. Liu, P. *et al.* SARS-CoV-2 ORF8 reshapes the ER through forming mixed disulfides with ER oxidoreductases. *Redox Biology* **54**, 102388 (2022).

152. Echavarría-Consuegra, L. *et al.* Manipulation of the unfolded protein response: A pharmacological strategy against coronavirus infection. *PLOS Pathogens* **17**, e1009644 (2021).

153. Tan, X. *et al.* Coronavirus subverts ER-phagy by hijacking FAM134B and ATL3 into p62 condensates to facilitate viral replication. *Cell Rep* **42**, 112286 (2023).

154. Kee, J. *et al.* SARS-CoV-2 disrupts host epigenetic regulation via histone mimicry. *Nature* 1–8 (2022) doi:10.1038/s41586-022-05282-z.

155. Lehrer, S. & Rheinstein, P. H. Alignment of human KAT2A (GCN5) histone acetyltransferase and SARS-CoV-2 Orf8 viral proteins. *Chronic Diseases and Translational Medicine* **9**, 263–265 (2023).

156. Liu, P., Hu, J. & Wang, L. SARS-CoV-2 ORF8 does not function in the nucleus as a histone mimic. *Protein & Cell* **15**, 79–82 (2024).

157. Matsuoka, K. *et al.* SARS-CoV-2 accessory protein ORF8 is secreted extracellularly as a glycoprotein homodimer. *J Biol Chem* **298**, 101724 (2022).

158. Li, J.-Y. *et al.* The ORF6, ORF8 and nucleocapsid proteins of SARS-CoV-2 inhibit type I interferon signalling pathway. *Virus Research* **286**, 198074 (2020).

159. Takatsuka, H. *et al.* In silico Analysis of SARS-CoV-2 ORF8-Binding Proteins Reveals the Involvement of ORF8 in Acquired-Immune and Innate-Immune Systems. *Frontiers in Medicine* **9**, (2022).

160. Rao, Y. *et al.* Targeting CTP Synthetase 1 to Restore Interferon Induction and Impede Nucleotide Synthesis in SARS-CoV-2 Infection. 2021.02.05.429959 Preprint at https://doi.org/10.1101/2021.02.05.429959 (2021).

161. Geng, H. *et al.* SARS-CoV-2 ORF8 Forms Intracellular Aggregates and Inhibits IFNγ-Induced Antiviral Gene Expression in Human Lung Epithelial Cells. *Frontiers in Immunology* **12**, (2021).

162. Zhang, Y. *et al.* The ORF8 protein of SARS-CoV-2 mediates immune evasion through down-regulating MHC-I. *Proc Natl Acad Sci U S A* **118**, (2021).

163. Yoo, J.-S. *et al.* SARS-CoV-2 inhibits induction of the MHC class I pathway by targeting the STAT1-IRF1-NLRC5 axis. *Nat Commun* **12**, 6602 (2021).

164. Lin, X. *et al.* ORF8 contributes to cytokine storm during SARS-CoV-2 infection by activating IL-17 pathway. *iScience* **24**, 102293 (2021).

165. Wu, X. *et al.* Viral Mimicry of Interleukin-17A by SARS-CoV-2 ORF8. *mBio* **13**, e00402-22 (2022).

166. Lin, X. *et al. Unconventional Secretion of Unglycosylated ORF8 Is Critical for the Cytokine Storm during SARS-CoV-2 Infection*. http://biorxiv.org/lookup/doi/10.1101/2021.12.03.471057 (2021) doi:10.1101/2021.12.03.471057.

167. Kohyama, M. *et al.* SARS-CoV-2 ORF8 is a viral cytokine regulating immune responses. *Int Immunol* dxac044 (2022) doi:10.1093/intimm/dxac044.

168. Beaudoin-Bussières, G. *et al.* SARS-CoV-2 Accessory Protein ORF8 Decreases Antibody-Dependent Cellular Cytotoxicity. *Viruses* **14**, 1237 (2022).

169. Hartl, D. *et al.* Innate Immunity of the Lung: From Basic Mechanisms to Translational Medicine. *Journal of Innate Immunity* **10**, 487–501 (2018).

170. Tengroth, L. *et al.* Functional Effects of Toll-Like Receptor (TLR)3, 7, 9, RIG-I and MDA-5 Stimulation in Nasal Epithelial Cells. *PLOS ONE* **9**, e98239 (2014).

171. Gopallawa, I., Dehinwal, R., Bhatia, V., Gujar, V. & Chirmule, N. A four-part guide to lung immunology: Invasion, inflammation, immunity, and intervention. *Frontiers in Immunology* **14**, (2023).

172. Williams, A. E. & Chambers, R. C. The mercurial nature of neutrophils: still an enigma in ARDS? *Am J Physiol Lung Cell Mol Physiol* **306**, L217-230 (2014).

173. Hartl, D. *et al.* Infiltrated neutrophils acquire novel chemokine receptor expression and chemokine responsiveness in chronic inflammatory lung diseases. *J Immunol* **181**, 8053–8067 (2008).

174. Effah, C. Y. *et al.* Neutrophil-Dependent Immunity During Pulmonary Infections and Inflammations. *Front Immunol* **12**, 689866 (2021).

175. Westphalen, K. *et al.* Sessile alveolar macrophages communicate with alveolar epithelium to modulate immunity. *Nature* **506**, 503–506 (2014).

176. Guan, T., Zhou, X., Zhou, W. & Lin, H. Regulatory T cell and macrophage crosstalk in acute lung injury: future perspectives. *Cell Death Discov.* **9**, 1–11 (2023).

177. Spits, H. *et al.* Innate lymphoid cells--a proposal for uniform nomenclature. *Nat Rev Immunol* **13**, 145–149 (2013).

178. Carbone, F. R. Unique properties of tissue-resident memory T cells in the lungs: implications for COVID-19 and other respiratory diseases. *Nat Rev Immunol* **23**, 329–335 (2023).

179. Lee, C. M. & Oh, J. E. Resident Memory B Cells in Barrier Tissues. *Front Immunol* **13**, 953088 (2022).

180. MacLean, A. J. *et al.* Secondary influenza challenge triggers resident memory B cell migration and rapid relocation to boost antibody secretion at infected sites. *Immunity* **55**, 718-733.e8 (2022).

181. Barker, K. A. *et al.* Lung-resident memory B cells protect against bacterial pneumonia. *J Clin Invest* **131**, e141810 (2021).

182. Allie, S. R. *et al.* The establishment of resident memory B cells in the lung requires local antigen encounter. *Nat Immunol* **20**, 97–108 (2019).

183. Szabo, P. A., Miron, M. & Farber, D. L. Location, location, location: Tissue resident memory T cells in mice and humans. *Sci Immunol* **4**, eaas9673 (2019).

184. Strugnell, R. A. & Wijburg, O. L. C. The role of secretory antibodies in infection immunity. *Nat Rev Microbiol* **8**, 656–667 (2010).

185. Heyman, B. & Shulman, M. J. Structure, Function, and Production of Immunoglobulin M (IgM). in *Encyclopedia of Immunobiology* (ed. Ratcliffe, M. J. H.) 1–14 (Academic Press, Oxford, 2016). doi:10.1016/B978-0-12-374279-7.05001-3.

186. Chapter 12 - Mucosal and Cutaneous Immunity. in *Primer to the Immune Response (Second Edition)* (eds. Mak, T. W., Saunders, M. E. & Jett, B. D.) 269–292 (Academic Cell, Boston, 2014). doi:10.1016/B978-0-12-385245-8.00012-1.

187. Breedveld, A. & van Egmond, M. IgA and FcαRI: Pathological Roles and Therapeutic Opportunities. *Front Immunol* **10**, 553 (2019).

188. Gommerman, J. L., Rojas, O. L. & Fritz, J. H. Re-thinking the functions of IgA(+) plasma cells. *Gut Microbes* **5**, 652–662 (2014).

189. Sutherland, D. B. & Fagarasan, S. IgA synthesis: a form of functional immune adaptation extending beyond gut. *Curr Opin Immunol* **24**, 261–268 (2012).

190. Pietrzak, B., Tomela, K., Olejnik-Schmidt, A., Mackiewicz, A. & Schmidt, M. Secretory IgA in Intestinal Mucosal Secretions as an Adaptive Barrier against Microbial Cells. *Int J Mol Sci* **21**, 9254 (2020).

191. Puchelle, E., Jacqot, J. & Zahm, J. M. In vitro restructuring effect of human airway immunoglobulins A and lysozyme on airway secretions. *Eur J Respir Dis Suppl* **153**, 117–122 (1987).

192. Kumar Bharathkar, S. *et al.* The structures of secretory and dimeric immunoglobulin A. *eLife* **9**, e56098.

193. Wei, H. & Wang, J.-Y. Role of Polymeric Immunoglobulin Receptor in IgA and IgM Transcytosis. *Int J Mol Sci* **22**, 2284 (2021).

194. He, T. *et al.* Associations of urinary polymeric immunoglobulin receptor peptides in the context of cardio-renal syndrome. *Sci Rep* **10**, 8291 (2020).

195. Stadtmueller, B. M. *et al.* The structure and dynamics of secretory component and its interactions with polymeric immunoglobulins. *eLife* **5**, e10640.

196. Mostov, K. E. & Deitcher, D. L. Polymeric immunoglobulin receptor expressed in MDCK cells transcytoses IgA. *Cell* **46**, 613–621 (1986).

197. Turula, H. & Wobus, C. E. The Role of the Polymeric Immunoglobulin Receptor and Secretory Immunoglobulins during Mucosal Infection and Immunity. *Viruses* **10**, 237 (2018).

198. Everett, M. L., Palestrant, D., Miller, S. E., Bollinger, R. R. & Parker, W. Immune exclusion and immune inclusion: a new model of host-bacterial interactions in the gut. *Clinical and Applied Immunology Reviews* **4**, 321–332 (2004).

199. Role of secretory immunoglobulin A and secretory component in the protection of mucosal surfaces | Future Microbiology. https://www.futuremedicine.com/doi/abs/10.2217/fmb.10.39.

200. Johansen, F.-E. & Kaetzel, C. S. Regulation of the polymeric immunoglobulin receptor and IgA transport: new advances in environmental factors that stimulate pIgR expression and its role in mucosal immunity. *Mucosal Immunol* **4**, 598–602 (2011).

201. Reikvam, D. H. *et al.* Epithelial-microbial crosstalk in polymeric Ig receptor deficient mice. *Eur J Immunol* **42**, 2959–2970 (2012).

202. Bruno, M. E. C. *et al.* Correlation of Biomarker Expression in Colonic Mucosa with Disease Phenotype in Crohn's Disease and Ulcerative Colitis. *Dig Dis Sci* **60**, 2976–2984 (2015).

203. Lin, H. *et al.* Polymeric immunoglobulin receptor deficiency exacerbates autoimmune hepatitis by inducing intestinal dysbiosis and barrier dysfunction. *Cell Death Dis* **14**, 1–12 (2023).

204. Krawczyk, K. M. *et al.* Localization and Regulation of Polymeric Ig Receptor in Healthy and Diseased Human Kidney. *The American Journal of Pathology* **189**, 1933–1944 (2019).

205. Polosukhin, V. V. *et al.* Secretory IgA Deficiency in Individual Small Airways Is Associated with Persistent Inflammation and Remodeling. *Am J Respir Crit Care Med* **195**, 1010–1021 (2017).

206. Polosukhin, V. V. *et al.* Bronchial secretory immunoglobulin a deficiency correlates with airway inflammation and progression of chronic obstructive pulmonary disease. *Am J Respir Crit Care Med* **184**, 317–327 (2011).

207. Wang, X., Zhang, J., Wu, Y., Xu, Y. & Zheng, J. SIgA in various pulmonary diseases. *Eur J Med Res* **28**, 299 (2023).

208. de Fays, C., Carlier, F. M., Gohy, S. & Pilette, C. Secretory Immunoglobulin A Immunity in Chronic Obstructive Respiratory Diseases. *Cells* **11**, 1324 (2022).

209. Gohy, S. T. *et al.* Polymeric immunoglobulin receptor down-regulation in chronic obstructive pulmonary disease. Persistence in the cultured epithelium and role of transforming growth factor-β. *Am J Respir Crit Care Med* **190**, 509–521 (2014).

210. Ladjemi, M. Z. *et al.* Bronchial Epithelial IgA Secretion Is Impaired in Asthma. Role of IL-4/IL-13. *Am J Respir Crit Care Med* **197**, 1396–1409 (2018).

211. Shkalim, V. *et al.* Selective IgA deficiency in children in Israel. *J Clin Immunol* **30**, 761–765 (2010).

212. Abo Ali, F. H. *et al.* Selective IgA Deficiency a Probable Risk of Recurrent Chest Infections in Asthmatics. *J Asthma Allergy* **14**, 1323–1333 (2021).

213. Mallano, A., Ascione, A. & Flego, M. Antibody Response against SARS-CoV-2 Infection: Implications for Diagnosis, Treatment and Vaccine Development. *International Reviews of Immunology* **41**, 393–413 (2022).

214. Shim, S.-M. *et al.* Persistence of the neutralizing antibody response after SARS-CoV-2 infection. *Clinical Microbiology and Infection* **28**, 614.e1-614.e4 (2022).

215. Marot, S. *et al.* Rapid decline of neutralizing antibodies against SARS-CoV-2 among infected healthcare workers. *Nat Commun* **12**, 844 (2021).

216. Sheikh-Mohamed, S. *et al.* Systemic and mucosal IgA responses are variably induced in response to SARS-CoV-2 mRNA vaccination and are associated with protection against subsequent infection. *Mucosal Immunol* **15**, 799–808 (2022).

217. Denis, J. *et al.* Long-term systemic and mucosal SARS-CoV-2 IgA response and its association with persistent smell and taste disorders. *Front Immunol* **14**, 1140714 (2023).

218. Sterlin, D. *et al.* IgA dominates the early neutralizing antibody response to SARS-CoV-2. *Sci Transl Med* **13**, eabd2223 (2021).

219. Cervia, C. *et al.* Systemic and mucosal antibody responses specific to SARS-CoV-2 during mild versus severe COVID-19. *Journal of Allergy and Clinical Immunology* **147**, 545-557.e9 (2021).

220. Quinti, I., Mortari, E. P., Fernandez Salinas, A., Milito, C. & Carsetti, R. IgA Antibodies and IgA Deficiency in SARS-CoV-2 Infection. *Frontiers in Cellular and Infection Microbiology* **11**, (2021).

221. Pilapitiya, D., Wheatley, A. K. & Tan, H.-X. Mucosal vaccines for SARS-CoV-2: triumph of hope over experience. *eBioMedicine* **92**, (2023).

222. Russell, M. W., Moldoveanu, Z., Ogra, P. L. & Mestecky, J. Mucosal Immunity in COVID-19: A Neglected but Critical Aspect of SARS-CoV-2 Infection. *Frontiers in Immunology* **11**, (2020).

223. Feng, Z. *et al.* Screening and Analysis of Serum Protein Biomarkers Infected by Coronavirus Disease 2019 (COVID-19). *Trop Med Infect Dis* **7**, 397 (2022).

224. Siwy, J. *et al.* CD99 and polymeric immunoglobulin receptor peptides deregulation in critical COVID-19: A potential link to molecular pathophysiology? *Proteomics* **21**, 2100133 (2021).

225. Zhang, K. *et al.* Nsp1 protein of SARS-CoV-2 disrupts the mRNA export machinery to inhibit host gene expression. *Science Advances* **7**, eabe7386 (2021).

226. Flower, T. G. & Hurley, J. H. Crystallographic molecular replacement using an in silico-generated search model of SARS-CoV-2 ORF8. *Protein Sci* **30**, 728–734 (2021).

227. Pires De Souza, G. A. *et al.* Choosing a cellular model to study SARS-CoV-2. *Frontiers in Cellular and Infection Microbiology* **12**, (2022).

228. Padmanabhan, P., Desikan, R. & Dixit, N. M. Targeting TMPRSS2 and Cathepsin B/L together may be synergistic against SARS-CoV-2 infection. *PLoS Comput Biol* **16**, e1008461 (2020).

229. Gehl, J. Electroporation: theory and methods, perspectives for drug delivery, gene therapy and research. *Acta Physiol Scand* **177**, 437–447 (2003).

230. Yu, T. *et al.* ORF8 protein of SARS-CoV-2 reduces male fertility in mice. *J Med Virol* **94**, 4193–4205 (2022).

231. Bruno, M. E. C., Frantz, A. L., Rogier, E. W., Johansen, F.-E. & Kaetzel, C. S. Regulation of the polymeric immunoglobulin receptor by the classical and alternative NF-κB pathways in intestinal epithelial cells. *Mucosal Immunol* **4**, 468–478 (2011).

232. Li, J.-Y. *et al.* The ORF6, ORF8 and nucleocapsid proteins of SARS-CoV-2 inhibit type I interferon signalling pathway. *Virus Research* **286**, 198074 (2020).

233. Annexin V Staining - CA. https://www.thermofisher.com/ca/en/home/life-science/cell-analysis/cell-viability-and-regulation/apoptosis/annexin-v-staining.html.

234. Fan, X. *et al.* Rab11-FIP1 and Rab11-FIP5 Regulate pIgR/pIgA Transcytosis through TRIM21-Mediated Polyubiquitination. *Int J Mol Sci* **22**, 10466 (2021).

235. Singer, K. L. & Mostov, K. E. Dimerization of the Polymeric Immunoglobulin Receptor Controls Its Transcytotic Trafficking. *Mol Biol Cell* **9**, 901–915 (1998).

236. Wang, J., Tian, S., Petros, R. A., Napier, M. E. & DeSimone, J. M. The Complex Role of Multivalency in Nanoparticles Targeting the Transferrin Receptor for Cancer Therapies. *J Am Chem Soc* **132**, 11306–11313 (2010).

237. Cell line - TFRC - The Human Protein Atlas. https://www.proteinatlas.org/ENSG00000072274-TFRC/cell+line#kidney_cancer.

238. Dev, S. & Babitt, J. L. Overview of Iron Metabolism in Health and Disease. *Hemodial Int* **21**, S6–S20 (2017).

239. Kleven, M. D., Jue, S. & Enns, C. A. Transferrin Receptors TfR1 and TfR2 Bind Transferrin through Differing Mechanisms. *Biochemistry* **57**, 1552–1559 (2018).

240. Pantopoulos, K., Porwal, S. K., Tartakoff, A. & Devireddy, L. Mechanisms of mammalian iron homeostasis. *Biochemistry* **51**, 5705–5724 (2012).

241. Nai, A. *et al.* The second transferrin receptor regulates red blood cell production in mice. *Blood* **125**, 1170–1179 (2015).

242. Fleming, M. D. *et al.* Nramp2 is mutated in the anemic Belgrade (b) rat: Evidence of a role for Nramp2 in endosomal iron transport. *Proc Natl Acad Sci U S A* **95**, 1148–1153 (1998).

243. Anderson, G. J. & Frazer, D. M. Current understanding of iron homeostasis. *Am J Clin Nutr* **106**, 1559S-1566S (2017).

244. Ohgami, R. S. *et al.* Identification of a ferrireductase required for efficient transferrin-dependent iron uptake in erythroid cells. *Nat Genet* **37**, 1264–1269 (2005).

245. Ganz, T. Systemic iron homeostasis. *Physiol Rev* **93**, 1721–1741 (2013).

246. Zhang, D.-L. *et al.* Hepcidin regulates ferroportin expression and intracellular iron homeostasis of erythroblasts. *Blood* **118**, 2868–2877 (2011).

247. Ni, S., Yuan, Y., Kuang, Y. & Li, X. Iron Metabolism and Immune Regulation. *Frontiers in Immunology* **13**, (2022).

248. Silva, A. M. N., Moniz, T., de Castro, B. & Rangel, M. Human transferrin: An inorganic biochemistry perspective. *Coordination Chemistry Reviews* **449**, 214186 (2021).

249. Sekyere, E. O., Dunn, L. L. & Richardson, D. R. Examination of the distribution of the transferrin homologue, melanotransferrin (tumour antigen p97), in mouse and human. *Biochimica et Biophysica Acta (BBA) - General Subjects* **1722**, 131–142 (2005).

250. Iatsenko, I., Marra, A., Boquete, J.-P., Peña, J. & Lemaitre, B. Iron sequestration by transferrin 1 mediates nutritional immunity in Drosophila melanogaster. *Proceedings of the National Academy of Sciences* **117**, 7317–7325 (2020).

251. Siqueiros-Cendón, T. *et al.* Immunomodulatory effects of lactoferrin. *Acta Pharmacol Sin* **35**, 557–566 (2014).

252. Bolat, E. *et al.* Lactoferrin for COVID-19 prevention, treatment, and recovery. *Front Nutr* **9**, 992733 (2022).

253. Miotto, M. *et al.* Molecular Mechanisms Behind Anti SARS-CoV-2 Action of Lactoferrin. *Front Mol Biosci* **8**, 607443 (2021).

254. Piacentini, R. *et al.* Lactoferrin Inhibition of the Complex Formation between ACE2 Receptor and SARS CoV-2 Recognition Binding Domain. *Int J Mol Sci* **23**, 5436 (2022).

255. Campione, E. *et al.* Lactoferrin Against SARS-CoV-2: In Vitro and In Silico Evidences. *Front Pharmacol* **12**, 666600 (2021).

256. Wotring, J. W., Fursmidt, R., Ward, L. & Sexton, J. Z. Evaluating the in vitro efficacy of bovine lactoferrin products against SARS-CoV-2 variants of concern. *Journal of Dairy Science* **105**, 2791–2802 (2022).

257. He, S. *et al.* Bovine lactoferrin inhibits SARS-CoV-2 and SARS-CoV-1 by targeting the RdRp complex and alleviates viral infection in the hamster model. *J Med Virol* **95**, e28281 (2023).

258. Serrano, G. *et al.* Liposomal Lactoferrin as Potential Preventative and Cure for COVID-19. in *International Journal of Research in Health Sciences* vol. 8 08–15 (2020).

259. Rosa, L. *et al.* Ambulatory COVID-19 Patients Treated with Lactoferrin as a Supplementary Antiviral Agent: A Preliminary Study. *J Clin Med* **10**, 4276 (2021).

260. Muhammad, J. S. *et al.* SARS-CoV-2-induced hypomethylation of the ferritin heavy chain (FTH1) gene underlies serum hyperferritinemia in severe COVID-19 patients. *Biochem Biophys Res Commun* **631**, 138–145 (2022).

261. Tural Onur, S. *et al.* Could ferritin level be an indicator of COVID-19 disease mortality? *Journal of Medical Virology* **93**, 1672–1677 (2021).

262. van Raaij, S. E. G., Srai, S. K. S., Swinkels, D. W. & van Swelm, R. P. L. Iron uptake by ZIP8 and ZIP14 in human proximal tubular epithelial cells. *Biometals* **32**, 211–226 (2019).

263. Cunningham, K. A. *et al.* Poly-immunoglobulin receptor-mediated transport of IgA into the male genital tract is important for clearance of Chlamydia muridarum infection. *Am J Reprod Immunol* **60**, 405–414 (2008).

264. Armitage, C. W., O'Meara, C. P. & Beagley, K. W. Chlamydial infection enhances expression of the polymeric immunoglobulin receptor (pIgR) and transcytosis of IgA. *American Journal of Reproductive Immunology* **77**, e12611 (2017).

265. Chen, Y.-M., Helm, E. T., Gabler, N., Hostetter, J. M. & Burrough, E. R. Alterations in Intestinal Innate Mucosal Immunity of Weaned Pigs During Porcine Epidemic Diarrhea Virus Infection. *Vet Pathol* **57**, 642–652 (2020).

266. Turula, H. *et al.* Natural Secretory Immunoglobulins Promote Enteric Viral Infections. *J Virol* **92**, e00826-18 (2018).

267. Iovino, F. *et al.* pIgR and PECAM-1 bind to pneumococcal adhesins RrgA and PspC mediating bacterial brain invasion. *Journal of Experimental Medicine* **214**, 1619–1630 (2017).

268. Iovino, F., Molema, G. & Bijlsma, J. J. E. Streptococcus pneumoniae Interacts with pIgR Expressed by the Brain Microvascular Endothelium but Does Not Co-Localize with PAF Receptor. *PLoS One* **9**, e97914 (2014).

269. Zhang, J. R. *et al.* The polymeric immunoglobulin receptor translocates pneumococci across human nasopharyngeal epithelial cells. *Cell* **102**, 827–837 (2000).

270. van der Wielen, P. A., Holmes, A. R. & Cannon, R. D. Secretory component mediates Candida albicans binding to epithelial cells. *Oral Dis* **22**, 69–74 (2016).

271. Lin, C. T. *et al.* The mechanism of Epstein-Barr virus infection in nasopharyngeal carcinoma cells. *Am J Pathol* **150**, 1745–1756 (1997).

272. Sixbey, J. W. & Yao, Q. Y. Immunoglobulin A-induced shift of Epstein-Barr virus tissue tropism. *Science* **255**, 1578–1580 (1992).

273. Li, D. *et al.* Expression of pIgR in the tracheal mucosa of SHIV/SIV-infected rhesus macaques. *Zool Res* **38**, 44–48 (2017).

274. Wang, Y. & Yang, Gb. Alteration of Polymeric Immunoglobulin Receptor and Neonatal Fc Receptor Expression in the Gut Mucosa of Immunodeficiency Virus-Infected Rhesus Macaques. *Scandinavian Journal of Immunology* **83**, 235–243 (2016).

275. Harcourt, J. L. & Haynes, L. M. Establishing a Liquid-covered Culture of Polarized Human Airway Epithelial Calu-3 Cells to Study Host Cell Response to Respiratory Pathogens In vitro. *J Vis Exp* 50157 (2013) doi:10.3791/50157.

276. Oztan, A., Rondanino, C. & Apodaca, G. Transcytosis of Polymeric Immunoglobulin A in Polarized Madin-Darby Canine Kidney Cells. *Methods Mol Biol* **440**, 157–170 (2008).

277. Tsai, H.-C., Lehman, C. W., Lin, C.-C., Tsai, S.-W. & Chen, C.-M. Functional evaluation for adequacy of MDCK-lineage cells in influenza research. *BMC Res Notes* **12**, 101 (2019).

278. Wang, L. *et al.* Susceptibility to SARS-CoV-2 of Cell Lines and Substrates Commonly Used to Diagnose and Isolate Influenza and Other Viruses. *Emerg Infect Dis* **27**, 1380–1392 (2021).

279. Maruthachalam, B. V. *et al.* Discovery and characterization of single-domain antibodies for polymeric Ig receptor-mediated mucosal delivery of biologics. *MAbs* **12**, 1708030 (2020).

280. Zuo, T., Feng, X., Zhang, N., Xue, C. & Tang, Q.-J. Establishment of a functional secretory IgA transcytosis model system in vitro for functional food screening. *Appl Microbiol Biotechnol* **99**, 5535–5545 (2015).

281. Collin, A. M. *et al.* Lung immunoglobulin A immunity dysregulation in cystic fibrosis. *EBioMedicine* **60**, 102974 (2020).

282. Grainger, C. I., Greenwell, L. L., Lockley, D. J., Martin, G. P. & Forbes, B. Culture of Calu-3 Cells at the Air Interface Provides a Representative Model of the Airway Epithelial Barrier. *Pharm Res* **23**, 1482–1490 (2006).

283. Loman, S., Radl, J., Jansen, H. M., Out, T. A. & Lutter, R. Vectorial transcytosis of dimeric IgA by the Calu-3 human lung epithelial cell line: upregulation by IFN-gamma. *Am J Physiol* **272**, L951-958 (1997).

284. Leung, C., Wadsworth, S. J., Yang, S. J. & Dorscheid, D. R. Structural and functional variations in human bronchial epithelial cells cultured in air-liquid interface using different growth media. *Am J Physiol Lung Cell Mol Physiol* **318**, L1063–L1073 (2020).

285. Ryu, G. & Shin, H.-W. SARS-CoV-2 Infection of Airway Epithelial Cells. *Immune Netw* **21**, e3 (2021).

286. Mulay, A. *et al.* SARS-CoV-2 infection of primary human lung epithelium for COVID-19 modeling and drug discovery. *Cell Rep* **35**, 109055 (2021).

287. Navigating challenges: optimising methods for primary cell culture isolation | Cancer Cell International | Full Text. https://cancerci.biomedcentral.com/articles/10.1186/s12935-023-03190-4#.

288. Booth, C. K., Dwyer, D. B., Pacque, P. F. & Ball, M. J. Measurement of immunoglobulin A in saliva by particle-enhanced nephelometric immunoassay: sample collection, limits of quantitation, precision, stability and reference range. *Ann Clin Biochem* **46**, 401–406 (2009).

289. Campos-Rodríguez, R. *et al.* Stress modulates intestinal secretory immunoglobulin A. *Frontiers in Integrative Neuroscience* **7**, (2013).

290. Hooper, L. V. *et al.* Molecular analysis of commensal host-microbial relationships in the intestine. *Science* **291**, 881–884 (2001).

291. Kurimoto, Y. *et al.* Voluntary exercise increases IgA concentration and polymeric Ig receptor expression in the rat submandibular gland. *Biosci Biotechnol Biochem* **80**, 2490–2496 (2016).

292. Matsuzaki, K. *et al.* Salivary Immunoglobulin A Secretion and Polymeric Ig Receptor Expression in the Submandibular Glands Are Enhanced in Heat-Acclimated Rats. *Int J Mol Sci* **21**, 815 (2020).

293. Moon, C., VanDussen, K. L., Miyoshi, H. & Stappenbeck, T. S. Development of a primary mouse intestinal epithelial cell monolayer culture system to evaluate factors that modulate IgA transcytosis. *Mucosal Immunology* **7**, 818–828 (2014).

294. Fan, C. *et al.* Animal models for COVID-19: advances, gaps and perspectives. *Signal Transduct Target Ther* **7**, 220 (2022).

295. Baringer, S. L., Palsa, K., Simpson, I. A. & Connor, J. R. Apo- and holo- transferrin differentially interact with ferroportin and hephaestin to regulate iron release at the blood-brain barrier. *bioRxiv* 2023.01.10.522344 (2023) doi:10.1101/2023.01.10.522344.

296. Woof, J. M. & Kerr, M. A. IgA function – variations on a theme. *Immunology* **113**, 175–177 (2004).

297. DuBourdieu, D. Colostrum Antibodies, Egg Antibodies and Monoclonal Antibodies Providing Passive Immunity for Animals. *Nutraceuticals in Veterinary Medicine* 245–257 (2019) doi:10.1007/978-3-030-04624-8_18.

298. Immunoglobulin IgM Class - CA. https://www.thermofisher.com/ca/en/home/life-science/antibodies/antibodies-learning-center/antibodies-resource-library/antibody-methods/immunoglobulin-igm-class.html.